Physics – Uspekhi **41** (11) 1049 – 1089 (1998)

REVIEWS OF TOPICAL PROBLEMS

PACS numbers: **52.55.–s**, 52.55.Lf, 52.55.Mg

On Galateas — magnetic traps with plasma-embedded conductors

A I Morozov, V V Savel'ev

Contents

Abstract. **The introduction of plasma-embedded magnetically insulated current-carrying conductors into a plasma trap magnetic system radically increases the number of possible trap designs. The present review focuses on the studies of $\beta = 1$ Galateas conducted in the 1990s. Both general and design-specific Galatea properties are discussed and for a number of specific schemes analytical and numerical calculations are performed. Experimental data on a number of electrical discharge Galateas are presented.**

A I Morozov Russian Research Center 'Kurchatov Institute'
pl. Kurchatova 1, 123182 Moscow, Russia
Tel. (7-095) 197 77 55
V V Savel'ev Keldysh Institute of Applied Mathematics, Russian Academy of Sciences, Miusskaya pl. 4, 125047 Moscow, Russia
Tel. (7-095) 250 78 37
E-mail: oyufed@spp.keldysh.ru

Received 24 March 1998
Uspekhi Fizicheskikh Nauk **168** (11) 1153 – 1194 (1998)
Translated by E N Ragozin; edited by S D Danilov

1. Introduction

Suppression of convective instabilities is a necessary condition for efficient plasma confinement. Only when they are suppressed can we look forward to suppressing different drift instabilities and thus attain the classical transfer mode. As a rule, convective instabilities are associated with plasma diamagnetism. It is therefore unnatural from general considerations to place a plasma in a magnetic field. Traditional traps (with a plasma to magnetic field pressure ratio $\beta < 1$) are operational because the path of a particle in a magnetic field is a spiral and not just a Larmor circle. As a result, a particle goes from a region with one magnetic field to a region with another one (e.g. as in a magnetic bottle with Ioffe rods), which can provide the particle confinement.

To radically suppress the confinement-prohibitive diamagnetic effect, the fields should be employed not as the 'habitat' of the plasma but as a 'fence' enclosing the plasma domain†. In this case, the diamagnetism becomes an assistant instead of an opponent. And this would be the case for an

† By convention, traps containing magnetic field-free domains are referred to as traps with $\beta_0 = 1$ (see Section 2.3).

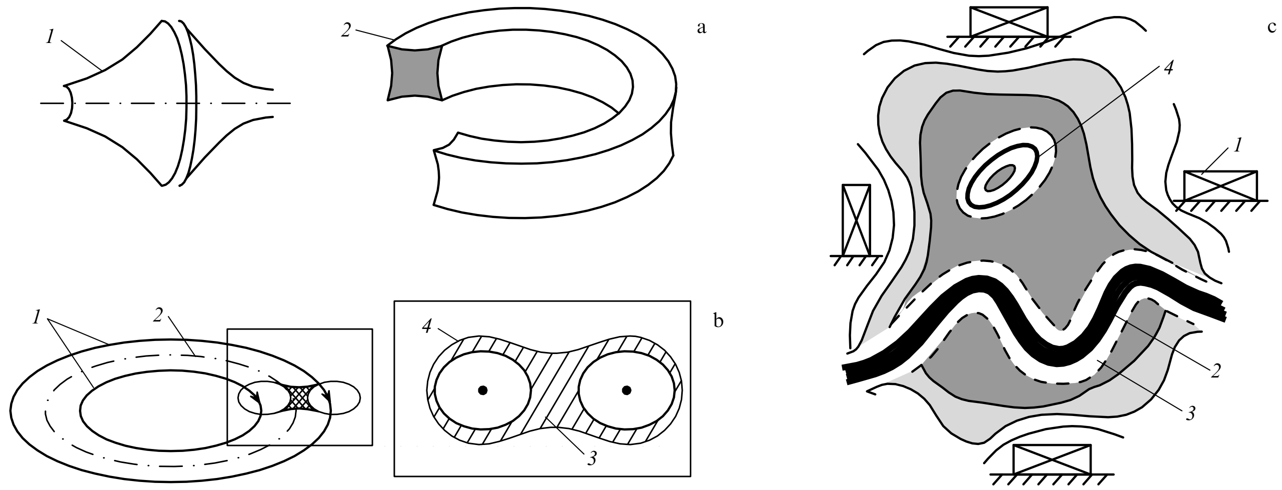

Figure 1. From acute-angled configurations towards Galateas: (a) acute-angled simply (*1*) and doubly-connected (*2*) configurations; (b) the general view and the cross section of the 'Dublon' trap: *1* — levitating current-carrying conductors, *2* — the line of zero magnetic field, *3* — acute-angled PPV, *4* — 'mantle,' (c) to the definition of the notions 'Galatea' and 'myxine': *1* — 'supporting coil,' *2* — 'jammed' myxine, *3* — magnetic sheath of a myxine (MSM), *4* — free myxines.

absolutely rigid and undistortable magnetic field. But the magnetic field is deformable, and therefore the sharp plasma – field boundary proves to be stable only provided

$$(\mathbf{n}^0, \nabla)H > 0\,. \tag{1.1}$$

Here $\mathbf{n}^0$ is the external normal to the plasma boundary. As a consequence the connected plasma volume necessarily appears to be 'acute-angled' (Fig. 1a). This implies that the configuration has gaps, its transverse dimension δ being of the order of the Larmor radius:

$$\delta \gtrsim \rho_{\mathrm{i}}\,. \tag{1.2}$$

All this has been well known since the mid-50s and has been the subject of investigations conducted by Russian and foreign scientists [1 – 4]. However, the problem of gaps was either totally ignored in these works or the estimates of their width were too optimistic ($\delta \approx \rho_{\mathrm{e}}$). But the first experiments with magnetic antibottles revealed that the actual gap widths were close to the estimate (1.2). This practically denudes such traps of the prospect of becoming reactors. Clearly a gapless fence can only be made with retention of stability by closing the acute angles to each other, as shown by the example of the 'Dublon' trap (Fig. 1b). But such closing is necessarily performed by magnetic 'sheaths' containing the separatrix, which leans upon the principal plasma volume (PPV) on one side and envelopes the current-carrying conductors on the other. In consequence the plasma from the PPV spreads along the separatrix to form plasma layers; following [5], they will be referred to as 'mantles.' The appearance of mantles necessarily calls for the detachment of conductors, which induce the magnetic configuration, from their base and for their transformation to levitating plasma-immersed elements with magnetic sheaths.

Following [6, 7], we shall refer to any traps (Fig. 1c) containing plasma-immersed current-carrying conductors as 'Galateas' and to plasma-immersed conductors as 'myxines.'† The appearance of levitating myxines calls for three new elements: 'supporting coils' (*1*) to induce the myxine-supporting field, 'locks' (*2*) to fix their relative position, and 'stabilizers' (*3*) to retain each myxine in its position.

By introducing the mantle into the plasma configuration, we stopped the gaps. But in the mantles the curvature of the magnetic field lines is unfavorable for stability. However, as calculations show, it is not difficult to compensate for the resulting tendency for the most dangerous hydrodynamic instabilities by portions of force lines adjoining the region where $H \to 0$ (see Section 8).

In the foregoing we came to Galateas starting from the problem of magnetic configurations, in which there is a zone free from magnetic field with a magnetic gapless barrier around the zone. This type of Galatea will be referred to as a 'Galatea with $\beta_0 = 1$.' But there are a number of interesting problems on Galateas with a nonzero magnetic field ($\beta_0 \neq 1$).

The simplicity of manipulating the magnetic fields of Galateas was the reason why they were popular even at the dawn of the conception of magnetic confinement. For example, described in A D Sakharov's fundamental work [8] was not the prototype of a tokamak but a Galatea. In the 50s, a series of theoretical studies on Galateas was made, and a number of configurations for these traps were proposed. The investigation made by D V Orlinskiĭ [9] was presumably the first attempt to devise and experimentally study a Galatea-type system.

In the 60s and the early 70s, the interest in Galateas grew steadily. Shown in Fig. 2 are the principal types of Galateas, which became the object of theoretical and experimental studies‡ by the mid-70s: tokamak-like 'levitrons' with $\beta_0 < 1$, Galateas with protective conductors ($\beta_0 = 1$), multipole Galateas ($\beta_0 = 1$), and tornado Galateas with a fixed myxine. At that time high-technology installations were made in the USSR, Western Europe, and the USA (Fig. 3). In particular, these studies demonstrated the feasibility of classical confinement, though in a relatively narrow parameter range [10].

† A myxine (Myxine glutinosa) is a lamprey 'relative' and resembles it. Myxines possess an astonishing ability to make a knot of themselves.

‡ Only a small part of the existing publications, primarily in Russian, are given in the figure captions. The preparation of a comprehensive review of the contributions of individual authors is a task for special study.

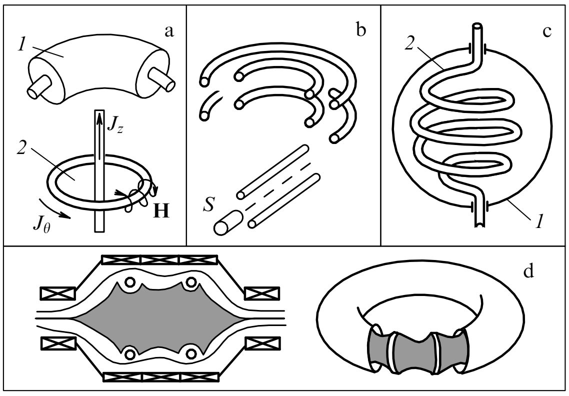

Figure 2. Classical Galatea types: (a) tokamak-like 'levitrons' [8, 10]; (b) multipole Galateas [4, 11 – 14]; (c) 'Tornado' [15, 16]; (d) traps with protective conductors [1, 9] (S is the plasma source).

By the mid-70s, most of the research on Galateas was terminated in connection with progress in tokamaks. The research on Galateas remained unfinished and was not brought to a logical end. Therefore, they are hard to comment on today. For the most part they were grouped on extremely low-β regimes (Fig. 3a). This stage of research on Galateas in the USA was summarized in the review by Yoshikawa [10]. The first sentence of the annotation to this review says: "Internal-conductor devices for low-β toroidal confinement are reviewed." Hence it is clear that it was not completely realized at that time that Galateas are required primarily to obtain high β. More recently the situation reversed: among the Galatea designs that appeared in the 60s, Galateas with $\beta_0 \approx 1$ were the subject of investigation for the longest. For example, the 'levitating octupole' of Wisconsin University (Fig. 3b) was operating as late as in the mid-80s while the 'Tornado' facilities in the Ioffe Physicotechnical Institute (St. Petersburg) are still in service [16] (Fig. 3c).

We are nevertheless convinced that the future may well lie with Galateas†. In the long run, the magnetic systems in traditional traps rest on the ground for two main reasons. First, for simplicity. Magnetic suspension requires more sophisticated devices. But now this no more presents an impenetrable barrier, which is especially well exemplified by the maglev train. Second, magnetic suspension requires either superconductors or the use of variable magnetic fields to induce the skin effect in supported elements. In many cases (in particular, for the CNF purposes in the context of the traditional approach) variable fields are unacceptable while the superconductors of the classical type require costly materials and special equipment. However, the situation is now reversed in connection with the advent of high-temperature superconductors and the technology for producing strips and wires around them. So, the technical complications and the inconveniences brought about by magnetic suspension have been left in the past and in the near future they will not even be taken into account. But then the fundamental advantages of Galateas are brought to the fore.

In addition, it is pertinent to note that plasma traps with $\beta_0 = 1$ are required for the solution not only of the CNF problem, but of a multitude of technical problems as well. One of the first problems of this kind emerged in connection with the demand for economic gas-discharge chambers (GDC) for space propulsion devices. For this purpose, R D Moor proposed covering the chamber surface with a system of positive anodes, protecting them against the penetration of electrons by an alternating magnetic field induced by small-sized permanent magnets [19]. More recently, systems of this kind came to be known as GDCs with a peripheral magnetic field and gained wide acceptance in the injectors for CNF etc. The plasma loss at the walls was thus radically reduced, allowing the price per ion to be cut by nearly an order of magnitude. 'Crustal' systems with a peripheral magnetic field are of prime interest for plasma technology as workpiece processing 'plasma baths.' Naturally, the change-over to Galateas will only improve the characteristics of such systems. Finally, the preparation of myxine-like (magnetically protected) bodies allowing for immersion in plasma will receive wide recognition in the future. The case in point could be, in particular, autonomous magnetically protected diagnostic tools for major

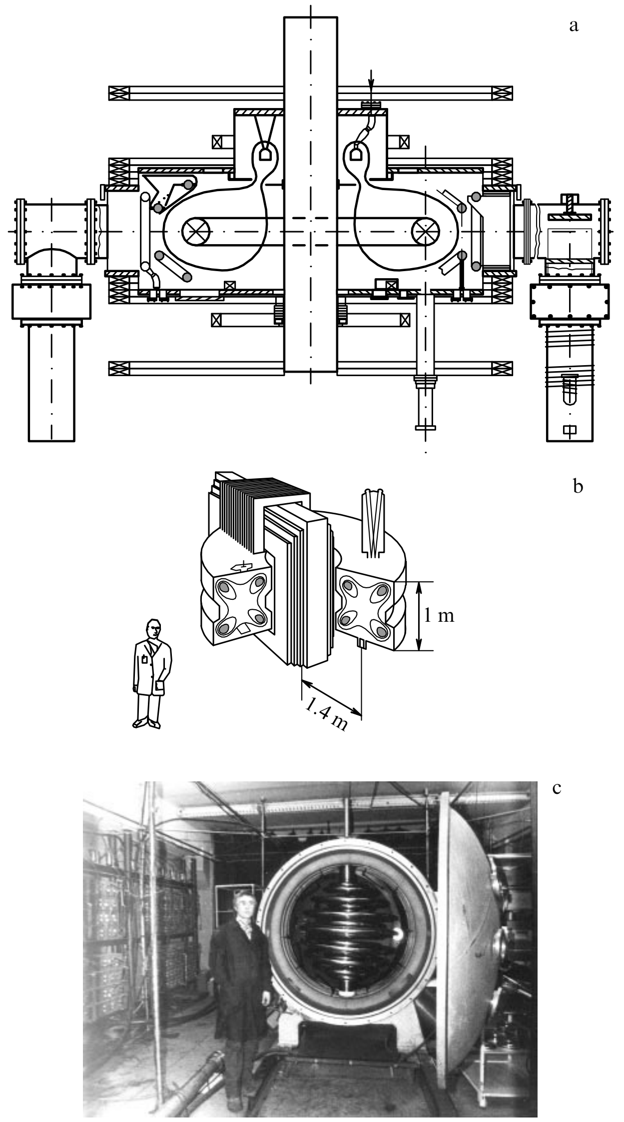

Figure 3. Examples of classical Galateas: (a) spherator [10], (b) levitating octupole [17], (c) 'Tornado' [16].

† Our opinion is shared by many. In particular, since the late 80s a long series of papers has appeared devoted to the 'Dipole' Galatea proposed by A Hasegawa (see Section 4.5).

plasma devices (see Section 4.5) and, probably, probes for the upper layers of the Sun.

This review covers the studies on Galateas conducted with participation of the authors since the late 80s (see Section 2.4). Three major features of these studies may be highlighted. First, we consider not one or two specific configurations but the fundamental possibilities offered by the use of levitating myxines. As a consequence, we have proposed a number of new Galatea configurations discussed below. Second, the emphasis is made on Galateas with $\beta_0 = 1$. Third, Galateas are studied experimentally in electric-discharge modes.

2. General description of Galateas

2.1 'Magnetic vessels.' 'Ideal' traps

One of indicators of the technical culture of a society is the nature of vessels intended for product storage. The advent of products with new features calls for the emergence of new vessels. There is a concurrent process of reduction of the ratio between the vessel material volume (mass) and the volume (mass) of the stored product. The vessels are not only reservoirs, but, as a rule, thermal (energy) barriers as well. A striking example is furnished by the Dewar flask. The advent of colliders can be regarded as the development of vessels for fast moving single-velocity flows.

The CNF problem has posed the problem of confinement of a hot plasma, a cloud of charged particles of either sign moving with high velocities which differ widely. Various configurations of plasma traps† emerged — first, toroidal and, later, open traps. Unfortunately, these plasma vessels have a fundamental drawback. Here, the plasma is 'mixed' with the magnetic field ($\beta < 1$ and even $\beta \ll 1$). As a consequence, the diamagnetism of Larmor circles provokes convective instabilities. In this case, the magnetic field occupies an unjustifiably large volume, whereas a magnetic crust ('shell') at the periphery of the plasma volume would in principle suffice to confine the plasma. This configuration makes it possible to reduce the volume occupied by the magnetic field by the factor $\theta_\mu = L/\delta$. Here, L is the diameter of the plasma volume and δ is the thickness of the magnetic crust.

However, it is not merely the smallness of the volume occupied by magnetic field that makes 'crustal' traps ('magnetic vessels') attractive. They are extremely economic as regards the field strength. It is evident from Table 1, which gives the data obtained for $\beta_0 = 1$, i.e. for $H^2/8\pi = nkT$.

Table 1.

Field strength, Oe	Concentration, 10^{11} cm^{-3}	Temperature, eV
10	1	30
100	10	300
1000	100	3×10^3
10000	1000	3×10^4

Magnetic vessels can be considered as 'ideal' traps. Of course, every particular problem advances specific optimization criteria. Therefore the concept of an ideal trap is to a degree conventional. Nevertheless introducing this notion as some ultimate reference point would be appropriate.

† Clearly 'trap' is an unfortunate term. Why then not call them 'plasma snares'?

By an ideal trap is naturally meant a gapless crustal-type trap ('magnetic vessel') that is stable with respect to convection and exhibits classical transfer of particles and energy.

In conventional gas dynamics, the suppression of convection is necessarily associated with classical transfer. In the case of magnetic confinement, currents flow through the plasma, which may result in the amplification of oscillations of relatively small perturbations. The latter give rise to convective cells capable of enhancing the transfer. Nevertheless, as indicated both by theory and experiment, when the convection is suppressed, it is possible, as a rule, to attain classical transfer by varying the plasma profile gradients. So, the feasibility of ideal traps is not doubted and, as is evident from the foregoing, these will be Galateas with $\beta_0 = 1$.

A fusion reactor is a different matter. This is not merely a trap for a plasma with 'thermonuclear parameters.' First, it is a trap to confine not only the hot 'fuel' (plasma), but, for some time, the charged reaction products as well. In addition to the second confinement problem (confinement of the charged reaction products), there are problems of 'fuel' injection and heating and of withdrawal of ash, i.e. reaction products. Finally, a reactor should provide radiation shielding. All this may force a divergence from ideal traps.

Nevertheless, there is hardly any doubt that Galateas will play an important part in the solution of the CNF problem. Their role will be especially important in going to hypertemperature reactors on D^{3}He, DD, etc. since the synchrotron radiation in Galateas with $\beta_0 = 1$ is minimum. A consideration of the complex of reactor problems is beyond the scope of this review; however, some of them will be touched on below.

The low cost of Galateas. Today the development of Galateas lags behind the corresponding development of tokamaks, stellarators, and magnetic mirror traps. This lag is often adduced as an argument against studies of Galateas. Disregarded in doing so is their exceptional cheapness stemming from design simplicity and efficient use of the magnetic field in Galateas. As for magnetic suspension, it is undoubtedly required for energy confinement times $\tau_E \geqslant 1$ ms; for lower values, it is possible to dispense with magnetic suspension. It should be taken into account (see Section 9) that the convection suppression in Galateas makes it possible to reduce the transfer to the classical level. Hopefully, the road to laboratory versions of traps with hydrogen plasmas of thermonuclear parameters (TTNP) ($n \sim 10^{14}$ cm^{-3}, $T_\mathrm{i} \sim T_\mathrm{e} \sim 10$ keV and $\tau_E \sim 1$ s) may be possible with highly modest means. Naturally, one-second confinement times will require superconducting chords in myxines. Assuming the field strength at the plasma-field transition $H \sim 10^4$ Oe, we have the ion Larmor radius $\rho_\mathrm{i} \sim 1$ cm and the diffusion coefficient for $\beta \sim 1$ and $T_\mathrm{e} \sim 10$ keV

$$D_\perp \approx \frac{c^2}{4\pi\sigma_0} \approx 10\ \mathrm{cm\,s^{-1}}\,. \tag{2.1}$$

Here σ_0 is the Spitzer plasma conductivity. Therefore the layer thickness through which the plasma can diffuse in one second is $\delta \leqslant 10$ cm.

2.2 Three technical complications associated with Galatea reactors [6]

Today it is still widely believed that the change-over to the magnetic suspension involves severe technical difficulties. Among these are: (i) devising the myxine suspension itself with a radiation shield; (ii) release of the myxine-related energy from the region of thermonuclear reactions; (iii) sustaining the required temperature in the superconducting myxine 'chord.'

(1) When traps (no reactions) are dealt with, the latter two difficulties are merely nonexistent while the first is greatly simplified because the radiation shield is no more required. Therefore, when evaluating the myxine mass, the mass of the superconducting chord can be used as the basis. Considering that the weight and the Ampere force acting on the superconductor are proportional to its volume (for a constant current density), the equilibrium equation can be written in the differential form

$$\rho g = 0.1 j_{SP} H_{\perp} . \tag{2.2}$$

Here, ρ is the chord density, j_{SP} is the current density in the chord, A cm^{-2}, and $H_{\perp}$ is the field strength of the external magnetic field which sustains the myxine in the gravitational field. Substituting the quantities $\rho = 10$ g cm^{-3}, $j_{SP} = 10^4$ A cm^{-2}, and $g \approx 10^3$ cm s^{-2} into (2.2), we find the magnitude of the sustaining magnetic field

$$H_{\perp} \approx 10 \text{ Oe} . \tag{2.3}$$

To state it in different terms, a magnetic field exceeding the Earth's magnetic field by only slightly more than an order of magnitude would suffice to suspend a myxine in the absence of a radiation shield.

Now we briefly† discuss the situation in the context of a fusion reactor. In this case, the superconducting chord would above all require shielding from the penetrating radiation. Depending on the type of the reactor working substance and the superconducting material, the shield thickness should be of the order of

$$\delta_m \sim 50-80 \text{ cm} .$$

For such a thickness, sustaining the myxine would require the transverse magnetic field

$$H_{\perp} \sim 150-300 \text{ Oe} .$$

If it is remembered that confining a thermonuclear plasma (DT, $n_i = n_e = 10^{14}$ cm^{-3}, $T_i = T_e = 10$ keV) for $\beta_0 = 1$ would require a barrier field $H_b \approx 10^4$ Oe, the magnitude of $H_{\perp}$ appears to be relatively low.

(2) The release of the fusion energy falling on a myxine with a density of ~ 1 MW m^{-2} can be accomplished (in the case of a DT mixture) by the thermal radiation of the surface heated to $T \approx 2000$ K.

(3) Finally, sustaining the cryoregion temperature at ~ 15 K when employing the classical Nb_3Sn superconductor or at ~ 70 K when employing new superconductors with a nitrogen operating temperature level can be accomplished either by cryogenerators built in the myxine or by cooling the entire myxine periodically with the use of external coolers (see Section 3.6).

So, there are no apparent serious problems of a technical nature today prohibiting the development of myxines for Galateas with an energy-passive or energy-producing plasma.

Clearly the situation with myxines will only improve in the future due to the inevitable increase of the operating semiconductor temperatures and to the change-over to low-flux neutron hypertemperature reactors.

† For more detail, see Section 3.5.

2.3 The Galatea as a subject of theoretical studies

In the preceding section we emphasized a fundamental feature of Galateas — the feasibility of gapless traps with $\beta_0 = 1$ in this class. Moreover, Galateas possess a series of important properties, some of which are noted here.

2.3.1 Completeness of the Galatea set. As is known, from the Fermi–Chandrasekhar virial theorem it follows that equilibrium static MHD configurations can be formed only in the presence of nonmagnetic forces. Under laboratory conditions, the only case in point is the elastic force of solids. In Galateas the solids are relieved of the artificial limitations — to rest on the ground and to touch the plasma only with one of its sides ('the first wall').

Hence, while the set of traditional traps $\{T\}$ is limited to simply connected (open) and doubly-connected (toroidal) traps, the Galatea set $\{\Gamma\}$ is immense both topologically and especially metrically. It is therefore safe to say that the Galatea set includes the set of traditional traps as a very special case:

$$\{\Gamma\} \supset \{T\} . \tag{2.4}$$

Galateas open up fresh opportunities for solving, in particular, the problem of large β on the metrical rather than topological level and thus to devise traps with

$$\beta_{loc} = \infty ,$$

i.e. magnetic vessels.

The inclusion (2.4) may seem to be an exaggeration but this is not so. Some new Galatea configurations have been obtained from traditional traps (Fig. 4). For instance, if the circle of fast particles (electrons or ions) in Christofilos's

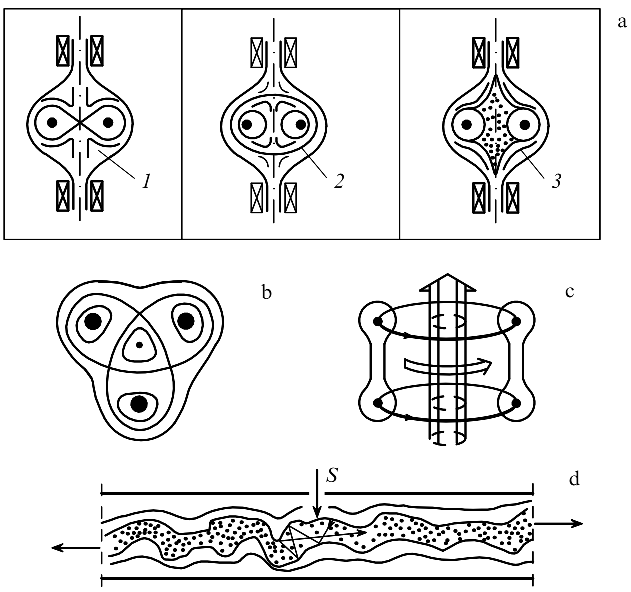

Figure 4. 'New' Galatea configurations: (a) solid-state analog of 'Astron' — Galatea-A: *1*, *2* — vacuum magnetic fields respectively with one and two zero points in the system axis, *3* — Galatea-A with a simply connected plasma volume, $\beta_0 = 1$; (b) Stellarator-Galatea (Stega); (c) Galatea-Belt; (d) diffusion-type Galateas with a weakly collisional plasma.

'Astron' is replaced by a current-carrying conductor, we obtain a Galatea-Astron, or Galatea-A (Gala). Its magnetic configuration can be of three types (Fig. 4a) [20, 21]. One of the present authors and V D Pustovitov proposed [22] a Stellarator-Galatea (Fig. 4b), which constitutes merely a torsotron; its primary coils do not rest on supports but are suspended by the magnetic field of the locks. In consequence, as the plasma flows along the separatrix, its mantle encloses the principal conductors. The so-accomplished flooding of the separatrix with the plasma would certainly improve the stability of the plasma configuration and increase the attainable magnitude of β. This is pointed out not only by the general considerations given in Ref. [22], but by the first calculation [23] as well. The possible change-over from the M S Ioffe 'Atoll' trap to a quadrupole trap is another example of such a switch from a traditional trap to a Galatea. Galateas can also form in a less trivial way. One example is the Galatea-Belt [24] (Fig. 4c). It is a quadrupole trap wherein the azimuth current flowing through the plasma is responsible for the formation of a current sheath. This Galatea is considered in detail in Section 8.

We therefore believe that the completeness of the Galatea set opens up new avenues for the development of the general theory of plasma confinement unrelated to the essentially accidental limitation of the set of traditional traps, namely, to the 'resting-on-ground' condition imposed on all the coils. And here developing the principles of classifying Galateas will presumably be the top-priority task.

2.3.2 Features of Galatea physics. Galateas differ essentially from traditional traps regarding their design and the processes involved. We emphasize the theoretically crucial ones:

(1) multiple connectedness of the plasma volumes and, in particular, the existence of 'holes;'

(2) the existence of three blocks (plasma, field, solid-state myxines with the electrodynamics of their own) rather than two (plasma and field), requiring a self-consistent description. In particular, both the plasma and the myxines should be in equilibrium;

(3) the existence of magnetic field-free regions in Galateas with $\beta_0 = 1$ whose representation is inherently kinetic;

(4) on the whole, investigation of the stability of the 'thin' (plasma-field transition and mantle) layers calls for a non-linear treatment in the kinetic approximation;

(5) the surface Galatea layers — magnetic vessels with relatively thin transition layers and mantles — can in many cases be treated as 'tiles,' i.e. consisting of quasi-autonomous blocks. This factor notably simplifies the studies on such Galateas as compared, for instance, with tokamaks and stellarators, in which the principal plasma volume is pierced by infinite force lines.

2.3.3 Terminology. Prior to passing to the consideration of specific issues, we define more precisely the meaning of some terms used below. This has already been done for the two opposite cases: the magnetic field in a vacuum ($\beta \to 0$) and the configurations with an abrupt plasma – field transition layer ($\beta_0 = 1$) with thickness $\delta \ll L$, where L is the characteristic transverse dimension of the principal plasma volume. In the former case, the surface $\Psi_{\mathrm{b}} = \mathrm{const}$ (Ψ is the magnetic flux function), which separates the regions of plasma stability and instability for $\beta \to 0$ according to one or other stability criterion (e.g. $U = \int H^{-1}\,\mathrm{d}l = \min$), will be referred to as the 'barrier surface.' If the configuration is toroidal, the line S (a point in the r, z-plane) on the surface Ψ_{b} where the field strength is minimum, is given the name 'saddle-point' and the field strength

$$H_{\mathrm{b}} = \min H(\Psi_{\mathrm{b}}) \tag{2.5}$$

is termed the 'barrier field' by the given stability criterion for $\beta \to 0$. In principle, we would do well to introduce the notions of the 'absolute maximum' S^* and the 'absolute barrier' H_{b}^*. The former signifies the locus (unrelated to stability criteria) of points where the magnetic field strength attains the absolute minimum H_{b}^* over the entire set of lines connecting the region with $H = 0$ at the center of the configuration and the external space where $H \to 0$.

In the case of configurations with an abrupt plasma-field transition, the 'plasma boundary' stands out, which can be defined as the magnetic surface Ψ_Γ at which the plasma pressure is $P_\Gamma = \theta P_0$. Here the quantity $\theta \sim 0.5$ and P_0 is the pressure in the principal plasma volume where $H \to 0$. Next we introduce the 'barrier' surface Ψ_{b} according to one or other stability criterion, as in the vacuum case. Needless to say

$$\Psi_\Gamma \leqslant \Psi_{\mathrm{b}}\,, \qquad \Psi > 0\,.$$

Similarly to the vacuum case, we define the 'saddle-point' S and the 'barrier field' H_{b}.

We now pass to defining the β parameter. Clearly this can be done in several ways:

(1) Local β parameter:

$$\beta_{\mathrm{loc}} = \frac{8\pi P}{H^2}\,. \tag{2.6a}$$

In the configurations with a steep profile it varies from ~ 0 to $\sim \infty$.

(2) The 'boundary' β_Γ for the principal plasma volume:

$$\beta_\Gamma = \left.\frac{8\pi P_0}{H_\Gamma^2}\right|_{\theta \to 0}. \tag{2.6b}$$

In the case of a steep profile, $\beta_\Gamma \approx 1$.

(3) The 'separatrix' β_{s} parameter:

$$\beta_{\mathrm{s}} = \frac{8\pi P_0}{H_{\mathrm{s}}^2}\,. \tag{2.6c}$$

Here H_{s} is the maximum field strength in the separatrix [17].

(4) The 'barrier' β parameter:

$$\beta_{\mathrm{b}} = \frac{8\pi P_0}{H_{\mathrm{b}}^2}\,. \tag{2.6d}$$

The above-introduced conventional β_0 parameter can be identified with β_Γ.

2.4 How we followed the path to Galateas

We have been on the road to Galateas since our presentation entitled "Stationary Plasma Accelerators and the Prospects for their Application in Fusion Research" [25] at the IAEA Conference in Novosibirsk in 1968. In that presentation a radically new, in a sense, configuration for a fusion reactor was proposed in the form of a long solenoid, the plasma heated to thermonuclear temperatures flowing along the

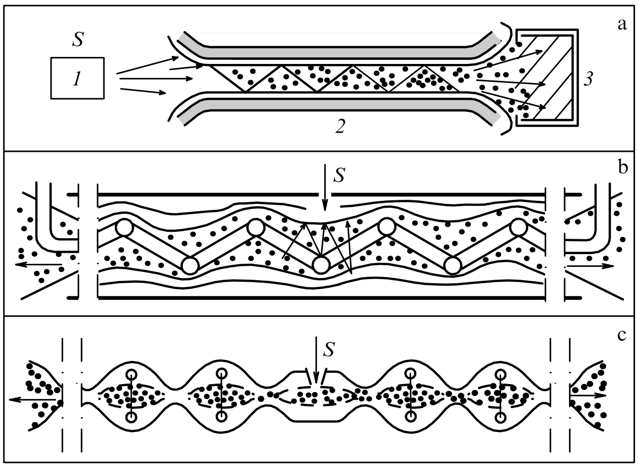

Figure 5. Traps with a moving plasma: (a) 'proletotron' with high-energy plasma injection: *1* — plasma source, *2* — solenoid, *3* — plasma receiver; (b) diffusion trap with a helical 'jammed' myxine (Gega); (c) sectioned diffusion trap with randomizing cells of the Galatea-A type (Gabi).

solenoid (Fig. 5). In its most crude form, the system comprises a high-current accelerator *1*, a solenoid *2*, and a receiver-recuperator *3*†. At the solenoid inlet a change-over occurs from a supersonic to subsonic plasma flow attended by heating to the required temperature. The convenience of such a configuration is evident. But all the problems are associated with the huge solenoid length. If we estimate the plasma velocity in the solenoid at $V_{\mathrm{s}} = 10^8$ cm s^{-1}, the minimum solenoid length L is given by the expression

$$L = V_{\mathrm{s}} \tau_E = V_{\mathrm{s}} \frac{A}{n} . \tag{2.7}$$

Here $A = (n\tau_E)_{\min}$ is the Artsimovich–Lawson constant, which is equal to 10^{14} s cm^{-3} for the D-T reaction. Assuming that the plasma density in the solenoid axis is $n_{\mathrm{s}} = 10^{16}$ cm^{-3}, we obtain $\tau_E = 10^{-2}$ s and $L \approx 10$ km. To the density n_{s} selected above corresponds the magnetic field strength $H_{\mathrm{s}} \sim 10^5$ Oe. For the specified flight time $\tau_0 = \tau_E = 10^{-1}$ s, the classical diffusion length is $\delta^{(\mathrm{c})} \approx 3$ mm. Hence the jet diameter will hardly change during the flight time if we put it equal to $\delta_{\mathrm{s}} \approx 4$ cm. Under these conditions, the fusion energy generated per meter of the jet will be $P_1 \approx 10$ MW. The total power of such a fusion reactor will amount to ~ 100 GW. If the diameter of the first solenoid wall is $D_{\mathrm{s}} \sim 3$ m, the power density at the wall is ~ 1 MW m^{-2}. The conception of a flight-tube reactor ('proletotron') can be implemented in many ways. In particular, when pellets are injected into the center of a previously 'ignited' reactor, the injector can be removed. The receiver of the outgoing plasma can be variously designed etc. The conception of a flight-tube reactor is appealing and many authors‡ would revert to it, proposing one or other version of the reactor. A realistic assessment of the proletotron was once given by G I Budker: "Such systems were considered, in particular, by Morozov, Tak, and others. Since no confinement or thermal insulation was intended, the installation length would be of the order of several hundred meters ... I would say that it is adequate for the problem of a fusion power plant of commercially significant output power. However, its modeling involves serious problems, and an immediate launch of the construction of a full-scale facility calls for exceptional courage on the part of the experimenter and the financing organization" [27].

Subsequently the conception advanced along two lines. On the one hand, the investigation and the improvement of a high-current quasistationary plasma accelerator was being continued. A conceptual sketch was proposed in the I V Kurchatov Institute of Atomic Energy [28–30] as early as the middle of 1959, and the experimental work on the accelerator commenced in the Institute in 1960. In essence, this accelerator is a magnetoplasmadynamic analog of the Laval nozzle (gas dynamic nozzle), the working substance being accelerated by the magnetic field pressure rather than the gas kinetic pressure. The development of such an accelerator proved to be a difficult task primarily due to the difficulties associated with matching the electric field in the accelerating channel and the field at the electrodes. Nevertheless they were overcome (Institute of Physics, Belarus; Kharkov Institute of Physics and Technology, Ukraine; Troitsk Institute for Innovation and Thermonuclear Research, Russia) in the early 90s, and the first-generation quasistationary high-current plasma accelerator (QHPA) was placed in service in the design mode. The QHPA delivered ~ 3 GW fluxes for a hydrogen ion energy of ~ 1 keV and a pulse duration of ~ 100 μs. Naturally, the advent of such an intense injector posed the problem of a trap design of 'modest' dimensions, which is nevertheless capable of withstanding the 'impact' of the QHPA plasma jet. Proceeding from a proletotron, the idea of replacing the specularly reflecting, magnetic cylindrical walls of the proletotron (Fig. 5a) with magnetic walls that scatter particles 'macrodiffusively' is natural. Thus comes the configuration of an 'extended tornado' (Fig. 5b), i.e. a solenoid with an asymmetric current-carrying helix inside it§. The asymmetry is required to ensure that no particle parameter (integral) is conserved during scattering by the magnetic walls. The lifetime of a particle, which moves in this trap with rare volume collisions and is chaotically, on average, scattered by the walls, is determined by the diffusion time

$$\tau^{\mathrm{dif}} \approx \frac{L_{\mathrm{s}}^2}{a_{\mathrm{s}} V_{\mathrm{s}}} . \tag{2.8}$$

Here a_{s} is the diameter of the magnetic channel. Putting $a_{\mathrm{s}} \approx 3$ m, $\tau^{\mathrm{dif}} \approx 10^{-2}$ cm, and $V_{\mathrm{s}} = 10^8$ cm s^{-1} with allowance made for the neutron shielding, we get

$$L_{\mathrm{s}} \sim 200 \text{ m} .$$

This length for a barrier field of ~ 100 kOe is acceptable for full-scale experiments. If the neutron shield is rejected, we can put $a_{\mathrm{s}} \approx 50$ cm to get

$$L_{\mathrm{s}} \sim 80 \text{ m} .$$

This trap proves to be smaller in size of a magnetic volume than the ITER. The term 'Galatea' appeared precisely after the conception of 'Gega' came into being. The interest in just the diffusion systems had certain historical grounds. Pre-

† A similar configuration was proposed by D L Tak at the same conference.

‡ In Ref. [26] Post described a version of a 'proletotron' under the name 'linear collider' without reference to the papers by A I Morozov and D L Tak.

§ In Ref. [20] this trap received the name 'Gelikon-Galatea' or, diminutively, 'Gega.' Gega, by the way, is a beautiful waterfall near the Ritsa lake in the Caucasus.

sumably the idea of such systems was first outlined in one of A I Morozov's reports in the following form in the late 50s (Fig. 5b). A trap will be termed a 'randomizing cell' if it has two end openings, through which particles can enter and exit the trap, and has a 'randomizing' capacity which implies the following: once a particle enters the trap, it 'forgets' which end the entry was made through and can exit by either with equal probability. If we prepare a chain of $2N+1$ randomizing cells, a particle placed in the center of the chain will remain inside, on average, for the period

$$\tau_N \approx \tau_1 N^2 \,. \tag{2.9}$$

Here τ_1 is the lifetime in a single cell.

The GOL† and ESPL traps were the first realizations of diffusion traps [31]. In GOL, a dense plasma system, randomization was accomplished by volume collisions. In ESPL, a rarefied plasma system, randomization was caused by the strong gradients of magnetic and electric fields. ESPL is discussed in more detail in Section 9. In the late 80s, a demand arose for the development of a trap for the QHPA. Then, in addition to the diffusion Gega trap, a diffusion trap termed bead Galatea, or Gabi was also proposed [20]. Here the Galatea-A trap was implied as the randomizing cell (Fig. 4a). The Gabi and Gega scales are commensurable.

At that time, in the early 90s, a decision was made to exemplify the advantages of Galateas by an extremely simple trap — a toroidal quadrupole — and to attempt to obtain a relatively high-energy plasma by a direct discharge, as was already done in the case of ESPL. Thus appeared multipole electric-discharge traps (EDTs): first, EDT-M ('Avos'ka') and then in 1998 the 'Octupole' trap. These are considered in Section 9, as are the experiments on a Galatea-A-type trap performed in the electric-discharge mode. All these experiments demonstrated the high efficiency of the Galateas with $\beta_0 = 1$.

In the early 90s, the Stellarator-Galatea and Galatea-Belt configurations were proposed (Fig. 4).

3. Myxines in the absence of plasma ($\beta = 0$)

3.1 The statics of myxines for $\beta = 0$

As a rule, the magnetic Galatea systems should be so designed that myxines remain in the equilibrium state even in the absence of plasma. Thus arise the simplest problems of the theory of Galateas — the statics of myxines and then their stability for $\beta = 0$.

We commence with the statics of perfectly conducting myxines. We need to solve the system of equations, which includes the equation for the irrotational magnetic field and the zero conditions on the forces and the torques acting on each of N myxines:

$$\Delta\phi = 0 \,, \tag{3.1a}$$

$$M_k \mathbf{g} + \frac{1}{c}\int_{V_k} \mathbf{j}\times\mathbf{H}\,\mathrm{d}V = 0 \,, \tag{3.1b}$$

$$\int_{V_k}\left(\rho_k \mathbf{g} + \frac{1}{c}\,\mathbf{j}\times\mathbf{H}\right)\times\mathbf{r}\,\mathrm{d}V = 0 \,. \tag{3.1c}$$

† GOL was proposed by G I Budker and D D Ryutov independently of the cited report and ESPL by V V Zhukov and A I Morozov.

Here ϕ is the scalar potential of the magnetic field, ρ_k is the density, and V_k the volume of the kth myxine. The equilibrium condition with respect to rotation (3.1c) is automatically fulfilled when the system is axially symmetric. Meanwhile the center-of-gravity equilibrium condition (3.1b) calls for special precautions. We illustrate this situation by two simple examples.

3.1.1 Galatea-A. If the trap axis is directed vertically (Fig. 4a), by action of gravity the myxine is displaced from the midplane by a distance ζ without breaking the symmetry. This shift is determined by Eqn (3.1b)

$$Mg = \frac{1}{c}\,2\pi R J_\mu H_r^{\mathrm{ex}}(R,\zeta) \,. \tag{3.2}$$

Here H_r^{ex} is the r-component of the 'external' field (the field of the mirror coils) and J_μ is the current traversing the myxine. If the myxine radius $R \ll L$, the distance between the magnetic mirrors, the magnetic field in the vicinity of the myxine can be described in the paraxial approximation [32]

$$\phi(r,z) = \int H_0(z)\,\mathrm{d}z - \frac{r^2}{4}\,H_0'(z) + \frac{r^4}{64}\,H_0''(z) + \ldots \tag{3.3}$$

Here $H_0(z)$ is the field in the system axis. From Eqn (3.3) it follows that

$$H_r = -\frac{rH_0'}{2} + \ldots \,, \tag{3.4a}$$

$$H_z = H_0 - \frac{r^2}{4}\,H_0'' + \ldots \tag{3.4b}$$

For simplicity of the following formulas we assume, putting $\zeta \ll L$, that

$$H_0(z) = H_{00}\left(1 + \frac{z^2}{b_1^2}\right) . \tag{3.5}$$

We substitute (3.5) and (3.4a) in Eqn (3.2) to obtain the shift:

$$\zeta = -\frac{Mgb_1^2 c}{2\pi R^2 H_{00}}\,\frac{1}{J_\mu} \equiv -\frac{A}{J_\mu} \,. \tag{3.6}$$

We take the parameter values not too far removed from reactor parameters and estimate the magnitude of ζ:

$$J_\mu = 5\times10^6~\mathrm{A}\,, \quad H_{00} = 10^4~\mathrm{Oe}\,, \quad b_1 = 6~\mathrm{m}\,,$$

$$R = 2~\mathrm{m}\,, \quad M_1 = \frac{M}{2\pi R} = 10~\mathrm{t~m^{-1}} \,. \tag{3.7}$$

The magnitude of M_1 was taken with allowance for the radiation shielding (see Section 3.5). Substituting (3.7) into Eqn (3.6) gives

$$\zeta \approx 36~\mathrm{cm} \,.$$

3.1.2 Quadrupole (Fig. 6a). Two myxines carrying current in one direction are known to be nonequilibrium and are forcefully attracted together for thermonuclear parameters. For example, for a myxine separation $2a = 2$ m and a current $J \sim 5\times10^6$ A traversing the myxine, the attracting force per unit length of the myxine is

$$F_1 \approx 250~\mathrm{t~m^{-1}} \,.$$

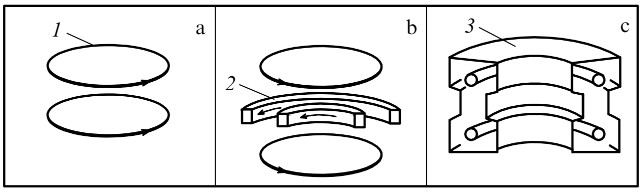

Figure 6. Mechanics of myxines in a quadrupole: (a) nonequilibrium system of two myxines *1*, (b) equilibrium but unstable system of myxines with rigidly supported locks *2*, (c) stable configuration of myxines in a transversely profiled superconducting case *3*.

Clearly the myxines should be 'relieved' with the aid of external magnetic fields. Such fields can be induced by one or several circular conductors. There are many versions. In essence, they reduce to inducing a quasiuniform field at the myxine surface whereby

$$\iint \frac{H^2}{8\pi} n_z^0 \, \mathrm{d}s = 0 \, .$$

Here n_z^0 is the z-component of the unit normal to the myxine surface. This can be attained by placing either rigidly fixed locks — 'stretchers' with current in the same direction as in the myxine or with current of the opposite direction — 'pushers' (Fig. 6b). In either case, the field inside the myxines is enhanced and the field outside is attenuated. To quantitatively illustrate the resulting situation avoiding cumbersome calculations, consider a quadrupole with a large aspect ratio $\alpha \equiv R/a \gg 1$, when the field of myxines and locks can be approximated by a field of straight lines. Assuming the locks to be pushing out, it is easily verified that the myxines will be in equilibrium with the proviso [7] that

$$\frac{J_\phi}{J_\mu} = \frac{a^2 + b^2}{4a^2} \, , \tag{3.8}$$

where b is the distance of the lock from the zero of the magnetic field.

Notice that the locks-pushers have the advantage of reducing the 'toroidal' effect, i.e. the radial displacement of the magnetic field zero for a finite aspect ratio. At the same time they reduce the working trap volume. We may readily check that the requisite configuration vanishes completely for $J_\phi \geqslant J_\mu$. So, in this case the force relief of myxines and the current compensation ($J_\phi = J_\mu$), which is important for the reduction of the toroidal effect, are incompatible. Clearly, in practice priority should be given to force relief. It is evident from the aforesaid that locks can impair the confinement ability of Galateas. Here we restrict the discussion to the two above examples. Several other examples of the statics of myxines for $\beta = 0$ are considered in Refs [33, 34]. For $\beta \neq 0$, the equilibrium of myxines will be discussed in Sections 6 and 8.

3.2 The stability of myxines for $\beta = 0$

Three major classes of problems on the stability of myxines for $\beta = 0$ are recognized: (i) determination of the instability increments developing in unstabilized but equilibrium myxine systems; (ii) development of active systems with feedback to suppress instabilities; (iii) development of self-stabilized systems with stable myxine positions.

The problems of the first class for Galatea-A and the quadrupole are considered in the next section. This simple type of Galatea is of practical interest at the initial stage of research when, on the one hand, the operation is not hindered by rigid myxine fixing and, on the other, the development of a superconducting complex is for some reason disadvantageous.

Systems with feedback were used in Galateas in the 60s and the 70s. The Yoshikawa spherator, which dates back to that time, with the specified myxine stabilization system is shown in Fig. 3a. But stabilization by feedback is hardly optimum for systems with $\beta_0 = 1$. This is caused by a strong field rearrangement on filling the trap with plasma, which is associated with a significant change of the forces acting on the myxines. Moreover, when the systems with feedback are operating, the magnetic field undergoes 'coarse' changes which may markedly affect the plasma confinement. Finally, such systems are, in a way, too 'technical' and are inevitably represented by cumbersome theoretical models. Therefore we do not dwell on them here and restrict the discussion to the self-stabilized magnetic systems of stationary Galateas. Considered below as universal stabilizing elements are superconducting screens — cases of fairly simple form. We emphasize immediately that we are concerned only with the fundamental aspects of the problem. The stabilizing role of the screen is clear from Fig. 6c depicting the quadrupole. We first introduce the fundamental scale for the angular oscillation frequency of screen-enclosed myxines — the levitation frequency. To do this, we consider the oscillation of a straight conductor with mass M_1 per unit length carrying a direct current J, which is placed above a perfectly superconducting plane. The following condition defines the height h_0 at which the conductor is in equilibrium:

$$M_1 g = \frac{2J_\mu^2}{2h_0 c^2} \, . \tag{3.9}$$

If the conductor is disturbed from equilibrium, its oscillations are described by the equation

$$M_1 \frac{\mathrm{d}^2 h}{\mathrm{d}t^2} = \frac{J_\mu^2}{hc^2} - M_1 g \, . \tag{3.10}$$

Linearizing (3.10) gives the usual equation for small-amplitude pendular oscillations

$$\frac{\mathrm{d}^2 \tilde{h}}{\mathrm{d}t^2} + \frac{g}{h_0} \tilde{h} = 0 \, , \qquad h = h_0 + \tilde{h} \, , \tag{3.11}$$

with the angular frequency of levitation oscillations equal [33] to

$$\Omega_J = \sqrt{\frac{g}{h_0}} = \sqrt{\frac{J_\mu^2}{c^2 M_1 h_0^2}} \, . \tag{3.12}$$

It will be seen below that this frequency, within a factor ~ 1, shows up in all systems with screens.

3.3 The dynamics of myxines in systems without stabilization

At the initial stage of experimental research on Galateas, unstable systems with a relatively small increment γ_F such that

$$S_F = \gamma_F \tau_E > 1 \tag{3.13}$$

may be of interest. Here τ_E is the characteristic plasma confinement time, e.g. with respect to energy. In addition to criterion (3.13) which characterizes the Galatea configuration lifetime, a role of practical importance is played by the parameter

$$S_J = \gamma_J \tau_E\,, \tag{3.14}$$

where γ_J is the damping decrement for the current in myxines, if they are made of conductors with a finite conductivity.

3.3.1 Deformation of a Galatea structure in the absence of screens. If the myxines can be regarded as perfect conductors, their dynamics in the general case are determined by the Lagrange function [2, 35]

$$\mathrm{L} = \sum_k \frac{MV_k^2}{2} + \sum_{k,\alpha,\beta} \frac{I_{k(\alpha,\beta)}\Omega_{k(\alpha)}\Omega_{k(\beta)}}{2} - \sum_k \frac{L_k J_k^2}{2c^2} - \sum_{i>k} \frac{M_{ik} J_i J_k}{c^2} - \sum_k \frac{1}{c}\,\Phi_k^e J_k\,. \tag{3.15}$$

Here $1 \leqslant k \leqslant N$ are the myxine numbers, L_k are the induction coefficients which we assume to be functions of the myxine coordinates q_k (q_k is the collection of the center-of-mass position and the orientation of the normal to the myxine plane $\mathbf{n}_k^0$), M_{ik} are mutual inductances dependent on all q_k and all $\mathbf{n}_k^0$, $\Phi_k^e(q_i, \mathbf{n}_i^0)$ are the magnetic fluxes of extraneous sources of magnetic field, $I^e_{k(\alpha,\beta)}$ are the components of the tensor of moment of inertia of the kth myxine, and $\Omega_{k(\alpha)}$ are the components of the angular velocity. Even in the axially symmetric case the system has a total of $5N$ geometric coordinates and $6N$ velocities. To this we should add N values of current in the myxines. Now we restrict ourselves to a simplified consideration of Galatea-A and a straight quadrupole with locks.

Myxine dynamics in Galatea-A. Here three kinds of shifts from equilibrium are possible: along the z-axis, the radial direction r, and the inclination of the myxine plane. Consider each perturbation separately, assuming them to be linear, and approximating the magnetic field of the supported mirror coils by formulas (3.4) and (3.5).

(1) In the linear approximation, the myxine motion along the z-axis is described by the equation

$$M_1 \frac{\mathrm{d}^2 z}{\mathrm{d}t^2} = -M_1 g + \frac{J_\mu}{c} H_r = -M_1 g + \frac{J_\mu}{c}(-R) H_{00} \frac{z}{b^2}\,. \tag{3.16}$$

Hence it follows that $z = \zeta + \tilde{z}$, with the expression (3.6) for ζ obtained above, and that the oscillations of $\tilde{z}$ proceed with the angular velocity

$$\omega_z = 2\sqrt{\frac{J_\mu R H_{00}}{cb^2 M_1}}\,. \tag{3.17}$$

With the data (3.7) we find $\omega_z \approx 8\ \mathrm{s}^{-1}$; hence the oscillation period ~ 1 s.

(2). The radial myxine shift ξ builds up exponentially in time, which is due to the radial dependence of H_z. The force acting on a myxine shifted, for definiteness, along the x-axis is

$$F = -\frac{RJ_\mu}{c} \int \cos\theta' H_z\big(r(\theta'), z\big)\,\mathrm{d}\theta'\,. \tag{3.18}$$

Here θ' is the polar angle whose vertex is at the center of the displaced myxine. To this angle corresponds the distance

$$r = \sqrt{\xi^2 + R^2 + 2R\xi\cos\theta'} \approx R + \xi\cos\theta'$$

to the trap axis. Substituting this quantity in expression (3.18), for H_z we obtain

$$H_z \approx H_0 - \frac{R^2 + 2R\xi\cos\theta'}{2} H_0'\,, \tag{3.19}$$

and, consequently,

$$F = \frac{RJ_\mu}{c}\,\xi R\pi H_0' = \frac{J_\mu H_{00}\pi R^2}{cb^2}\,\xi\,.$$

So, the radial shift is described by the equation

$$\frac{\mathrm{d}^2\xi}{\mathrm{d}t^2} - \frac{J_\mu H_{00} R}{2cM_1 b^2}\,\xi = 0\,. \tag{3.20}$$

Hence we find the growth increment ξ

$$\gamma_F = \sqrt{\frac{J_\mu H_{00} R}{2cM_1 b^2}} = \frac{\omega_z}{\sqrt{2}}\,. \tag{3.21}$$

We notice that this quantity is close to the angular frequency of oscillations in z. Clearly the radial shift can be stabilized if $H_0'(0) < 0$ but then the shift along the z-axis becomes unstable.

(3) The case of plane rotation is more complicated. Qualitatively, if in the vicinity of the $z = -\zeta$ plane for $r = R$ the magnetic force lines lie in the sphere to a good approximation, the orientation of the myxine plane is in indifferent equilibrium. If the magnetic surface in the region involved can be approximated by an ellipsoid flattened along the z-axis, the orientation of the myxine plane is stable. Conversely, if the approximating ellipsoid is extended, the orientation is unstable.

Myxine dynamics in a quadrupole with locks. A rigorous analysis of the dynamics of two toroidal myxines in a quadrupole system with locks involves a treatment of ten equations, the forces between the conductors appearing to be elliptic functions. This is an unwieldy procedure and therefore we restrict ourselves to a simple model by assuming that the myxine planes are not inclined while the aspect ratio is high. Then, with obvious reservations, we can consider the oscillations of two straight myxines in the presence of two straight locks (3.8). We denote the vector radii of the former by $\mathbf{r}_1$ and $\mathbf{r}_2$ while the latter by $\mathbf{x}_b$ and $(-\mathbf{x}_b)$ to write the following system of equations:

$$\begin{aligned}
M_1 \frac{\mathrm{d}^2\mathbf{r}_1}{\mathrm{d}t^2} &= \frac{2J_\mu J_\phi}{c^2}\,\frac{\mathbf{r}_1 - \mathbf{x}_b}{(\mathbf{r}_1 - \mathbf{x}_b)^2} + \frac{2J_\mu J_\phi}{c^2}\,\frac{\mathbf{r}_1 + \mathbf{x}_b}{(\mathbf{r}_1 + \mathbf{x}_b)^2} - \frac{2J_\mu^2}{c^2}\,\frac{\mathbf{r}_1 - \mathbf{r}_2}{(\mathbf{r}_1 - \mathbf{r}_2)^2}\,,\\
M_1 \frac{\mathrm{d}^2\mathbf{r}_2}{\mathrm{d}t^2} &= \frac{2J_\mu J_\phi}{c^2}\,\frac{\mathbf{r}_2 - \mathbf{x}_b}{(\mathbf{r}_2 - \mathbf{x}_b)^2} + \frac{2J_\mu J_\phi}{c^2}\,\frac{\mathbf{r}_2 + \mathbf{x}_b}{(\mathbf{r}_2 + \mathbf{x}_b)^2} - \frac{2J_\mu^2}{c^2}\,\frac{\mathbf{r}_2 - \mathbf{r}_1}{(\mathbf{r}_2 - \mathbf{r}_1)^2}\,.
\end{aligned} \tag{3.22}$$

Assuming the equilibrium condition (3.8) to be fulfilled and the currents traversing the conductors to be constant, in the linear approximation we obtain

$$M_1 \frac{d^2\xi_1}{dt^2} = \frac{4J_\mu J_\phi}{a^2+b^2}\,\xi_1 - \frac{2J_\mu^2}{c^2}\,\frac{\xi_1-\xi_2}{a^2+b^2}\,,$$

$$M_1 \frac{d^2\xi_2}{dt^2} = \frac{4J_\mu J_\phi}{a^2+b^2}\,\xi_2 - \frac{2J_\mu^2}{c^2}\,\frac{\xi_2-\xi_1}{a^2+b^2}\,. \tag{3.23}$$

Here $\xi_1 = \mathbf{r}_1 - a\mathbf{y}^0$ and $\xi_2 = \mathbf{r}_2 + a\mathbf{y}^0$; J_μ and J_ϕ are taken positive since their signs are accounted for by the signs of the terms in the right-hand side. Evidently, in the general case the myxine positions are unstable. Indeed, we add together Eqns (3.23) to obtain the equation of center-of-mass motion

$$M_1 \frac{d^2}{dt^2}(\xi_1+\xi_2) = \frac{4J_\mu J_\phi}{a^2+b^2}(\xi_1+\xi_2)\,. \tag{3.24}$$

Hence it is clear that accidental center-of-mass displacements grow in time with the increment

$$\gamma = \sqrt{\frac{4J_\mu J_\phi}{M_1(a^2+b^2)}}\,. \tag{3.25}$$

Obviously, the qualitative conclusion that the myxine center-of-mass positions are unstable would still stand for a finite aspect ratio.

3.4 The fall of myxines with a finite conductivity in Galatea-A

If the myxine in a vertically mounted Galatea-A is disconnected from the power supply, for a finite resistance R_Ω the current traversing the myxine decays gradually and the myxine falls down.

As it falls, the myxine cuts the external field and the changes of current obey the equation

$$J_\mu R_\Omega = -\frac{L}{c^2}\frac{dJ_\mu}{dt} + 2\pi R\,\frac{V_z H_r}{c}\,. \tag{3.26}$$

If the current decays sufficiently slowly, the myxine position can be treated as quasi-equilibrium. Then, from Eqn (3.6)

$$V_z \approx \frac{d\zeta}{dt} = \frac{cMgb_1^2}{H_{00}2\pi R^2}\,\frac{d}{dt}\,\frac{1}{J_\mu} \equiv -\frac{a}{J_\mu^2}\,\frac{dJ_\mu}{dt}\,,$$

$$a \equiv \frac{cMgb_1^2}{H_{00}2\pi R^2}\,, \qquad J_\mu < 0\,. \tag{3.27}$$

With (3.4), we have

$$H_r(\zeta, R) = -\frac{RH_0'(\zeta)}{2} = -RH_{00}\,\frac{\zeta}{b_1^2}$$

$$= -\frac{RH_{00}}{b_1^2}\,\frac{a}{J_\mu} = -\frac{cMg}{2\pi R}\,\frac{1}{J_\mu}\,. \tag{3.28}$$

The following equation results for the decay of the current carried by the myxine:

$$\frac{L}{c^2}\frac{dJ_\mu}{dt}\left(1 - \frac{c^2}{L}\,\frac{aMg}{J_\mu^3}\right) + R_\Omega J_\mu = 0\,. \tag{3.29}$$

Evidently, owing to the fall of myxines in the field of magnetic mirrors, instead of the conventional induction coefficient L there appears an effective one

$$L_{\text{eff}} = L + \frac{c^3(Mg)^2 b_1^2}{H_{00}2\pi R^2}\,\frac{1}{|J_\mu|^3} = L\left(1 + \frac{Mg|\zeta|8\pi}{LH_J^2R^2}\,\frac{\pi}{2}\right),$$

$$H_J \equiv \frac{2\pi J_\mu}{cR}\,. \tag{3.30}$$

Putting $L = 2\pi R\theta$, where $\theta \sim 1$, we obtain a sufficiently descriptive expression

$$L_{\text{eff}} = L\left(1 + \frac{Mg|\zeta|}{W_J}\right), \tag{3.31}$$

where

$$W_J = \frac{H_J^2}{8\pi}\,4\theta R^3$$

is the energy scale of the magnetic field induced by the current through the myxine.

Equation (3.29) is readily integrated:

$$-\frac{R_\Omega c^2}{L}\,t = \ln\frac{J_\mu}{J_0} + \frac{c^2 aMg}{3L}\left(\frac{1}{J_\mu^3} - \frac{1}{J_0^3}\right). \tag{3.32}$$

While the conventional induction coefficient plays an important part at the initial stage of current decay, the induced one does so late in the process. In this case, the current decays not exponentially but by the law

$$J_\mu(t) \approx J_0\left(\frac{1}{1+At}\right)^{1/3}, \qquad A \equiv \frac{3R_\Omega}{Mga}\,, \tag{3.33}$$

where J_0 is the initial current in the myxine. If time is expressed in terms of the dimensionless quantity $\tau = (c^2R_\Omega/L)t$, as is clear from Eqn (3.32) the J/J_0 ratio is a function of τ and the dimensionless parameter

$$\varkappa \equiv \frac{c^2 aMg}{3L|J_0|^3}\,. \tag{3.34}$$

3.5 The dynamics of ideal myxines inside superconducting screens

The oscillations of perfectly conducting myxines in a vacuum volume surrounded by a superconducting screen reduces to the solution of Eqn (3.1) with the boundary condition $H_n = 0$ at the screen surface. As a rule, the calculation of 3-D fields and the inclusion of their impact on the myxine dynamics are required. In the general case this problem can well be solved by the existing codes and computers. Meanwhile, it is instructive to have relatively simple analytical models, even though they provide a coarse approximation to the reality. Certain of the methods of analytical treatment of this problem are considered in Refs [33, 34]. We outline one of them.

A simple technique for calculating myxine oscillation models termed the 'hose' approximation was proposed in Ref. [33]. This approximation rests on the two assumptions: (i) the screen is a toroidal tube with a large aspect ratio, i.e. $\alpha = R/a \gg 1$; (ii) the minor cross section of the torus is a circle. When these conditions are met, any portion of the torus as long as several minor diameters can be regarded as a straight cylinder while the portion of the myxine inside it as a straight conductor drawing a current directed along the axis of the straight cylinder. Since the screen is assumed to be perfectly conducting, the magnetic field near an arbitrary point P lying in the torus axis can be represented as the field of two currents, viz. the conductor itself carrying current J and its image with current $-J$ located at a distance

$$\boldsymbol{\rho} = \frac{a^2}{\xi^2}\,\boldsymbol{\xi} \tag{3.35}$$

from the center of the tube cross section. Here a is the minor torus radius.

Now we can write the general expression for the force acting on a myxine element ds located inside the toroidal screen†. The radius vector of this element can be written as $\mathbf{r}(\theta) = \mathbf{r}_0(\theta) + \boldsymbol{\xi}(\theta, t)$, where parameter θ determines the point in the axial line of the torus corresponding to the position of the element of interest in the absence of a shift ($\boldsymbol{\xi} = 0$).

Clearly the force exerted by the myxine image on the element involved is

$$\mathrm{d}\mathbf{F} = -\frac{2J_\mu}{c^2}\,\frac{\boldsymbol{\xi}_\perp}{a^2 - \xi_\perp^2}\,\mathrm{d}s\,. \tag{3.36}$$

Here $\boldsymbol{\xi}_\perp$ is the shift component normal to the torus median line. Integration of (3.36) gives the expression for the force acting on the entire myxine,

$$\mathbf{F} = -\frac{2J_\mu^2}{c^2}\int_\theta \mathrm{d}s\,\frac{\boldsymbol{\xi}_\perp}{a^2(\theta) - \xi_\perp^2}\,. \tag{3.37}$$

Here $\boldsymbol{\xi}_\perp = \boldsymbol{\xi} - \boldsymbol{\tau}_0(\boldsymbol{\xi}, \boldsymbol{\tau}_0)$ and $\boldsymbol{\tau}_0 = \mathrm{d}\mathbf{r}_0/\mathrm{d}s$ is the unit vector tangent to the hose axis.

A similar formula can be derived for the torque acting on the myxine and causing its plane to oscillate.

We highlight three specific examples of the use of formula (3.37) to calculate the oscillations of conductors inside superconducting screens.

Straight current-carrying line in a straight tube. In this case from (3.36) follows

$$M_1\,\frac{\mathrm{d}^2\boldsymbol{\xi}}{\mathrm{d}t^2} + \frac{2J_\mu}{c^2}\,\frac{\boldsymbol{\xi}}{a^2 - \xi^2} = 0\,.$$

If $|\boldsymbol{\xi}| \ll a$, harmonic oscillations occur with the levitation frequency

$$\Omega = \sqrt{\frac{2J_\mu^2}{c^2 M_1 a^2}}\,. \tag{3.38}$$

This expression differs from the frequency defined by formula (3.12) by a factor ~ 1.

An annular myxine in a torus of circular section. Let the major radius R_μ of the myxine torus be equal to the median torus radius R_0. If the myxine shifts along the z-axis conserving the orientation of the plane, the oscillation frequency will be given by Eqn (3.38) as before. If the myxine shifts along the x-axis, i.e. remaining in the $z = 0$ plane, the oscillation frequency will decrease by the factor $\sqrt{2}$ and be equal to

$$\Omega^* = \sqrt{\frac{J_\mu^2}{c^2 a^2 M_1}}\,. \tag{3.39}$$

† In principle, it is not necessary that the axial line of the screen be a circle in the reasoning conducted.

Oscillations of two myxines of different radius with current in one direction, lying in one plane (the 'Dublon' configuration), and located inside a toroidal screen with minor radius *a*. In this case, two factors compete: on the one hand, the myxines tend to 'stick together' owing to the attraction of the currents flowing in one direction but, on the other, they are repelled from the screen. The analysis of linear oscillations of such a system conducted in Ref. [33] revealed that the configuration is stable if the ring separation

$$\Delta = R_2 - R_1 \geqslant a\,,$$

but unstable in the opposite case.

3.6 Parameters of a myxine designed for a reactor

To be clear in one's mind what the Galatea reactors may look like, it is instructive to estimate the design parameters of a myxine in the context of a reactor. These parameters were first estimated in Ref. [36]. The estimates yielded reasonable values but were not too well substantiated. Therefore we present the results of Ref. [37] in which the myxine radiation dynamics were neatly calculated on the basis of the ITER code [38].

The calculations were performed for a demonstration reactor with an operating cycle of 1000 s. In doing so it was assumed that a neutron flux with intensity $P_1 = 1$ MW m^{-2} is incident on the myxine surface and that a Nb_3Sn-based composite is employed as the superconductor. The major objective of the calculations was to choose the shielding parameters in such a way as to provide the superconducting state for 1000 s for relatively modest dimensions. Since the operating cycle is limited to a short period, a three-region radiation-accumulative myxine design was proposed. The outer (red) region should intercept $\geqslant 95\%$ of the energy incident on the myxine. In a time $\leqslant 100$ s, this region inevitably will be heated up to a temperature $\geqslant 1700$ K and will begin to release the major part of the incident energy in the form of thermal radiation. In the optimized model this region is made of tungsten, which not only ensures its resistance to high temperature, but notably reduces the inward radiation flux owing to the high (60%) fusion-neutron albedo as well.

The next (gray) region operates in the accumulative mode, i.e. it does not release heat anywhere but is continuously heated by the radiation throughout the operating cycle. In consequence, $\sim 10^{-5}$ of the energy incident on the myxine surface throughout the operating time reaches the cryoregion (blue region) located at the myxine center. The cryoregion, too, operates in the accumulative mode. Selected as the coolant in Ref. [38] was a hydrogen sludge (at a melting temperature of hydrogen of 14 K) containing equal volumes of liquid and solid phases. The energy penetrating the cryoregion goes first to melt the ice and later to heat the liquid hydrogen to its vaporization temperature (~ 17 K for atmospheric pressure).

Next, the regions were assumed to be separated from each other by a multilayer vacuum-screen insulation and, in a few places, held together by firm, relatively low-section heat insulators.

Several versions of the 15-layer shielding were calculated in the context of the above configuration, with the additional conditions that the myxine's magnetic sheath thickness was 50 cm and $H = 10^4$ Oe at its external boundary. The optimization goal was to lower the myxine price and minimize its dimensions, the layer thicknesses serving as the optimization parameters. One of the best compositions thus found is given in Table 2.

Table 2.

Layer thickness, cm	Material	Absorbed energy density, W cm^{-3}
15	Hydrogen sludge	1.82×10^{-3}
5	Nb_3Sn	8.39×10^{-3}
5	Hydrogen sludge	2.11×10^{-3}
5	Water	3.97×10^{-3}
5	Stainless steel	1.56×10^{-2}
5	Stainless steel	3.02×10^{-2}
5	Stainless steel	1.06×10^{-1}
5	Water	4.52×10^{-2}
5	Stainless steel	1.67×10^{-1}
5	Stainless steel	2.63×10^{-1}
5	Stainless steel	8.38×10^{-1}
5	Water	4.30×10^{-1}
5	Tungsten	2.08×10^{0}
5	Tungsten	2.35×10^{0}
5	Tungsten	5.38×10^{0}

Its integral characteristics per linear meter are as follows: external diameter 1.7 m, mass 27 t m^{-1}, current in the superconducting chord ($j_{\mathrm{SP}} = 1.2 \times 10^4$ A cm^{-2}) $J_\mu \sim 6.6$ MA, transverse magnetic field to support the myxine $H_\perp = 400$ Oe.

The myxine operation scenario is simple. Prior to the operating cycle the myxine rests on the supports with tubes for the coolant, its regions are properly cooled, and the required field is induced in the superconducting chord. Then the transverse magnetic field $H_\perp$ begins to build up and raises the myxine to the operating position. On completion of the operating cycle, the myxine goes down to rest on the same supports, which contain cooling systems and power sources inside, and the cycle is repeated.

4. Magnetic sheaths of myxines

By a magnetic sheath of myxines (MSM) is meant a domain with field and plasma, which is bounded by the solid myxine surface on one side and by the separatrix of the magnetic field on the other. Clearly there are two characteristic situations: either a portion of the separatrix borders on a volume without a field or the entire separatrix is contiguous with a strong magnetic field. An open MSM will be referred to in the former case and a closed one in the latter.

Consider the equilibrium, the stability, and the heat transfer only in an open MSM assuming in addition that the MSM radius $b_\mu < R_\mu$, where R_μ is the major myxine radius.

The pattern of the processes in a MSM differs notably from that in the vicinity of the first wall of a tokamak or a stellarator. This is related to the two circumstances: the increase in the field strength in the MSM as the myxine is approached, which efficiently provides the hydrodynamic plasma stability, and the absence of the diverting layer to intercept the impurities going from a solid surface to the principal plasma volume†.

Here we restrict ourselves to hydrodynamic MSM models and the inclusion of the simple convective Rosenbluth–Longmire–Kadomtsev instability (RLK). This restriction arises primarily from the fact that the problems of kinetics and sophisticated instabilities are, as a rule, completely reconsidered after experiments, as indicated by a wealth of experiments on plasma systems and, mostly, traps for the CNF. Therefore such *a priori* models are of little significance. Nevertheless, below we give the familiar references to the papers relevant to this topic but not touched upon in this review.

† In the future, one might expect the development of myxines enclosed by magnetic layers to capture impurities and direct them inside the myxine.

4.1 Plasma equilibrium in an MSM

The fundamental feature of an MSM plasma configuration is the existence of a temperature difference between its external boundary and the myxine surface. In consequence, a current is maintained in the MSM owing to thermal diffusion, which causes the pressure to decrease towards the myxine surface. Even though this fact was noted by A D Sakharov [8], we present its derivation here because we are concerned with its generalizations, too.

Simplest is the case of axial symmetry and a single poloidal magnetic field. We will restrict ourselves to this case because it holds the greatest interest for us.

Assuming the plasma to be quasistatic, we have two equations of motion [39]

$$\frac{\nabla P_{\mathrm{i}}}{en} = \mathbf{E} + \frac{1}{c}[\mathbf{V}_{\mathrm{i}}\mathbf{H}] + \mathbf{R}\,,$$
$$-\frac{\nabla P_{\mathrm{e}}}{en} = \mathbf{E} + \frac{1}{c}[\mathbf{V}_{\mathrm{e}}\mathbf{H}] - \mathbf{R}\,, \tag{4.1}$$

where

$$\mathbf{R} = \left(\frac{\mathbf{j}_\parallel}{\sigma_\parallel} + \frac{\mathbf{j}_\perp}{\sigma_\perp}\right) - 0{,}71\, n\nabla_\parallel kT_{\mathrm{e}} - \frac{3}{2}\frac{n}{\omega_{\mathrm{e}}\tau_{\mathrm{e}}}\frac{[\mathbf{H}, \nabla kT_{\mathrm{e}}]}{H}\,. \tag{4.2}$$

Directing the x-axis normal to the magnetic surfaces, the y-axis along the symmetry (azimuth) direction, and the z-axis along $\mathbf{H}$, we obtain the y-component of the second equation of (4.1) in the form

$$\frac{j_y}{\sigma} = \frac{3}{2}\frac{n}{\omega_{\mathrm{e}}\tau_{\mathrm{e}}}\frac{\partial}{\partial x}kT_{\mathrm{e}}\,. \tag{4.3}$$

We took into account that $\partial P_{\mathrm{e}}/\partial y = 0$, $E_y = 0$, and $V_{\mathrm{e}x} = 0$. Substituting (4.3) in the MHD equilibrium equation

$$\nabla P = \frac{1}{c}[\mathbf{j}, \mathbf{H}]\,,$$

which follows from (4.1), we get

$$\frac{\partial}{\partial x}n(T_{\mathrm{i}} + T_{\mathrm{e}}) = \frac{3}{2}n\frac{\partial T_{\mathrm{e}}}{\partial x}\,. \tag{4.4}$$

If it is assumed that $T_{\mathrm{i}} = T_{\mathrm{e}} = T$, we have [8]

$$nT^{1/4} = \theta_m = \mathrm{const}\,. \tag{4.5}$$

Putting at the outer MSM surface $n_0 = 10^{14}$ cm^{-3} and $T_0 = 10$ keV, for a plasma temperature $T_1 = 1$ eV near the myxine surface we have the plasma density $n_\mu = 10^{15}$ cm^{-3}.

However, in the general case $T_{\mathrm{i}} \neq T_{\mathrm{e}}$, and if it is assumed that $T_{\mathrm{e}}/T_{\mathrm{i}} = \omega = \mathrm{const}$, instead of (4.5) we obtain

$$nT^{(1-\omega/2)/(1+\omega)} = \mathrm{const}\,. \tag{4.6}$$

Hence, in the case of cold electrons ($\omega = 0$)

$$P = \mathrm{const}\,. \tag{4.7}$$

If the electron temperature increases, the T-dependence of the plasma density becomes progressively weaker and for $\omega = 2$ vanishes completely. For $\omega > 2$ the dependence of n on T_i qualitatively changes its manner.

We make two remarks to conclude: (i) in the derivation of formulas (4.5) and (4.6) it was assumed that electrons do not cut the magnetic surfaces. However, in Section 9 the traps in 'electric-discharge' modes are considered. In this case $V_{ex} \neq 0$ and, accordingly, formulas (4.4) – (4.6) break down; (ii) under the MSM conditions, the relationship between n and T just obtained automatically provides the stability of the magneto-plasma configuration with respect to hydrodynamic convection. This is evident from the RLK stability criterion

$$\frac{\partial}{\partial \Psi} PU^{\gamma} \geqslant 0\,, \tag{4.8}$$

where $U = \int H^{-1}\,\mathrm{d}l$ is the specific volume of the magnetic force tube and Ψ is measured from the myxine surface. Inequality (4.8) is the condition for the increase of the entropy of a unit mass of plasma with distance away from the myxine.

For an estimate, we take the field of a straight conductor to obtain

$$U \propto \frac{c}{2J_{\mu}}\,\frac{r^2}{2}\,. \tag{4.9}$$

Combining (4.8) and (4.9), for $\gamma = 5/3$ we obtain

$$\frac{\partial}{\partial r}\, T^{3/4} r^{10/3} > 0\,. \tag{4.10}$$

This condition is knowingly fulfilled with a reserve since T increases with distance from the myxine.

4.2 Thermal conduction in an MSM

The classical thermal conduction in MSM was considered in Ref. [40]. We outline the major results of this work.

The complete set of equations for an axially symmetric MSM configuration is of the form [39]

$$\Delta^* \Psi = -\frac{\mathrm{d}P(\Psi)}{\mathrm{d}\Psi}\,, \tag{4.11a}$$

$$T_i = T_i(\Psi)\,, \qquad T_e = T_e(\Psi)\,, \tag{4.11b}$$

$$\mathrm{div}\,\varkappa_{i\perp} \nabla T_i = Q_i\,, \tag{4.11c}$$

$$\mathrm{div}\,\varkappa_{e\perp} \nabla T_e = Q_e - \frac{j_\theta^2}{\sigma} + S\,, \tag{4.11d}$$

$$\frac{j_\theta}{\sigma} = \frac{3}{2}\,\frac{1}{e\omega_e \tau_e}\left[\frac{\mathbf{H}}{H}\,, \nabla k T_e\right]_\theta\,. \tag{4.11e}$$

Here

$$\varkappa_{i\perp} = \frac{2nkT_i}{M\omega_i^2 \tau_i}\,, \qquad \varkappa_{e\perp} = 4{,}66\,\frac{nkT_i}{m\omega_e^2 \tau_e}\,,$$

$$\tau_i = \frac{3}{4}\sqrt{\pi}\,\frac{\sqrt{M}}{\Lambda e^4}\,\frac{(kT_i)^{3/2}}{n}\,, \qquad \tau_e = \frac{3}{4}\sqrt{\pi}\,\frac{\sqrt{m}}{\Lambda e^4}\,\frac{(kT_e)^{3/2}}{n}\,, \tag{4.12}$$

Λ is the Coulomb logarithm, and the quantities Q_i and Q_e respectively are

$$Q_i = \frac{3m}{M}\,\frac{nk}{\tau_e}(T_e - T_i)\,,$$

$$Q_e = -Q_i - \alpha n^2 \sqrt{kT_e}\,, \qquad \alpha = \mathrm{const}\,.$$

The last term in Q_e allows for bremsstrahlung radiation.

System (4.11) is very complex. However, regarding our calculations as an estimate, it is easily verified that in the first approximation the magnetic field can be viewed as a vacuum field, the ohmic heating and the electron heat transfer can be neglected, and the temperatures of ions and electrons can be taken to be equal. In consequence, the problem reduces to the solution of one equation

$$\mathrm{div}(\varkappa_\perp \nabla T) = \alpha n^2 \sqrt{T}\,. \tag{4.13}$$

In view of Eqn (4.5), it can be written as

$$\mathrm{div}(\varkappa_\perp \nabla T) = \alpha \theta^2\,. \tag{4.14}$$

4.2.1. Plane model. First consider the plane model, when n and T are functions of the Cartesian x-coordinate and the magnetic field $H = \mathrm{const}$. The characteristic dimensional parameter determining the solutions of Eqn (4.14) is the quantity A_*:

$$A_*^2 = \frac{8\sqrt{\pi}\,\Lambda e^2 c^2}{3\alpha}\,\sqrt{M}\,. \tag{4.15}$$

Then

$$\varkappa_{i\perp} = \frac{A_*^2 \alpha \theta^2}{H^2 T}\,. \tag{4.16}$$

For a deuterium plasma,

$$A_* \approx 5 \times 10^5\ \mathrm{Oe\ cm}\,. \tag{4.17}$$

With this parameter Eqn (4.14) in the one-dimensional case can be written as

$$\frac{\mathrm{d}^2}{\mathrm{d}x^2} \ln T = \frac{H^2}{A_*^2} \equiv \frac{1}{L_*^2}\,. \tag{4.18}$$

Hence it follows that

$$\frac{T}{T_1} = \left(\frac{T_1}{T_0}\right)^{x/L} \exp\left(\frac{x^2 - Lx}{2L_*^2}\right). \tag{4.19}$$

It is assumed that the temperature is equal to T_0 at the boundary with the plasma volume and to T_1 at the myxine surface ($x = L$).

For arbitrary T_0 and T_1, the resulting dependence $T(x)$ turns out to be nonmonotonic and has a minimum for

$$x_{\min} = \frac{L}{2} - \frac{L_*^2}{L} \ln \frac{T_1}{T_0}\,.$$

Naturally, we are concerned with the mode wherein the heat flows only in one direction, viz. towards the myxine. The inequality $x_{\min} \geqslant L$ should therefore be fulfilled. Assuming the MSM thickness to be $L = x_{\min}$, we obtain the relationship between L and T_1/T_0:

$$\ln\frac{T_0}{T_1} = \frac{L^2}{2L_*^2}\,.$$

This formula is used to obtain L, putting $T_0 = 10^4$ eV, $T_1 = 10$ eV, $H = 10^4$ Oe and taking the value of (4.17) for A_*. Then

$$L = \frac{A_*}{H}\sqrt{2\ln\frac{T_0}{T_1}} \approx 190\ \text{cm}\,. \tag{4.20}$$

This is a relatively large value, which has evidently been overrated because the magnetic field value taken here is minimum for a reactor and the quasicylindrical field geometry in the vicinity of the myxine is not taken into account. Moreover, in real plasmas a certain amount of impurities with $Z > 1$ (e.g. α-particles) are always present to notably decrease A_* and, consequently, L.

4.2.2. Axisymmetric case. In the axially symmetric case equation (4.14) can be integrated along the force lines ($\Psi = \text{const}$) to give the equation for the temperature

$$\frac{\mathrm{d}}{\mathrm{d}\Psi}\left(\frac{1}{T}\frac{\mathrm{d}T}{\mathrm{d}\Psi}\oint r^2\,\frac{\mathrm{d}l}{H}\right) = \frac{1}{A^2}\oint\frac{\mathrm{d}l}{H}\,. \tag{4.21}$$

This equation can be integrated in the general form in quadratures

$$T = T_0\exp\left[-c\int_{\Psi_0}^{\Psi}\left(\oint r^2\,\frac{\mathrm{d}l}{H}\right)^{-1}\mathrm{d}\Psi + \frac{1}{A_*^2}\int_{\Psi_0}^{\Psi}\mathrm{d}\Psi\left(r^2\,\frac{\mathrm{d}l}{H}\right)^{-1}\int_{\Psi_0}^{\Psi}\mathrm{d}\Psi\oint\frac{\mathrm{d}l}{H}\right]. \tag{4.22}$$

A specific calculation using formula (4.22) for a reactor on D^3He was considered in Ref. [40]. As shown in the paper, for $n_0 = 4\times10^{14}$ cm^{-3}, $T_0 = 50$ keV, $H_0 = 40$ kOe, $T_0/T_1 = 10^4$, $\Lambda = 20$, and the MSM thickness $L = 70$ cm, the thermal flux vanishes at a distance of 50 cm from the myxine surface.

So, in the region between $x_{\min}$ and L a cold plasma occurs with specific features of its own, which we do not consider here.

To conclude, estimates of the synchrotron radiation flux at the myxine reveal that its intensity is low [40].

The equilibrium and the heat transfer in the MSM was considered in the context of a kinetic model in Refs [41, 42].

4.3 The MSM thickness

The actual MSM thickness will be determined by many factors: the flows of charged particles at the myxine surface, the thermal plasma conductivity in the MSM, the design considerations, the dynamics of impurities proceeding from the myxine surface etc. Here we highlight two criteria.

Heat transfer length. As shown earlier, for an MSM thickness $L \sim 1$ m the classical heat flux transferred by particles is 'depleted' by 'pure' bremsstrahlung alone. If it is considered that the bremsstrahlung power is proportional to Z^2, there is little doubt that $L_{\text{MSM}} \sim 1$ m is sufficient to suppress the heat transfer to the myxine surface.

Shielding from fast charged reaction products. The necessity of shielding is compelling. As a case in point, consider the D-T reaction. The resulting α-particles have energies ~ 4 MeV. Considering that they are decelerated by electrons, which is not attended by strong scattering, about two Larmor circles (deformed owing to the nonuniformity of the magnetic field) can be adopted as the natural MSM shielding thickness. The Larmor radius of an α-particle in the field $H_0 = 10^4$ Oe is $\rho_\alpha \approx 40$ cm. In accordance with the thickness of the radiation myxine shielding ($b_\mu \sim 80$ cm) stated in Section 3.6, we can assume that $H_1 \sim 20$ kOe near the myxine surface. So, by this criterion, too, the MSM thickness can be taken to be $L_{\text{MSM}} \sim 1$ m. It is not improbable that the actual MSM thickness will prove to be of the order of ~ 0.5 m.

4.4 The 'Dipole' Galatea trap

Previously, myxines were spoken of as elements of complex magnetic systems. However, a single myxine in an 'infinite' space, too, can be a plasma trap. Such traps are, in particular, planetary magnetospheres with their radiation belts. In this case the plasma confinement owes its stability to the fulfillment of the entropy growth criterion (4.8) when moving to the periphery. It was precisely these astrophysical considerations that prompted A. Hasegawa to come up with the idea of a myxine trap, which was termed 'Dipole' [18]. Subsequently, a relatively large number of theoretical papers were devoted to it [43–45]. This trap is conceptually some extreme version of the Galatea-A depicted in Fig. 4a.

Under laboratory conditions, the dimensions of the region occupied by the magnetic field are limited by the values n_Γ and T_Γ at the external field boundary or, more precisely, by the difference in the specific volume of the magnetic force tube from U_Γ at the external boundary to U_0 in the region of maximum parameters

$$U_\Gamma^\gamma \geqslant \frac{P_0 U_0^\gamma}{P_\Gamma}\,. \tag{4.23}$$

If it is considered that the P_0/P_Γ ratio should be at the level $\sim 10^7 - 10^8$ and that

$$U_\Gamma \propto x_\Gamma^4\,, \qquad U_0 \propto R_\mu^4\,, \tag{4.24}$$

we obtain

$$x_\Gamma \propto 10R_\mu\,. \tag{4.25}$$

Here x_Γ is the external radius of the field boundary for $z = 0$. It was precisely this scale x_Γ that was indicated in Ref. [44] in which the authors considered the configuration of a possible fusion reactor. The diameter of the region occupied by the field was estimated at 60 m. For details, the reader is referred to the cited papers considering at greater length the processes, schematic reactor designs, and a rocket propulsion system based around a 'Dipole' trap [45]. Here we only highlight the configuration of a laboratory model of this Galatea [46], which is contemplated for construction in the foreseeable future (Fig. 7). The parameters of this facility are as follows: current drawn by the myxine is 1.24 MA, the myxine radius 0.34 m, the high-energy plasma volume 0.2 m^3, the total plasma volume 15 m^3, the (equilibrium) temperature 1 keV, the hot-electron temperature 250 keV, the plasma density 10^{13} cm^{-3}, and the parameter $\beta \sim 10\%$. The plasma will be produced through electron heating by microwave techniques.

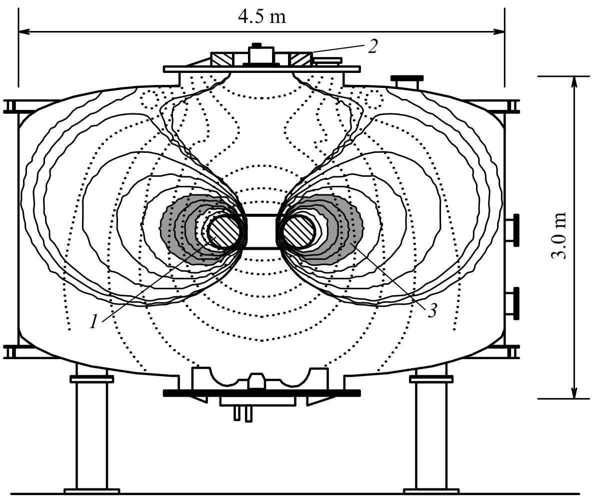

Figure 7. Schematic of a laboratory model of the 'Dipole' Galatea trap: *1* — levitating ring (1.24 MA), *2* — supporting coil (0.3 MA), *3* — hot-electron plasma.

4.5 MicroGalateas, or myxine probes

The feasibility of employing current-carrying rings as carriers of diagnostic tools to probe the interior of large plasma volumes, e.g. large tokamaks, was considered in a series of papers [47–49]. These rings were termed 'microGalateas' despite the fact that the term 'myxine probe' (MP) used hereafter is more adequate. Below we consider three groups of issues: (i) the features of myxine probe operation in a plasma volume; (ii) thermomagnetic processes when employing a ring made of a finite-conductivity material, (iii) perturbation of the structure of the tokamak magnetic field by the myxine probe field.

Bearing in mind the MP injection into a tokamak it would be reasonable to employ a diamagnetic orientation of the MP with respect to external field H_0 in order to minimize the dimensions of the perturbation region, which is assumed in the subsequent discussion (Fig. 8a).

4.5.1. Some estimates. The minimum magnitude of the current through the MP required for magnetic shielding from the plasma is close to $J_{\min} = (5/\pi)H_0 a$, where a is the major radius of the ring. Putting the medium diameter of the ring section $b = (2/3)a$, we find the characteristic current density $j_{\min} \approx 5H_0 a$. So, even for $H_0 = 15$ kOe and $a = 3$ cm this density $j_{\min} \approx 25$ kA cm^{-2} notably exceeds that typical of 'cold' superconductors (~ 10 kA cm^{-2}). That is why we will be oriented to cooled copper as the conductor, with the external field $H_0 \sim 15$ kOe, and $a \sim 2-3$ cm.

Let the MP-enclosing separatrix be a sphere of radius r_s, b_z be the z-dimension of the ring equal to $2b$, and $a = 2$ cm. The plasma configuration near the MP may be considered as being stable because the specific volume of magnetic force tubes decreases rapidly as the MP surface is approached. Assuming the transfer to be classical and $\omega_e \tau_e \to \infty$, we find the density of the heat flux towards the MP surface [47]†

$$q = -nD\,\frac{\partial T_i}{\partial \nu}\,, \qquad D = \frac{\rho_{iH}^2}{t_i}\,. \tag{4.26}$$

† Taking into account the estimative nature of the accompanying calculation, we do not consider the surface layer structure.

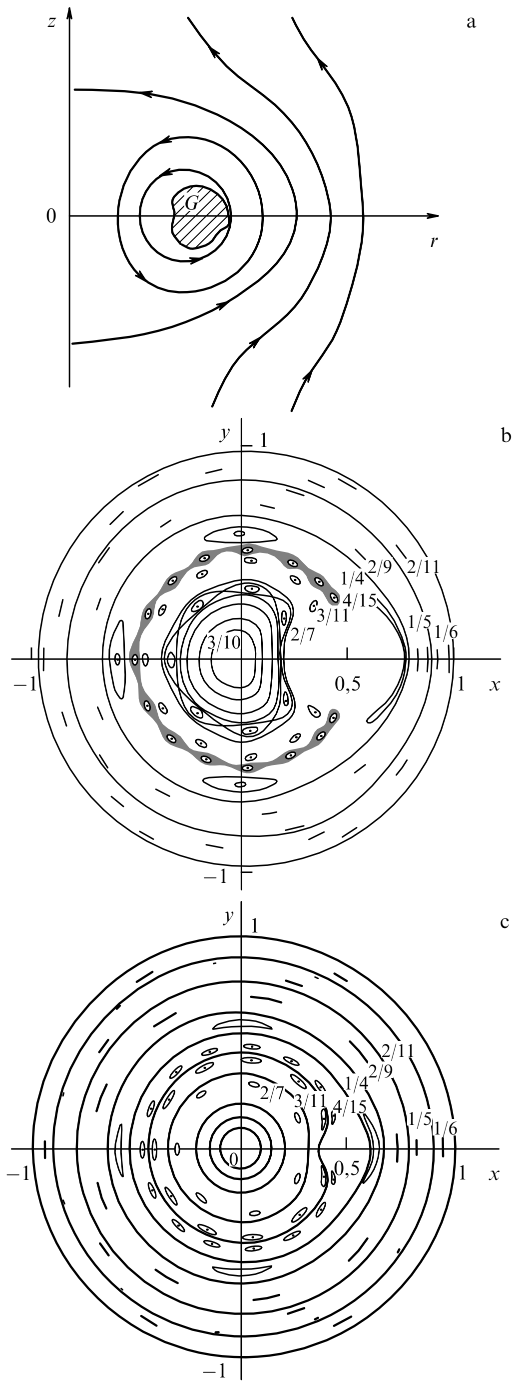

Figure 8. Myxine probe: (a) initial magnetic configuration near the myxine probe, (b), (c) perturbation of the magnetic surfaces of the quasitoroidal tokamak magnetic field.

Here ν is the normal to the surface and t_i is a quantity of the order of the ion–ion collision time. Assuming the parameter differences across the shielding layer l to be constant, we can write

$$q = kT_i n\,\frac{D}{l}\,. \tag{4.27}$$

In experimental conditions ($H_0 = 10^4$ Oe, $T_i = T_e = 10^2$ eV, $l = 1$ cm, $n = 10^{13}$ cm^{-3}) we have $q \approx 0.5 \times 10^5$ erg cm^{-2}.

So, during the MP time of flight through the plasma volume ($\tau_f \sim 0.1$ s), about $Q = q\tau_f \approx 1.5 \times 10^{-3}$ J will be released per 1 cm^2 of the surface, which is nearly 10^6 times smaller than is required to initiate noticeable material evaporation. Thus it is possible to do without the magnetic shielding at all. However, this possibility is of little interest for 'reactor' applications of MPs.

It is advantageous to freeze the field in an MP in the uniform external magnetic field. In consequence, both inside the ring and in the volume the field will have the same value $H_1 \sim (1.5-2)H_0$. Upon entry into the tokamak field, the intrinsic field 'blankets' the MP, moving the external field away. The disruption of the frozen-in field begins at the outer side of the ring and passes two stages: first the current penetrates into the volume of the ring and then the current in the ring decays. As shown in Ref. [47], the total current decay time at the first and second stages is $\tau_J \sim 0.5$ s.

So, the estimates suggest that it is possible to develop magnetically isolated autonomous probes (MPs) around cooled copper. In the future, the use of superconductors will dramatically simplify the preparation of MPs. Clearly, mastering the MP technology will open up new avenues for the operation of large-scale plasma volumes.

4.5.2. Thermomagnetic processes in a ring with finite conductivity. Consider the mathematical model of the following physical process [48]. A conducting ring with a toroidal magnetic field is placed in a uniform external magnetic field parallel to the ring axis. The current induces a poloidal field which encloses the ring and is separated from the external field by a separatrix surface. In time, the current in the ring decays owing to the ohmic resistance and the intrinsic magnetic field is attenuated. In consequence, the external field approaches the ring and penetrates it eventually to become uniform over all space.

If the axis of the current ring is adopted as the z-axis of the cylindrical (r, θ, z) coordinate system (Fig. 8a), the problem becomes two-dimensional and axially symmetric: the magnetic field has only two poloidal components H_r and H_z. Inside the ring, the time evolution of the magnetic field is described by the diffusion equation, which can be expressed in terms of magnetic flux function Ψ as

$$\frac{\partial \Psi}{\partial t} = \frac{c^2}{4\pi\sigma(T)}\, \Delta^* \Psi \,,$$

$$\Delta^* = r\,\frac{\partial}{\partial r}\left(\frac{1}{r}\,\frac{\partial}{\partial r}\right) + \frac{\partial^2}{\partial z^2} \,. \tag{4.28}$$

Here σ is the conductivity of the ring material (copper) dependent on the temperature T, which varies in time according to the equation

$$\rho C_p\,\frac{\partial T}{\partial t} = \frac{j^2}{\sigma(T)} \,, \tag{4.29a}$$

$$j = j_\theta = -\frac{c}{4\pi r}\, \Delta^* \Psi \,. \tag{4.29b}$$

The term in the right-hand part of (4.29a) arising from thermal conduction has been omitted: estimates show that its role is insignificant compared with the Joule heating. The heat capacity C_p is also temperature-dependent. The expressions for σ and C_p are specified by the tables† and are interpolated by polynomials in the temperature range of interest.

The magnetic field in vacuum is described by the equation

$$\Delta^* \Psi = 0 \,. \tag{4.30}$$

At the vacuum – conductor interface the magnetic field, viz. Ψ and the normal derivative $\partial\Psi/\partial n$, is bound to be continuous. The constant external magnetic field $H_r = 0$, $H_z = H_0$ is given at 'infinity' or

$$\Psi = \frac{H_0 r^2}{2} \,, \qquad r, z \to \infty \,. \tag{4.31}$$

For $t = 0$, the prescribed magnetic field is uniform and is directed in opposition to the external field: $H_r = 0$, $H_z = H_1 < 0$. Then the field at infinity changes in a short time to assume the constant value (4.31). This change corresponds to the transition of the ring from the chamber, where the magnetic field is frozen in it, to the plasma volume to be probed. The initial ring temperature is assumed to be equal to $T = 20$ K across the section.

A long series of calculations was conducted for copper rings of different cross sections (round, elliptic, square) [48]. If the ring section diameter is small relative to the diameter of the ring itself, the results for the rings with variously shaped cross sections differ insignificantly. As one of the main calculation results, we present the empirical formula for estimating the time it takes for the magnetic field separatrix to approach the ring and touch its surface:

$$t_s \approx \frac{2}{H_0}\,\frac{abh}{5b + h} \,. \tag{4.32}$$

Here a is the ring radius, b and h are its halfwidth and halfheight (cm), and H_0 is the external field strength (kOe).

4.5.3. Structural changes of the toroidal magnetic field induced by a point-like magnetic dipole. Although the magnetic field of the toroidal plasma configuration will flow around the magnetic MP-produced cavity, the existence of this cavity will nevertheless cause the structure of the magnetic surfaces to change. Here we consider a model problem of the perturbation of symmetric magnetic field $\mathbf{H}_0$ induced by an asymmetrically immersed point-like magnetic dipole [49]. Instead of the torus, we consider a straight cylinder with identical ends. Considering that the characteristic ratio between the major R_0 and minor r_0 radii of the tokamak torus is ~ 3, the cylinder length is taken to be

$$L = 6\pi r_0 \,. \tag{4.33}$$

The unperturbed magnetic field is prescribed as

$$H_\theta^{(0)} = h H_0\,\frac{r}{r_0}\left(1 - \frac{r^2}{2r_0^2}\right) , \qquad H_z^{(0)} = H_0 = \text{const} \,, \tag{4.34}$$

where $h = 2H_\theta^{(0)}/H_0|_{r=r_0}$ is a parameter.

The magnetic field of an MP is approximated by the field of a dipole with moment m_0 aligned with the z-axis. The magnitude of m_0 is related to the current J_0 carried by the ring and its medium radius a by the expression

$$m_0 = \frac{J_0}{c}\,\pi a^2 \,.$$

† *Handbook of a Chemist* Vol. 1 (Moscow, Leningrad: Gostekhteorizdat, 1963).

The dipole magnetic field is conveniently given by the scalar potential

$$\Phi_{\mathrm{m}} = m_0 \frac{\partial}{\partial z} \frac{1}{\rho} \,. \tag{4.35}$$

Here ρ is the distance from the dipole $(x_{\mathrm{m}}, y_{\mathrm{m}}, z_{\mathrm{m}})$ to the point under consideration. From here on the relative magnitude of the dipole field will be characterized by the dimensionless parameter

$$\chi = \frac{m_0}{H_0 r_0^3} = \frac{\pi J_0 a^2}{c H_0 r_0^3} \,. \tag{4.36}$$

To ensure the identity of the cylinder ends, the magnetic field should be periodic. For this purpose, consider an infinite chain of cylinders of length L each containing a dipole. Instead of (4.35), in the calculations we use the sum

$$\Phi_{\mathrm{ms}}(\mathbf{x}) = \sum_{n=-N}^{N} \Phi_{\mathrm{m}}(\mathbf{x}, x_{\mathrm{m}}, y_{\mathrm{m}}, z_{\mathrm{m}} + nL) \,. \tag{4.37}$$

Our estimates indicate that it will suffice to limit the summation in (4.37) to $N = 2$. The stated problem reduces to the solution of the system of equations

$$\frac{\mathrm{d}r}{\mathrm{d}z} = \frac{H_r}{H_z} \,, \qquad \frac{r\,\mathrm{d}\theta}{\mathrm{d}z} = \frac{H_\theta}{H_z} \,, \qquad \mathbf{H} = \mathbf{H}^{(0)} + \mathbf{H}_{\mathrm{m}} \tag{4.38}$$

in the multiply repeated interval $(-3\pi, 3\pi)$ in z. For each force line, the intersection points with the $z = 0$ plane are noted. The numerical integration of (4.38) was accomplished by the fourth-order Runge – Kutta method.

In the absence of the dipole, the magnetic force lines wind around the embedded cylinders and rotate through the angle

$$\delta\theta = 6\pi h \left(1 - \frac{r^2}{2r_0^2}\right)$$

for the length $L = 6\pi r_0$. Accordingly, the rotation number $\mu = \delta\theta / 2\pi$ changes from $\mu(r = 0) = 3h$ to $\mu(r_0) = 3/2h$. In this case, there is a family of concentric circles in the $z = 0$ section passed through the cylinders.

The existence of perturbations significantly changes this simple picture. This is due to the fact that the magnetic surfaces formed by periodic force lines, i.e. the lines with rational rotation numbers $\mu = n/m$ (n is the number of circuits in azimuth and m the number of periods in z following which the force line closes to itself), are not conserved under the perturbation. They split to form a filamentary structure or collapse altogether. As this takes place, in the $z = 0$ plane a chain of m magnetic islands appears in lieu of a circle. With a strong perturbation, the island structure may collapse to form a chaotic layer.

The calculations were made for three versions of the parameters h and χ: (1) $h = 0.1$, $\chi = -0.01$ (Fig. 8b); (2) $h = 1/30$, $\chi = -0.01$; (3) $h = 0.1$, $\chi = -0.001$ (Fig. 8c). The structure of magnetic islands and their reconstruction with increasing perturbation were considered. Flow around the cavity occupied by the dipole field is inherent in all the versions. The cavity center is close to the dipole center ($x_{\mathrm{m}} = 0.5 r_0$). According to the calculations, the resonances most pronounced in the first version (Fig. 8b) are those with $\mu = 1/4$, $2/7$, and $3/11$. The resonance with $\mu = 4/15$ is noteworthy. It is on the verge of regeneration of an elliptic point to a hyperbolic one with a jump, i.e. is imbedded in the stochastic layer. This layer is shown schematically in Fig. 8b. In the second case, significant splitting occurs for $\mu = 1/11$ and $1/12$, i.e. as in all other instances the greatest changes are experienced by the rational surfaces located close to the dipole region. Inherent in the third version (Fig. 8c) was a notable attenuation of the same resonances as in the first one. A more than twofold decrease of the dipole cavity is noteworthy.

As also evidenced by the calculations, in the case that $r_0/a \approx 10$, i.e. when the radii of the plasma cylinder and the myxine probe differ by an order of magnitude, the perturbation may be thought of as being small.

5. Certain kinetic effects in Galateas

Due to the existence of plasma – field transition layers in Galateas for $\beta_0 = 1$, whose thickness can be commensurable with the ion Larmor radius ρ_{i}, in many cases there is a need to analyze both the dynamics of individual particles and the kinetic models for the equilibrium and the stability of plasma configurations. Some of the issues are considered in this section.

5.1 Co- and counter-collisions of charged particles with a magnetic barrier [50]

Consider a simple model of a magnetic barrier in the form of a step in which the field for $x > 0$ is aligned with the z-axis (Fig. 9a). Let a charged particle (e.g. an ion) with velocity $\mathbf{V}_0 = (V_{0x}, V_{0y})$ be confronted by the barrier at point A. If $H_z > 0$ and $V_{0y} < 0$, the Lorentz force points toward the $x < 0$ domain, and so the particle describes an arc smaller than a semicircle to exit from the field region with velocity $\mathbf{V}_1 = (-V_{0x}, V_{0y})$ at point B.

Now, if the same particle with velocity $\mathbf{V}_{1^*} = -\mathbf{V}_1$ is directed to point B, it will traverse quite another path and describe an arc greater than a semicircle. This path difference is due to the fact that the Newton – Lorentz equations are not invariant under change of the sign of time.

The collision of the first particle depicted in Fig. 9a will be termed a 'co-collision' while the particles experiencing it in the given context will be termed the 'co-particles.' The collision of the second particle will be named the 'counter-collision' and such particles the 'counter-particles.'

The existence of two types of collisions can have a profound effect on the plasma confinement in traps. This is amply manifested in open axisymmetric traps with a poloidal

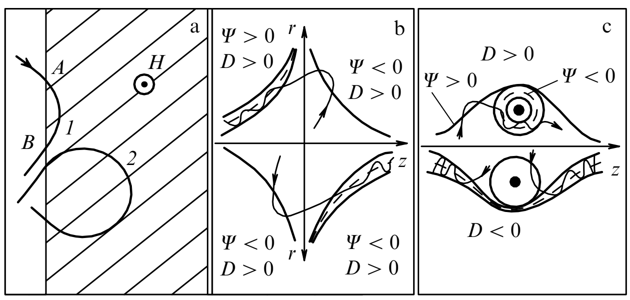

Figure 9. Co- and counter-collisions of particles with a magnetic barrier: (a) co-collisions *1* and counter-collisions *2*; (b) collisions with a magnetic barrier in a magnetic antibottle; (c) collisions with a barrier in a Galatea-A.

magnetic field: magnetic antibottles and Galateas-A. In the specified cases, the generalized angular momentum

$$MrV_\theta + \frac{e}{c}\,\Psi \equiv D = \text{const} \tag{5.1}$$

is conserved and the motion in r and z can be represented as the motion in the field with the effective potential

$$U = \frac{1}{2Mr^2}\left(\frac{e}{c}\,\Psi - D\right)^2 . \tag{5.2}$$

The magnetic field in the central part is taken to be zero and here we can put $\Psi = 0$. Now consider some region of the magnetic barrier where we put $\Psi > 0$ for definiteness. Then, a particle for which $D < 0$ cannot penetrate through the barrier since the potential U monotonically increases outside. However, if Ψ and D are opposite in sign, the potential has a dip for $\Psi = D$ which can capture particles.

Consider a magnetic antibottle more closely (Fig. 9b). In this trap, in the plasma-surrounding barrier the direction of the magnetic field changes and so does the sign of Ψ. Therefore, regardless of the sign of the momentum D, an escape channel appears in the potential contour ('charge pattern') $U(r, z, D)$ either to the left or to the right of the radial slit. To be captured in the channel, a particle should have a longitudinal (along the continuous boundary line) velocity component directed to the axial trap exit. Referring to Eqn (5.2), as r decreases the height of the channel walls increases and the particle is captured. Whether it escapes through the axial mirror or not is determined by the mirror ratio $\chi = H_{\max}/H_*$ ($H_{\max}$ is the magnetic mirror field and H_* is the field at the point of capture).

So, there are two factors that cause a particle to leave the magnetic antibottle: the existence of the capture channel and the 'appropriate' components (across and along the channel) of the particle velocity after its entry. It is precisely these factors that cause the effective areas of the axial openings, permitting the particles to escape the trap, to be unexpectedly large:

$$S^{\mathrm{ax}} \propto 2\pi R \rho_{\min} . \tag{5.3}$$

Here R is the maximum radius of the plasma volume and $\rho_{\min}$ is the ion Larmor radius in the mirror.

The case of Galatea-A is more complicated. Here the plasma boundary also consists of two elements, viz. the myxine surface S_μ and the 'general' magnetic surface S_0 (Fig. 9c) at which Ψ is opposite in sign. However, the S_μ surface does not go beyond the plasma volume. Therefore, for those particles whose angular momentum D is of the same sign (let it be positive) as Ψ at the myxine surface, the existence of a capture channel in the potential pattern U is not associated with particle loss.

But when confronted by the 'general' barrier, these same particles turn out to be co-particles for which there is no escape channel. Therefore the effective escape cross section for them is

$$S^{\mathrm{co}} \propto \pi \rho_{\min}^2 . \tag{5.4}$$

The situation reverses for particles with $D < 0$. They are co-particles for the magnetic sheath of a myxine and counter-particles for the general magnetic sheath. Therefore

$$S^{\mathrm{con}} \propto 2\pi R \rho_{\mathrm{i}} . \tag{5.5}$$

From the above discussion it follows: if a Galatea-A is filled with a non-magnetized plasma, the particles with $D\Psi^0 > 0$ (Ψ^0 is the magnitude of Ψ near the axis) are first to escape the trap. After that, the plasma of particles with $D\Psi^0 < 0$ will remain in the trap volume. This plasma rotates and the particle escape from the trap drops sharply. This is associated not only with the reduction of the escape cross section by the factor R/ρ_{i}, but with the rotation-induced particle extrusion from the axial region as well. However, the plasma rotation may induce a poloidal magnetic field in its volume and cause the trap to transfer to a class of traps with an azimuth volume current. What occurs in reality remains unknown.

5.2 A class of equilibrium kinetic configurations [51]

Today there is no way to calculate three-dimensional equilibrium Galatea configurations along with ion and electron distribution functions of a sufficiently general form. However, kinetic models of equilibrium configurations can be constructed with relative ease for axisymmetric systems with poloidal magnetic fields and quasi-equilibrium electron and ion distribution functions. In this case, the quasi-equilibrium implies that two conditions are fulfilled. First, collisions are infrequent and in the first approximation the Vlasov equation

$$\mathbf{V}\,\frac{\partial f_{\mathrm{i,e}}}{\partial \mathbf{x}} \pm \frac{1}{m_{\mathrm{i,e}}}\left(-\nabla\Phi + \frac{1}{c}\,\mathbf{V}\times\mathbf{H}\right)\frac{\partial f_{\mathrm{i,e}}}{\partial \mathbf{V}} = 0 \tag{5.6}$$

may be thought of as holding good. Second, the system is studied over time periods $\tau > \tau_{\mathrm{mix}}$, where τ_{mix} is the phase-volume mixing time, which is the time of forgetting the adiabatic invariants. It is assumed that τ_{mix} is no greater than $\tau_{\mathrm{i,i}}$, the ion-ion collision time.

In this case, the particles forget their initial conditions and we can write

$$f_{\mathrm{i}} = F_{\mathrm{i}}\left(\frac{M\mathbf{V}^2}{2} + e\Phi, MrV_\theta + \frac{e}{c}\,\Psi\right) \equiv F_{\mathrm{i}}(\mathcal{E}_{\mathrm{i}}, \mathcal{P}_{\mathrm{i}}) ,$$

$$f_{\mathrm{e}} = F_{\mathrm{e}}\left(\frac{m\mathbf{V}^2}{2} - e\Phi, mrV_\theta - \frac{e}{c}\,\Psi\right) \equiv F_{\mathrm{e}}(\mathcal{E}_{\mathrm{e}}, \mathcal{P}_{\mathrm{e}}) . \tag{5.7}$$

Here $F_{\mathrm{i,e}}(\mathcal{E}_{\mathrm{i,e}}, \mathcal{P}_{\mathrm{i,e}})$ are, in principle, arbitrary functions to be prescribed from specific considerations. If they are given, from the Maxwell equations

$$\Delta\Phi = -4\pi e \int (f_{\mathrm{i}} - f_{\mathrm{e}})\,\mathrm{d}\mathbf{V} , \tag{5.8a}$$

$$\Delta^*\Psi = -\frac{4\pi e}{c}\int V_\theta (f_{\mathrm{i}} - f_{\mathrm{e}})\,\mathrm{d}\mathbf{V} , \tag{5.8b}$$

$$\Delta^* \equiv r\,\frac{\partial}{\partial r}\,\frac{1}{r}\,\frac{\partial}{\partial r} + \frac{\partial^2}{\partial z^2} ,$$

it is possible to find the electric and magnetic fields and thus calculate the configuration completely.

However, the assumption of quasineutrality simplifies the problem substantially. Then,

$$\int F_{\mathrm{i}}(\mathcal{E}_{\mathrm{i}}, \mathcal{P}_{\mathrm{i}})\,\mathrm{d}\mathbf{V} = \int F_{\mathrm{e}}(\mathcal{E}_{\mathrm{e}}, \mathcal{P}_{\mathrm{e}})\,\mathrm{d}\mathbf{V} \tag{5.9}$$

and it is possible to determine the relationship

$$\Phi = \Phi(r, \Psi) . \tag{5.10}$$

Hence it follows that the magnetic force lines under the given assumptions are, to the r-dependence, equipotential while the plasma density also depends only on r and Ψ. Substituting (5.10) into (5.8b) reduces the problem to one equation of the Grad – Shafranov type

$$\Delta^* \Psi = -Q(r, \Psi) . \tag{5.11}$$

Examples of the numerical solution of this equation are given in Section 7.

We complement the aforesaid by three remarks concerning the transition layer itself, with the assumption that it is stationary and can be thought of as being one-dimensional.

(1) In this case, the magnetic field can have two components:

$$\mathbf{H} = \big(0, H_y(x), H_z(x)\big) .$$

Now the Vlasov equations can be solved in the general case and have three integrals

$$\mathcal{E}_{\mathrm{i,e}} = \frac{m_{\mathrm{i,e}}\mathbf{V}^2}{2} \pm e\Phi ,$$

$$\mathcal{P}^{(y)}_{\mathrm{i,e}} = m_{\mathrm{i,e}}V_y \pm \frac{e}{c}\,A_y , \qquad \mathcal{P}^{(z)}_{\mathrm{i,e}} = m_{\mathrm{i,e}}V_z \pm \frac{e}{c}\,A_z , \tag{5.12}$$

so that $f = F(\mathcal{E}, \mathcal{P}^{(y)}, \mathcal{P}^{(z)})$.

(2) The system of Maxwell equations

$$\frac{\mathrm{d}^2\Phi}{\mathrm{d}x^2} = -4\pi e \int (f_{\mathrm{i}} - f_{\mathrm{e}})\,\mathrm{d}\mathbf{V} ,$$

$$\frac{\mathrm{d}^2 A_{y,z}}{\mathrm{d}x^2} = -\frac{4\pi e}{c}\int V_{y,z}(f_{\mathrm{i}} - f_{\mathrm{e}})\,\mathrm{d}\mathbf{V} \tag{5.13}$$

given $F_{\mathrm{i,e}}$ and the quasineutrality condition, determines the ultimate relationship

$$\Phi = \Phi(A_y, A_z) \tag{5.14}$$

in the general case and reduces to two equations for A_y and A_z.

When the transition layer is considered in a system with only the poloidal field, $A_z = 0$, as in the axisymmetric case, the treatment reduces to the solution of the simple equation

$$\frac{\mathrm{d}^2 A_y}{\mathrm{d}x^2} = Q(A_y) . \tag{5.15}$$

(3) In principle, the potentials of the force lines can be determined either by electrodes (see Section 9.1) or by ion beams, which deliver one or other charge. If the potential $\Phi(x)$ is assumed to be given, for a known function $F_{\mathrm{i}}(\mathcal{E}_{\mathrm{i}}, \mathcal{P}_{\mathrm{i}})$ it is possible (for simplicity assuming the magnetic field to be poloidal) to write the equation for A_y in the quasineutrality case:

$$\frac{\mathrm{d}^2 A_y}{\mathrm{d}x^2} = -4\pi e\left(\int V_y F_{\mathrm{i}}\,\mathrm{d}\mathbf{V} + \frac{E_x}{H}\int F_{\mathrm{i}}\,\mathrm{d}\mathbf{V}\right) . \tag{5.16}$$

Clearly different distributions can be prescribed. We note the isodrift mode among them, when $E/H = \text{const}$ or $\Phi = \varkappa A_y$. In this case, all transition-layer electrons drift with a common velocity.

5.3 Flow stability in the multipole Padalka plasma guide [52, 53]

The problem of plasma stability in traps, as shown by the vast CNF research experience, can be solved efficiently only with a close relationship between experiment and theory. In line with this statement, we now consider the paper by V G Padalka et al. in which the stability of the plasma flow in a multipole plasma guide was studied experimentally. The research was based on the criteria of stability [10] with respect to permutational instability for plasmas in multipole traps. The theoretical treatment was performed in the context of kinetics though with a large number of assumptions (a linear approximation, an absence of electric fields in the unperturbed state, the drift nature of the particle motion, a Maxwellian ion distribution etc.). Eventually two stability criteria were obtained, i.e. the existence of two plasma confinement barriers was established. These owe their existence, first, to the minimum of the specific volume of magnetic force tubes

$$U = \int \frac{\mathrm{d}l}{H} , \qquad \frac{\partial U}{\partial n} < 0 , \tag{5.17}$$

and, second, to the minimum of the path length of a force line

$$\Lambda = \int \mathrm{d}l , \qquad \frac{\partial \Lambda}{\partial n} < 0 . \tag{5.18}$$

The latter criterion signifies the existence of force lines with a peak average strength $\bar{H} = \int H\,\mathrm{d}l / \int \mathrm{d}l$ of the magnetic field. The first criterion was obtained with the proviso that $k_z\rho_{\mathrm{i}} \ll 1$ and the second with the inverse inequality. Here k_z is the wave vector component along the direction of symmetry and ρ_{i} the ion Larmor radius. One would expect criterion (5.18) to be valid with the existence of a zero of the magnetic field. This was clearly demonstrated by V G Padalka with the plasma guides, which constituted either a system of two conductors drawing current in one direction and spaced 12 cm apart (a quadrupole plasma guide) or a system of four conductors also carrying current in one direction (an octupole plasma guide). The conductors measured 160 cm in length, and the current was 10 kA (Fig. 2d).

Preparatory to the experiment, a calculation was performed of the functions $U(\Psi)$ and $\Lambda(\Psi)$ or, which is the same, the functions $U(x)$ and $\Lambda(x)$, where x is the coordinate of the force line Ψ measured along the line drawn from the system center through the midpoint between the conductors (Fig. 10a, b). Referring to the figure, the region enclosed by barrier U is broader than that enclosed by barrier Λ.

The plasma source was a pulse gun delivering a ~ 1.5-m-long hydrogen plasma flux with density $\sim 10^{13}\ \mathrm{cm}^{-3}$, velocity $\sim 4\times 10^6\ \mathrm{cm\ s}^{-1}$, and the temperatures $T_{\mathrm{i}} \sim T_{\mathrm{e}} \sim 10$ eV. Prior to the pulse the chamber was pumped to ~ 10 Torr.

The oscillations were studied using single and double probes. In the process n_{e}, T_{e}, the potential Φ, and the electric field strength E were measured. The equipotential feature of magnetic force lines was verified. The oscillograms (Fig. 10c), which were recorded by two probes separated by 90°, clearly demonstrate the synchronism of the oscillations at different points in a common force line. After that, the oscillograms of the oscillations of plasma parameters at different distances from the axis were recorded (Fig. 10d).

Next the auto- and cross-correlation dependences were monitored for different modes. They revealed that the typical

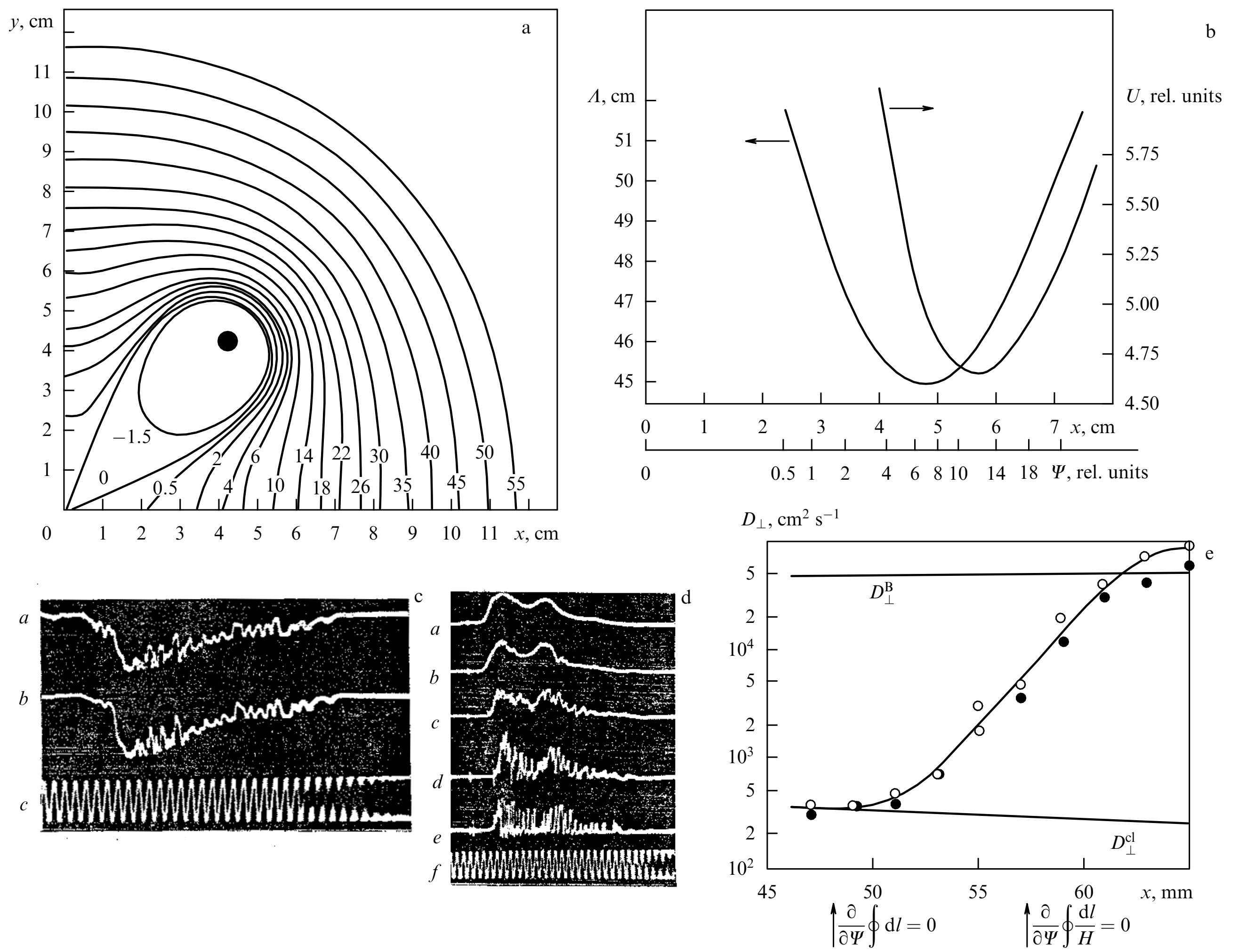

Figure 10. Stability of flow in an octupole plasma guide: (a) magnetic force lines (Ψ = const) in a straight octupole; (b) dependences of $U = \oint H^{-1}\,\mathrm{d}l$ and $\Lambda = \oint \mathrm{d}l$ on Ψ; (c) oscillograms of the plasma potential in an octupole plasma guide. The probes are located in one force line ($x = 65$ mm) and are separated by 90° in azimuth. The calibration in time was accomplished by a 250 kHz signal, the current drawn by the rods was 9.3 kA, $z = 105$ cm; (d) oscillograms of the plasma potential in the octupole plasma guide at different distances from the system axis: *a* — $x = 46$ mm, *b* — $x = 50.6$ mm, *c* — $x = 55$ mm, *d* — $x = 60$ mm; (e) magnitude of the plasma diffusion coefficient $D_\perp$ at different distances from the system axis.

correlation lengths under the conditions at hand were $l_c \sim 1.5$ cm and the corresponding time was $\tau_c \sim 1$ μs.

With knowledge of the plasma parameters, it is possible to calculate the diffusion coefficients: classical

$$D_\perp^{\mathrm{cl}} = \frac{mc^2 k(T_\mathrm{i} + T_\mathrm{e})}{e^2 H^2 \tau_{\mathrm{ei}}} \tag{5.19}$$

and Bohm diffusion coefficient

$$D_\perp^{\mathrm{B}} = \frac{ckT}{16eH}\,. \tag{5.20}$$

Plotted in Fig. 10e are the magnitudes of these coefficients as well as of the coefficients calculated from the correlation measurements employing the formulas

$$D_{\perp(1)} = c^2\,\frac{\langle \tilde{E}^2 \rangle}{H^2}\,\tau_c\,,$$

$$D_{\perp(2)} = -\frac{c}{H|\nabla H|}\,\langle \tilde{n}\tilde{E} \rangle\,. \tag{5.21}$$

It is clear that the transfer is classical in the limits $0 < x < x(\Lambda_{\min})$. Then, for $x > x(\Lambda_{\min})$ the diffusion is enhanced to eventually attain the Bohm level.

6. 2-D problems with an abrupt plasma – field transition

Interest in the equilibrium problems of ideal plasmas is traditional for plasma theory. The first analytical treatment of equilibrium plasma configurations with $\beta = 1$ and the derivation of the stability criterion were performed by S I Braginskiĭ and B B Kadomtsev [1]. Some general properties of equilibrium states and the independent derivation of their stability criteria were set forth in the classical papers by Berkovich, Grad, and Rubin [2, 3]. As is known, the principal result is simple: the interface should be concave toward the plasma.

There is one more circumstance that attaches much importance to the studies of such systems. V D Shafranov pointed out that the MHD equilibrium equations

$$\nabla P = \frac{1}{c}\,\mathbf{j} \times \mathbf{H}\,, \qquad \mathbf{j} = \frac{c}{4\pi}\,\mathrm{rot}\,\mathbf{H}\,, \qquad \mathrm{div}\,\mathbf{H} = 0 \tag{6.1}$$

are formally equivalent to the equations of stationary motion of an ideal incompressible liquid

$$(\mathbf{v}\nabla)\mathbf{v} = -\frac{\nabla P}{\rho}\,, \qquad \operatorname{div}\mathbf{v} = 0\,,$$

and therefore studies of configurations with $\beta = 1$ are simultaneously studies on some fluid dynamics problems.

Analytical methods are efficient only for plane symmetry problems. Presented below is an analytical treatment of several simple magnetic field – plasma systems in which a resting ideal plasma free of magnetic field occupies some finite volume in space and is confined by the surrounding magnetic field [55, 56].

6.1 Plane figures of equilibrium

Consider the formulation of the problem of plane equilibrium geometries of ideal plasmas ($\sigma = \infty$) embedded in the magnetic field of rectilinear currents. The plasma configuration is in this case a body of constant section D (D is the region in the plane with Cartesian x, y coordinates to be determined) extending along the z-axis. The electric currents $\mathbf{j}(\mathbf{r})$ and magnetic field $\mathbf{H}(\mathbf{r})$ are prescribed outside the plasma region (in vacuum). The two-dimensional property and the plane symmetry imply in this case that

$$\frac{\partial}{\partial z} = 0\,, \qquad \mathbf{j} = \big(0, 0, j(x,y)\big)\,, \qquad \mathbf{H} = \big(H_x(x,y), H_y(x,y), 0\big)\,.$$

We introduce the magnetic potential $A(x, y)$ with the relationships $H_x = \partial A/\partial y$ and $H_y = -\partial A/\partial x$ to obtain for the vacuum

$$\Delta A = -\frac{4\pi}{c}\, j(x,y)\,, \qquad (x,y) \notin D\,, \tag{6.2}$$

where $\Delta = \partial^2/\partial x^2 + \partial^2/\partial y^2$ is the Laplace operator.

This equation should be complemented by the boundary conditions at the plasma surface and at infinity. Since the normal component H_n of the magnetic field is continuous at the plasma – vacuum boundary and $\mathbf{H} \equiv 0$ inside the plasma, $H_n = 0$ at the plasma surface, i.e. the magnetic field is tangent to the plasma boundary ∂D, and therefore the first condition becomes

$$A = \text{const}\,, \qquad (x,y) \in \partial D\,.$$

The second is the equilibrium condition. If the plasma pressure $P(x, y) \equiv P_0 = \text{const}$ in D, we have

$$\frac{H^2}{8\pi} = \frac{1}{8\pi}\left(\frac{\partial A}{\partial n}\right)^2 = P_0\,, \qquad (x,y) \in \partial D\,. \tag{6.3}$$

Here n is the normal to ∂D. Condition (6.3) signifies that the modulus of the magnetic field is constant along the boundary.

The third condition can be obtained as follows. We integrate the equation $\operatorname{rot}\mathbf{H} = 4\pi/c\,\mathbf{j}$ over the D region to obtain

$$\oint_{\partial D} H_\tau\,\mathrm{d}\tau = \oint_{\partial D} \frac{\partial A}{\partial n}\,\mathrm{d}\tau = \frac{4\pi}{c}\,J_\mathrm{p}\,. \tag{6.4}$$

Here J_p is the total current traversing the plasma. Condition (6.4) is equivalent to some condition at infinity. If, for instance, the total current traversing the vacuum region is J, we get

$$A \cong -\frac{2(J + J_\mathrm{p})}{c}\ln R\,, \qquad R^2 = x^2 + y^2\,, \qquad R \to \infty\,. \tag{6.5}$$

Problems of similar structure have long been the subject of study in the hydrodynamic theory of incompressible ideal-fluid jets. It will suffice to mention the classical monographs [57, 58]. However, it is pertinent to note that the flow configurations studied in the theory of jets are of no particular interest for plasma physics (presumably, the reverse is equally true).

Evidently, the case of a single current of the form $j(x, y) = j_0\delta(x - x_0)\delta(y - y_0)$ (a singlet) is logically and physically simplest. But equally evident is that no equilibrium configurations occupying a finite spatial region (in the x, y plane) exist in the magnetic field of a singlet.

The simplest though nontrivial system of currents that produces a magnetic configuration with a zero point and separatrices not going to infinity is a superposition of two currents equal in magnitude and sense (a doublet),

$$j(x,y) = J_0\big[\delta(x - x_0)\delta(y) + \delta(x + x_0)\delta(y)\big]\,. \tag{6.6}$$

The currents flow through the points $(\pm x_0, 0)$, the zero point is at the origin. Consider this case in greater detail.

First, we rewrite the initial problem in new terms. The units of length, electric current, and magnetic field will respectively be x_0, J_0, and $H_0 = (4\pi/c)x_0 J_0$. In the new terms we have

$$\begin{aligned} &\Delta A = -\big[\delta(x-1)\delta(y) + \delta(x+1)\delta(y)\big]\,, \qquad (x,y) \notin D\,,\\ &A = \text{const}\,, \qquad (x,y) \in \partial D\,,\\ &\left|\frac{\partial A}{\partial n}\right| = h\,, \qquad (x,y) \in \partial D\,,\\ &\oint_{\partial D} \frac{\partial A}{\partial n}\,\mathrm{d}\tau = g\,. \end{aligned} \tag{6.7}$$

The problem (6.7) has two dimensionless parameters

$$h = \frac{c\sqrt{P_0}\,x_0}{\sqrt{2\pi}\,J_0}\,, \qquad g = \frac{J_\mathrm{p}}{J_0}\,, \tag{6.8}$$

whose significance is obvious (in particular, it is easily seen that $\beta = h^2$).

The methods developed in the theory of ideal-fluid jets make it possible to obtain a complete solution of this problem. The procedure is discussed at length elsewhere [55, 56]. Here we restrict ourselves to only the principal definitions and introduce the required notation. The x, y-plane is considered as the plane of the complex variable $z = x + \mathrm{i}y$. The exterior of region D (as yet unknown) is conformally mapped onto the exterior of a unit circle in the plane of the complex variable t. In doing this, let the points $z = \pm 1$ (the points of current location) go over respectively into the points $t = \pm t_1$ ($\operatorname{Im} t_1 = 0$, $t_1 > 1$).

We introduce the complex potential of the magnetic field $F(z) = \varphi + \mathrm{i}A$, where $\partial\varphi/\partial x = H_x$, $\partial\varphi/\partial y = H_y$. According to Eqns (6.7), $\operatorname{Im} F = \text{const}$ at ∂D. Also, we define the function $\zeta(z)$ by the relationship

$$\zeta(z) = \frac{1}{h}\frac{\mathrm{i}\,\mathrm{d}F}{\mathrm{d}z} = \frac{1}{h}(H_x - \mathrm{i}H_y)\,. \tag{6.9}$$

Then from Eqns (6.7) we obtain $|\zeta(z)| = 1$ for $z \in \partial D$.

Next we construct the functions F and ζ of variable t: $F(t) = F\big(z(t)\big)$ (by the method of images) and $\zeta(t) = \zeta\big(z(t)\big)$ (in the construction of this function, a special method is used involving analytic continuation of a meromorphic function along the arc in which its modulus is constant), where $z(t)$ is the above-specified conformal mapping $z \to t$ (yet to be constructed). In consequence we obtain

$$F(t) = \frac{1}{2\pi\mathrm{i}}\left[\ln\frac{(t-t_1)(t+t_1)t^{2+g}}{(tt_1-1)(tt_1+1)} + 2\ln t_1\right],$$

$$\zeta(t) = -\mathrm{i}\,\frac{t^2 t_1^2 - 1}{(t^2 - t_1^2)t}\,. \tag{6.10}$$

It is easily seen that for $|t| = 1$ the following holds: $\operatorname{Im} F(t) = \mathrm{const}$, $\big|\zeta(t)\big| = 1$. However, in accordance with Eqn (6.9) we have

$$z(t) = \frac{1}{h}\int \zeta^{-1}(t)\,\frac{\mathrm{d}F}{\mathrm{d}t}\,\mathrm{d}t\,. \tag{6.11}$$

With Eqns (6.10) and (6.11) we obtain

$$z(t) = \frac{1}{h}\,\Pi(t, t_1, g)\,, \tag{6.12}$$

where

$$\Pi(t, t_1, g) = \frac{1}{2\pi}\,t_1^{-3}\left[(2+g)t_1 t - (t_1^4 - 1)\frac{t_1 t}{t^2 t_1^2 - 1} + (1+g)\frac{t_1^4 - 1}{2}\ln\frac{t_1 t + 1}{t_1 t - 1}\right]. \tag{6.13}$$

The initial problem has two parameters, h and g, but $z(t)$ in Eqn (6.12) depends on the auxiliary quantity t_1. To exclude it, we invoke the 'normalization' condition $z(t_1) = 1$, which gives

$$\delta(t_1, g) \equiv \Pi(t_1, t_1, g) = h\,. \tag{6.14}$$

The latter relationship makes it possible, in principle, to determine the dependence $t_1 = t_1(h, g)$. Mapping (6.12) yields the complete solution, if it exists, to the problem and, in particular, the shape of the figure of equilibrium

$$w(\theta) \equiv z\big(\exp(\mathrm{i}\theta)\big)\,, \qquad 0 \leqslant \theta \leqslant 2\pi\,. \tag{6.15}$$

We first consider the case of $g = 0$ (the total current in the plasma is zero). The function $\delta_0(t_1) \equiv \delta(t_1, 0)$ is plotted in Fig. 11a. Some of the features of this function are noteworthy:

$$\delta_0(t_1) \approx \frac{1}{2\pi}\big[1 - 2(t_1 - 1)\ln(t_1 - 1)\big]\,, \qquad t_1 \geqslant 1\,,$$

$$\delta_0(t_1) \approx \frac{1}{\pi t_1}\,, \qquad t_1 \to \infty\,.$$

The function $\delta_0(t_1)$ peaks at $t_1 = t_{\max} \approx 1.2$, assuming the value $\delta_0(t_{\max}) = h_{\max} \approx 0.22$. The following conclusions can readily be drawn from Fig. 11a: (1) for $h > h_{\max}$, the solution of the problem does not exist; (2) two solutions exist for $1/2\pi = h_0 < h < h_{\max}$; (3) for $h < h_{\max}$ there exists a single solution. The examples of equilibrium geometries are given in Fig. 11b–d, with t_1 varying from 1.01 to 2.0.

So, no equilibrium plasma geometry exists for $h > h_{\max} \approx 0.22$. For $h = h_{\max}$, the figure has convex (unstable) and concave (stable) portions of the boundary. For $h_0 < h < h_{\max}$ there are two solutions. If we follow the figure proceeding along the right branch of the curve in Fig. 11a, both the x- and y-dimensions of the figure decrease as parameter h decreases. For sufficiently small h the figure has only concave boundaries. If we proceed by the left branch of the curve from $h = h_{\max}$, with decreasing h the figure dimension in x decreases (tends to zero as $h \to h_0$) while the dimension in y increases (tends to two as $h \to h_0$). For $h \to h_0$ the figure is as if ruptured at zero and connected by spinodes enclosing the currents.

The above problem of the properties of equilibrium plasma geometries in the field of a doublet (6.6) is, on the one hand, most elementary but, on the other, sufficiently

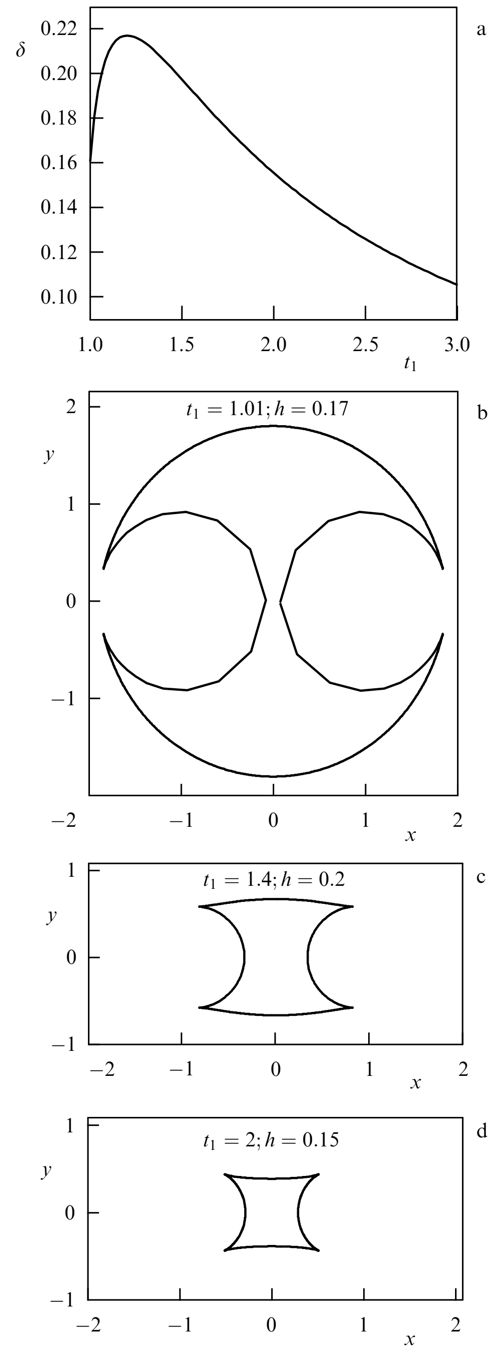

Figure 11. (a) Plot of the $\delta(t_1)$ function. (b–d) Examples of the figures of equilibrium for different values of the $t_1(h)$ parameter.

universal because it describes in fact the properties of the figures of equilibrium in the vicinity of any nondegenerate zero of the magnetic field.

The natural extensions and complications of the doublet problem are the problems with three (a triplet), four (quartet) etc. currents flowing in one direction and located at the corners of a regular triangle, quadrangle etc. We describe the principal qualitative features of these cases but do not give detailed calculations here. It can be inferred that with increasing the number of currents: (i) $t_{\max}$ decreases; (ii) h_0 and $h_{\max}$ increase; (iii) $h_{\max} - h_0$ decreases. So, the greater the number of currents, the higher the critical value $h_{\max}$, the narrower the h-parameter range whereby a two-valued solution exists, and the broader the h range whereby the figure has only concave boundaries.

Now we revert to the general case when the total current flowing through the plasma is nonzero ($g \neq 0$). Here the situation is more complicated and a wholly satisfactory representation is possible only in the plane of two parameters t_1, g [56]. The main results in this case are as follows. When the plasma current flows in the same direction as the currents flowing along the conductors ($g > 0$), a solution of the problem exists if the h parameter satisfies the conditions $h_{\min} < h < h_{\max}$, where $h_{\min}$ and $h_{\max}$ are functions of g. But when the plasma current and the external current are oppositely directed ($g < 0$), for g smaller than $g_{\min} \approx -0.3$ no stationary equilibrium configurations exist, no matter what the h parameter value may be (i.e. whatever the pressure). Examples of equilibrium geometries for different values of h and g are given in Fig. 12. In particular, for not-too-high values of the h parameter and a sufficiently large value of g the resulting configuration has the appearance of an arbitrarily thin current sheath lying in the (x, z) plane. Its horizontal dimension is limited by the conductor separation.

We have considered systems in which the magnetic field is induced by the currents flowing in one direction and has only closed separatrices. When differently directed currents are admitted, the simplest system of interest is the system of four currents, with the direction changing in checkerboard order. This system (it would be natural to identify it as a quadrupole if the total current is zero) is well known in connection with research on antimirror traps. An important quadrupole's distinction from the doublet etc. is that now the separatrices go to infinity. Here we briefly consider (for the sake of completeness of information) the main results that were obtained for this system employing the method used above.

Let the currents with $j = 1$ be located at the points $z = z_1$ ($|z_1| = 1$) and $z = z_4 = -z_1$ while the currents with $j = -1$ at the points $z = z_2 = z_1^*$ and $z = z_3 = -z_1^*$ (the asterisk signifies complex conjugation). The points in the t plane are t_1, $t_2 = t_1^*$, $t_3 = -t_1^*$, and $t_4 = -t_1$. Then the complex potential of the magnetic field as a function of t is given by the following expression:

$$F(t) = \frac{1}{2\pi \mathrm{i}} \left[\ln \frac{(t - t_1)(t + t_1)(t_1 t - 1)(t_1 t + 1)}{(t - t_1^*)(t + t_1^*)(t_1^* t - 1)(t_1^* t + 1)} + 2 \ln \frac{t_1^*}{t_1} \right]. \tag{6.16}$$

Constructing the $\zeta(t)$ function (the quadrupole's total current and dipole moment are equal to zero) gives

$$\zeta(t) = \frac{(t_1^{2*} t^2 - 1)(t_1^2 t^2 - 1)}{(t^2 - t_1^2)(t^2 - t_1^{2*}) t^3}. \tag{6.17}$$

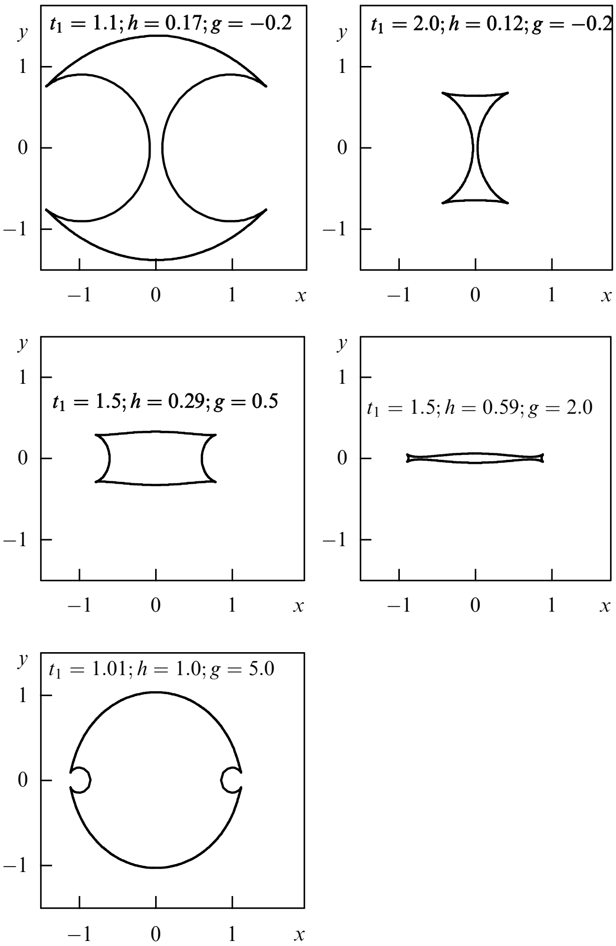

Figure 12. Examples of equilibrium geometries for a nonzero plasma current ($g \neq 0$).

After rather lengthy calculations we obtain Eqn (6.12), where

$$\begin{aligned} \Pi(t, t_1) = {} & \frac{|t_1|^4 - 1}{\pi \mathrm{i} (t_1^2 - t_1^{2*})} \left[\frac{(t_1^2 - t_1^{2*})^2}{|t_1|^8}\, t + \frac{t_1^4 - 1}{2 t_1^4} \frac{t}{t_1^2 t^2 - 1} \right. \\ & + \frac{t_1^{4*} - 1}{2 t_1^{4*}} \frac{t}{t_1^{2*} t^2 - 1} + \frac{3 t_1^4 - 7}{4 t_1^5} \ln \frac{t_1 t + 1}{t_1 t - 1} \\ & + \frac{3 t_1^{4*} - 7}{4 t_1^{5*}} \ln \frac{t_1^* t + 1}{t_1^* t - 1} \\ & \left. + \frac{|t_1|^4}{t_1^2 - t_1^{2*}} \left(\frac{t_1^4 - 1}{t_1^7} \ln \frac{t_1 t + 1}{t_1 t - 1} - \frac{t_1^{4*} - 1}{t_1^{7*}} \ln \frac{t_1^* t + 1}{t_1^* t - 1} \right) \right]. \end{aligned} \tag{6.18}$$

Next we restrict ourselves to the case of a symmetric quadrupole, when $x_1 = y_1$. Analyzing (6.18) leads to the following conclusions.

The solution of the problem for the quadrupole does not exist if $h > h_{\max} \approx 0.31$. For $h \leqslant h_{\max}$, a unique solution exists. The figure boundaries (its general view is well known) are always concave. With increasing h, the dimensions of the figure increase, and for $h = h_{\max}$ the ultimate figure of unit size in x and y (in our units $x_1 = y_1 = 1/2^{1/2} \approx 0.7$) is realized.

More complex systems can comprise currents of different sense and magnitude located at arbitrary points. Separatrices going to infinity and closed ones may exist simultaneously. The large number of parameters and the complex geometries of the vacuum magnetic field hinder the efficient implementation of the above analytical approach even in the two-dimensional case.

6.2 The force between the conductors (myxines)

In connection with the above-given exact solutions of several problems on equilibrium geometries, we can pose the problem of the force of interaction between the conductors in the presence of a plasma. We consider this issue by the example of the doublet problem for $g = 0$ [59]. Dimensional quantities will be used here.

Let $\mathbf{B}_\mu$ be the magnetic field strength induced at the point $x = x_0$, $y = 0$ (the position of the right-hand conductor) by plasma currents and by the current of the left-hand conductor. From Eqns (6.9)–(6.13) we obtain $\mathbf{B}_\mu = (0, B_y)$, where

$$B_y = \frac{\pi h J_0}{c x_0 t_1^2}\,(t_1^4 - 1)\,. \tag{6.19}$$

Hence it is evident that the force $\mathbf{f}$ acting on a section of the right-hand conductor of length L is determined by the following equalities:

$$\mathbf{f} = (f_x, 0)\,, \qquad f_x = -\frac{J_0 L}{c}\,B_y = -\frac{\pi J_0^2 L h}{c^2 x_0 t_1^3}\,(t_1^4 - 1)\,. \tag{6.20}$$

In the absence of plasma, this force is given by the expressions

$$\mathbf{f}^0 = (f_x^0, 0)\,, \qquad f_x^0 = -\frac{J_0^2 L}{c^2 x_0}\,. \tag{6.21}$$

Analyzing Eqns (6.20) and (6.21) suggests the following. The force of attraction of the myxines in the presence of a plasma is always smaller than in a vacuum. With stable configurations (concave figure boundaries), the force of attraction is attenuated more strongly, the greater the h parameter value. However, the force of attraction vanishes only for $t_1 \to 1 + 0$, i.e. for an unstable plasma configuration shielding the myxines completely.

7. Axisymmetric configurations

7.1 Equilibrium configurations in the hydrodynamic approximation

With axial symmetry, the MHD equilibrium equations (6.1) for ideal plasmas reduce (e.g. see Ref. [60]) to one scalar Grad–Shafranov (GSh) equation for the magnetic flux function Ψ. In the cylindrical coordinate system (r, θ, z) we have

$$\Psi = \int_0^r H_z \times 2\pi r\,\mathrm{d}r\,, \qquad H_r = -\frac{1}{2\pi r}\,\frac{\partial\Psi}{\partial z}\,, \qquad H_z = \frac{1}{2\pi r}\,\frac{\partial\Psi}{\partial r}\,. \tag{7.1}$$

The electric current density will be considered to have only an azimuth component ($j_r = j_z = 0$, $j_\theta \neq 0$) and, consequently, the magnetic field is poloidal ($H_\theta = 0$). Let $j_{\mathrm{ex}}(r, z)$ denote the given distribution of external azimuth currents. Then the GSh equation takes the form:

$$-\Delta^*\Psi = \frac{8\pi^2 r}{c}\,j_{\mathrm{ex}}(r, z) + 16\pi^3 r^2\,\frac{\mathrm{d}P}{\mathrm{d}\Psi}\,,$$

$$\Delta^*\Psi = r\,\frac{\partial}{\partial r}\,\frac{1}{r}\,\frac{\partial\Psi}{\partial r} + \frac{\partial^2\Psi}{\partial z^2}\,, \tag{7.2}$$

where $P(\Psi)$ is some prescribed function determining the dependence of the plasma pressure on the magnetic field.

We pursue the goal to obtain from Eqns (7.2) some axisymmetric analogs of the analytic solutions for plane systems (doublet, quadrupole) to start with. The corresponding vacuum fields are induced by two turns with the currents flowing in one direction (magnetic bottle) in the first case or with oppositely directed currents (magnetic antibottle) in the second. Let the whole system be placed in a perfectly conducting cylinder with radius $R_{\max}$ and length $2Z_{\max}$.

We go to the units of measurements well suited for the problem: the radius R_{c} of the current-carrying turn serves as the unit of length, the characteristic magnitude of the current density j_0 in the turn as the unit of current, the characteristic pressure value P_0 as the unit of pressure, and the quantity $8\pi R_{\mathrm{c}}^3 j_0/c$ as the unit of Ψ. In these units Eqns (7.2) become:

$$-r\,\frac{\partial}{\partial r}\,\frac{1}{r}\,\frac{\partial\Psi}{\partial r} - \frac{\partial^2\Psi}{\partial z^2} = r\,j_{\mathrm{ex}}(r, z) + \beta r^2\,\frac{\mathrm{d}P}{\mathrm{d}\Psi}\,, \tag{7.3}$$

with the dimensionless parameter

$$\beta = \frac{c^2 P_0}{4\pi R_{\mathrm{c}}^2 j_0^2}\,. \tag{7.4}$$

In view of symmetry the treatment of Eqn (7.3) is restricted to a halfcylinder $0 < z < Z_{\max}$.

In what follows three configurations of the vacuum magnetic field are studied: (1) a magnetic antibottle (Fig. 13a), (2) a magnetic bottle (Fig. 13b), (3) Galatea-A (Fig. 13c). Plotted in each drawing of Fig. 13 are, from top to bottom, the vacuum magnetic field, the field in the presence of the plasma, and the plasma pressure.

The boundary-value problems for equation (7.3) will be solved approximately, employing the finite difference method. We use a uniform square grid and the standard five-point difference approximation of the second-order elliptic differential operator Δ^*. The resulting system of nonlinear equations is solved by iterations, i.e. the solution of the difference boundary-value problem is in fact found by the relaxation of the solution of the transient problem for a heat conduction-type equation. The longitudinal-lateral scheme was used (e.g. see Ref. [61]).

The function $j_{\mathrm{ex}}(r, z)$, which determines the distribution of external azimuth currents, is defined as follows:

$$j_{\mathrm{ex}}(r, z) = \exp\left[-\frac{(r - r_{\mathrm{c}})^2 + (z - z_{\mathrm{c}})^2}{r_0^2}\right] + j_{\mathrm{b}}\exp\left[-\frac{(r - r_{\mathrm{b}})^2 + z^2}{r_0^2}\right].$$

In this formula, the points $(r_{\mathrm{c}}, z_{\mathrm{c}})$ and $(r_{\mathrm{b}}, 0)$ specify the positions of the 'point-like' currents and the r_0 parameter determines the 'spread' radius for these currents (for the first two configurations $j_{\mathrm{b}} = 0$).

The results of calculations in the case of a magnetic antibottle are presented first. The boundary conditions: $\Psi = 0$ at all boundaries. The geometric parameters: $Z_{\max} = R_{\max} = 2$, $z_{\mathrm{c}} = r_{\mathrm{c}} = 1$, $r_0 = 0.2$. The $P(\Psi)$ function was so selected that the plasma was located primarily near the zeros of the magnetic field and along the separatrices. That is why the following function form appears to be natural:

$$P(\Psi) = \exp\left(-\frac{\Psi^2}{\alpha^2}\right). \tag{7.5}$$

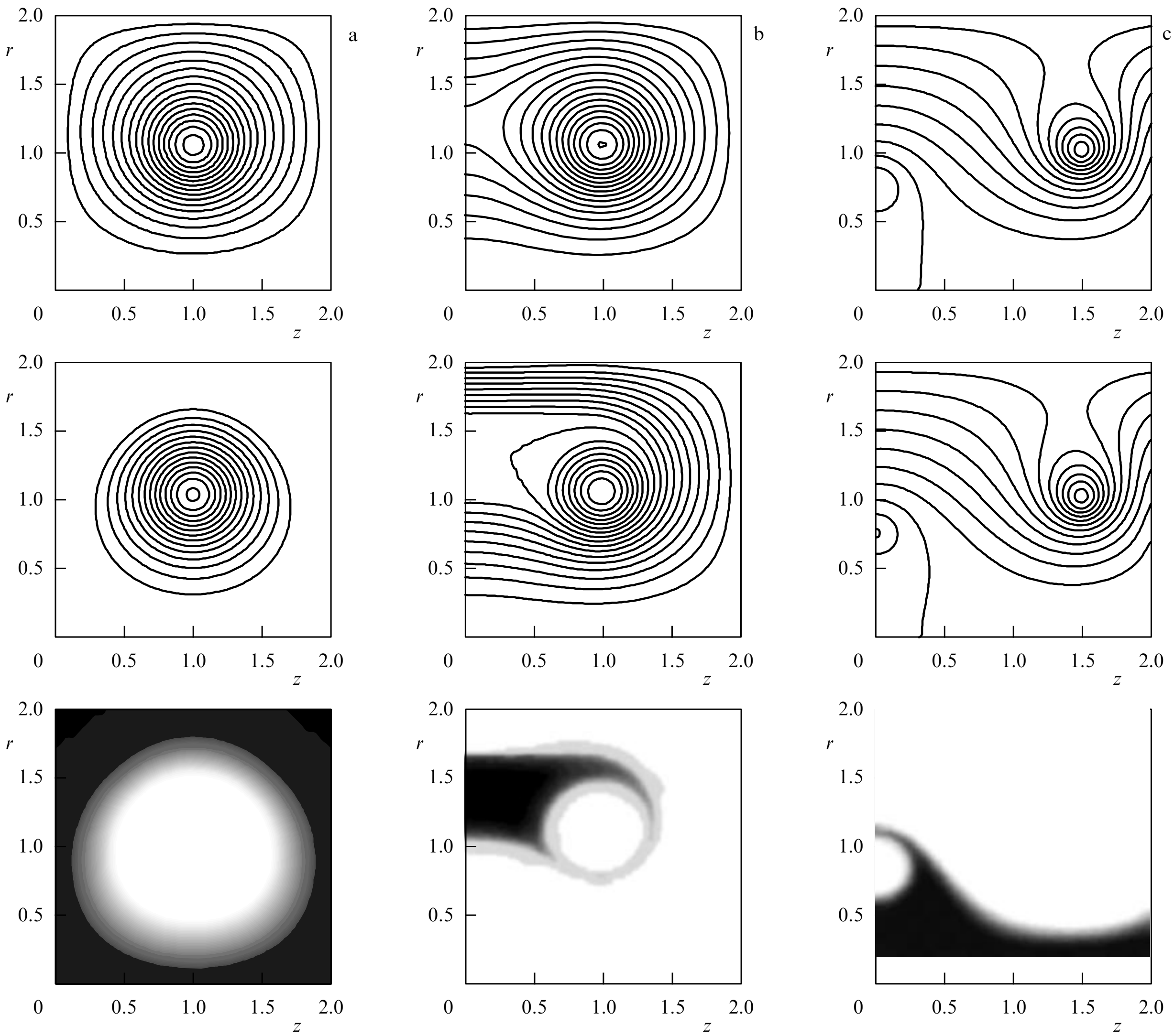

Figure 13. Distributions of the vacuum magnetic field, the magnetic field, and the plasma pressure for a magnetic antibottle (a), a magnetic bottle (b), and Galatea-A (c) in the (r, z) plane.

So, $P = 1$ for $\Psi = 0$ and decays with increasing Ψ. We will seek to obtain the minimum α parameter.

Shown in Fig. 13a are the lines of equal Ψ (magnetic field lines) for $\beta = 0$ (the vacuum configuration), for $\beta = 0.0003$ and $\alpha = 0.002$, and the lines of equal $P(\Psi)$. As is evident, in the presence of the plasma the magnetic field backs off the plasma region boundaries. The transition from $P = 1$ to $P \approx 0$ occurs in a rather thin layer which can be treated as the plasma – vacuum boundary.

Now consider the case of a magnetic bottle. Here the choice of the $P(\Psi)$ function is not that evident. Figure 13b displays the results of calculations of the vacuum configuration ($\beta = 0$) (the boundary conditions: $\partial\Psi/\partial z = 0$ for $z = 0$, $0 < r < R_{\max}$, and $\Psi = 0$ at the remaining boundaries). The vacuum magnetic field has a separatrix corresponding to $\Psi = \Psi_s \approx 0.02$. We therefore select $P(\Psi)$ in a form somewhat different from Eqn (7.5):

$$P(\Psi) = \exp\left(-\frac{(\Psi - \Psi_s)^2}{\alpha^2}\right). \tag{7.6}$$

Also plotted in Fig. 13b are the lines of magnetic field and pressure for $\beta = 0.0005$ and $\alpha = 0.001$. The formation of the region, where $\Psi \approx \Psi_s$, near the zero of the magnetic (vacuum) field is clearly visible. In this region $P \approx 1$, i.e. it is occupied by the plasma.

Qualitatively, the figure of the region (more exactly, the section of the region by the r, z plane) occupied by the plasma resembles the figure of equilibrium for a doublet (see Fig. 11). However, there is a significant distinction. Since the line $\Psi = \Psi_s$ bypasses the current region, the plasma region now surrounds the current and closes into itself in thin bridges around it.

And, finally, the third configuration (Galatea-A). In this case it would be convenient to add complexity to the formulation of the problem. Let a uniform longitudinal field H_{z0} be imposed on the magnetic field of three turns. Then the boundary conditions imposed on Ψ are as follows: $\partial\Psi/\partial z = 0$ (left boundary), $\Psi = 0$ (lower), $\Psi = \pi r^2 H_{z0}$ (right), $\Psi = \pi R_{\max}^2 H_{z0}$ (upper). Now solving (7.3) with $\beta = 0$ we so select the current j_b in the middle turn and the magnitude of the longitudinal field H_{z0} that the vacuum field has a separatrix bypassing the middle current and going into the system axis near the point $r = z = 0$. The parameter values $j_b = -0.5$ and $H_{z0} = 0.0006$ provide the required geometry of the magnetic field. The remaining parameters assume the values: $Z_{\max} = R_{\max} = 2$, $z_c = 1.5$, $r_c = 1$, $r_b = 0.75$, and $r_0 = 0.1$. Then, with $P(\Psi)$ of the form (7.5) (the separatrix goes into the axis, where $\Psi = 0$), we increase β.

The magnetic field and the pressure are shown in Fig. 13c for $\beta = 0.00003$ and $\alpha = 0.0002$. The plasma occupies the region near the axis and, in the form of a thin envelope, bypasses the central current (the myxine). In our opinion, it is precisely this type of configuration that holds the greatest interest today as regards pure theory and applications.

7.2 2-D stationary plasma configurations

The hydrodynamic models do not represent the structure of transition layers whose thicknesses are of the order of the ion Larmor radius in the cases of primary interest. Any consideration of such layers calls for a kinetic description of the ion and electron dynamics or at least for hybrid models, when ions are described kinetically and electrons in the context of hydrodynamics. Initially such layers were treated in the one-dimensional approximation. Noteworthy here is the Chapman–Ferraro model for the interaction of the solar wind with the Earth's magnetosphere [62]. A comprehensive analysis of one-dimensional collisionless kinetic configurations is given in Ref. [51]. A series of two-dimensional transition layers was calculated in Ref. [4].

Following [63] (also see Section 5.2) here we make an attempt to describe the general approach to the construction of consistently kinetic stationary configurations. To do this, we need the stationary kinetic equations for electrons and ions and the Maxwell equations:

$$\begin{aligned}
&\mathbf{v}\,\frac{\partial f_i}{\partial \mathbf{x}} + \frac{e}{M}\left(\mathbf{E} + \frac{1}{c}[\mathbf{v}, \mathbf{H}]\right)\frac{\partial f_i}{\partial \mathbf{v}} = 0\,,\\
&\mathbf{v}\,\frac{\partial f_e}{\partial \mathbf{x}} - \frac{e}{m}\left(\mathbf{E} + \frac{1}{c}[\mathbf{v}, \mathbf{H}]\right)\frac{\partial f_e}{\partial \mathbf{v}} = 0\,,
\end{aligned} \tag{7.7}$$

$$\operatorname{rot}\mathbf{H} = \frac{4\pi e}{c}\int \mathbf{v}(f_i - f_e)\,\mathrm{d}\mathbf{v}\,,$$

$$\operatorname{div}\mathbf{H} = 0\,, \qquad \mathbf{E} = -\nabla\Phi\,, \tag{7.8}$$

$$\Delta\Phi = -4\pi e\int (f_i - f_e)\,\mathrm{d}\mathbf{v}\,. \tag{7.9}$$

As in Section 7.1, we consider stationary axisymmetric plasma motion in a cylindrical coordinate system (r, θ, z) assuming the magnetic field to be poloidal and the electric currents to be toroidal:

$$\mathbf{H} = (H_r, 0, H_z)\,, \qquad \mathbf{j} = (0, j, 0)\,.$$

Then the equation for the magnetic flux function can be written in the following form:

$$\begin{aligned}
&\Delta^*\Psi = -\frac{4\pi r}{c}\,j\,,\\
&\Delta^*\Psi = r\,\frac{\partial}{\partial r}\,\frac{1}{r}\,\frac{\partial \Psi}{\partial r} + \frac{\partial^2 \Psi}{\partial z^2}\,.
\end{aligned} \tag{7.10}$$

In equations (7.10), $j = j_{ex} + j_{pl}$, where $j_{ex} = j_{ex}(r, z)$ is a given distribution of external currents and j_{pl} is the current density in the plasma. Depending on the model adopted for plasma representation, Eqns (7.10) can now be closed in different ways. If, for instance, the MHD model of the plasma equilibrium is used, the task reduces to the Grad–Shafranov equation with $j_{pl} = 8\pi^2 r\,\partial P/\partial\Psi$ (see Section 7.1), where $P(\Psi)$ (the plasma pressure) is a given function.

In the consistent kinetic description of ions and electrons, for the plasma current we obtain by definition

$$j_{pl} = e\int V_\vartheta (f_i - f_e)\,\mathrm{d}\mathbf{v}\,. \tag{7.11}$$

Then Eqns (7.7), (7.9), and (7.10) make up a complete self-consistent set of equations.

The assumption that the plasma is quasineutral simplifies the problem substantially:

$$\int f_i\,\mathrm{d}\mathbf{v} = \int f_e\,\mathrm{d}\mathbf{v}\,. \tag{7.12}$$

In essence, (7.12) serves as an additional equation to determine the potential Φ in lieu of Eqn (7.9). The closed set of equations is now made up by Eqns (7.7), (7.10), and (7.12).

The general solution of Eqns (7.7) is represented by arbitrary integrals of electron and ion motion in stationary electric Φ and magnetic Ψ fields. The complete collection of these integrals can be found only through a self-consistent problem solution. Under the circumstances (two-dimensional axisymmetric case), two integrals always exist. They are the integrals of energy and generalized angular momentum for ions and electrons:

$$\begin{aligned}
&\mathcal{E}_i = \frac{M\mathbf{V}^2}{2} + e\Phi\,, \qquad \mathcal{P}_i = MrV_\vartheta + \frac{e}{c}\,\Psi\,,\\
&\mathcal{E}_e = \frac{m\mathbf{V}^2}{2} - e\Phi\,, \qquad \mathcal{P}_e = mrV_\vartheta - \frac{e}{c}\,\Psi\,.
\end{aligned} \tag{7.13}$$

Let the functions $f_i = f_i(\mathcal{E}_i, \mathcal{P}_i)$ and $f_e = f_e(\mathcal{E}_e, P_e)$ be given. Then the expression for Φ as a function of r and Ψ can be obtained from Eqn (7.12):

$$\Phi = \Phi(r, \Psi)\,. \tag{7.14}$$

From (7.11) we obtain the expression for j_{pl} as a function of r and Ψ:

$$j_{pl} = j_{pl}(r, \Psi)\,. \tag{7.15}$$

So, in the *kinetic* case the problem reduces to the solution of one nonlinear elliptic equation

$$\Delta^*\Psi = -\frac{4\pi}{c}\,r\left[j_{ex}(r, z) + j_{pl}(r, \Psi)\right]. \tag{7.16}$$

Now consider the *hybrid* model. The dynamics of ions are determined by their distribution function $f_i = f_i(\mathcal{E}_i, \mathcal{P}_i)$ as before while electrons obey the hydrodynamic equation of motion. Assuming an infinite conductivity and a zero electron mass, the equation can be written as

$$\nabla P_e + en\left(\mathbf{E} + \frac{1}{c}[\mathbf{V}_e, \mathbf{H}]\right) = 0\,. \tag{7.17}$$

Let us assume that $P_e = P_e(n)$. We introduce the functions $W(n) = \int \mathrm{d}P_e/n$, electron enthalpy, and $\Phi_T = \Phi - (1/e)W$, the thermalized potential. From Eqn (7.17) it follows that $\Phi_T = \Phi_T(\Psi)$. The expression for the azimuth electron velocity is also easily obtainable:

$$V_e = cr\,\frac{\mathrm{d}\Phi_T}{\mathrm{d}\Psi} \equiv V_e(r, \Psi)\,. \tag{7.18}$$

Now let the functions $\Phi_T(\Psi)$ and $f_i(\mathcal{E}_i, \mathcal{P}_i)$ be prescribed. Then the current j_{pl} is calculated as follows.

We have the relationships

$$n = \int f_i(\mathcal{E}_i, \mathcal{P}_i)\, d\mathbf{V} \equiv n(r, \Phi, \Psi)\,, \qquad \Phi = \Phi_T(\Psi) + \frac{1}{e}\, W(n)\,.$$

With these, Φ and n are expressed as functions of r and Ψ:

$$n = n(r, \Psi)\,, \qquad \Phi = \Phi(r, \Psi)\,. \tag{7.19}$$

Next we calculate the azimuth component of the ion current

$$j_i = e \int V_\theta f_i(\mathcal{E}_i, \mathcal{P}_i)\, d\mathbf{V} \equiv j_i(r, \Psi) \tag{7.20}$$

and, finally, the plasma current

$$j_{pl}(r, \Psi) = j_i(r, \Psi) - en(r, \Psi) V_e(r, \Psi)\,. \tag{7.21}$$

Once again, the problem reduces to the solution of one equation of the type (7.16). Once $\Psi(r, z)$ has been determined from it, we find n, Φ, P_e, etc. as functions of r and z.

The equation resulting in the context of both the kinetic and hybrid approaches resembles the Grad – Shafranov equation. However, with the GSh equation prescribing only one function $P(\Psi)$ of one variable would suffice (in the presence of only the poloidal field) while two functions are required now — $f_i(\mathcal{E}_i, \mathcal{P}_i)$ and $f_e(\mathcal{E}_e, \mathcal{P}_e)$ in the context of the kinetic model or $f_i(\mathcal{E}_i, \mathcal{P}_i)$ and $\Phi_T(\Psi)$ in the hybrid one.

The main physical complication associated with the treatment of Eqn (7.16) is that the form of these function is not easily selected *a priori*. It may well be that some 'test firing' would be required to obtain the required configuration. To conclude the general discussion concerning the approach proposed for calculating kinetic and hybrid axisymmetric configurations, we emphasize that only configurations with a poloidal field can be studied to advantage in the framework of this approach.

Next we commence considering Eqn (7.16) with the hybrid model intending to realize the 'crustal'-type configurations with $\beta \approx 1$ and the transition layers with thicknesses of the order of an ion Larmor radius.

7.3 The hybrid model [64]

Consider (also see Section 7.1 and Fig. 13b) the configuration of a vacuum magnetic field induced by two circular turns with current J_0, radius r_c, and separation $2z_c$. In Section 7.1 such a configuration was studied on the basis of the Grad – Shafranov equation.

To determine the right-hand part of Eqn (7.16), we should specify the functions $f_i(\mathcal{E}_i, \mathcal{P}_i) = f(\mathcal{E}, \mathcal{P})$, $\Phi_T(\Psi)$, and $P_e(n)$. For simplicity the electrons are assumed to be isothermal, i.e. $P_e(n) = T_e n$, $T_e = \text{const}$. Accordingly, $W(n) = T_e \ln n$. In this case, the functions $n(r, \Psi)$ and $\Phi(r, \Psi)$ in Eqns (7.19) are defined explicitly and analytically.

The ion distribution function is given by the following expression:

$$f(\mathcal{E}, \mathcal{P}) \propto \exp\left[-\frac{\mathcal{E}}{T_i} - \frac{(\mathcal{P} - \mathcal{P}_0)^2}{D^2}\right], \tag{7.22}$$

where $T_i = \text{const}$, $D = \text{const}$, and $\mathcal{P}_0 = \text{const}$ are parameters.

As in Section 7.1, we assume that the entire system is placed in a perfectly conducting cylindrical casing with length $2Z_{max}$ and radius R_{max}, and that the system as a whole is symmetric with respect to the $z = 0$ plane. Then Eqn (7.16) is solved in the region $0 \leqslant z \leqslant Z_{max}$, $0 \leqslant r \leqslant R_{max}$.

The boundary conditions on Ψ are as follows: $\Psi = 0$ for $r = 0$, $r = R_{max}$, and $z = Z_{max}$; $\partial\Psi/\partial z = 0$ for $z = 0$. We also note here the normalization conditions. It is assumed that $\Phi(0, 0) = 0$. Then, from the definition of $\Phi_T(\Psi)$ and in view of the condition $\Psi(0, 0) = 0$ it follows that $n(0, 0) = \exp\left[-e\Phi_T(0)/T_e\right]$. Since Eqns (7.7) and (7.17) are homogeneous respectively in f and n, we can put $n(0, 0) = 1$, and therefore $\Phi_T(0) = 0$.

Next we use 'dimensionless' units of measurements. The new units are r_c (the unit of length), T_i/e (the unit of potential), $J_0/\pi r_c^2$ (the unit of current density), $\Psi_0 = 4\pi J_0 r_c/c$ (the unit of Ψ), and $H_0 = \Psi_0/r_c^2$ (the unit of magnetic field).

Under the specified assumptions, the functions $n(r, \Psi)$ and $\Phi(r, \Psi)$ are written as

$$n(r, \Psi) = b(r)^{-1/[2(1+\alpha)]} \exp\left\{-\frac{1}{1+\alpha}\left[\Phi_T(\Psi) - v^2\varphi_0^2 + v^2\frac{(\Psi - \varphi_0)^2}{b(r)}\right]\right\}, \tag{7.23}$$

$$\Phi(r, \Psi) = \frac{1}{1+\alpha}\left[\Phi_T(\Psi) - \frac{\alpha}{2}\ln b(r) + \alpha v^2\varphi_0^2 - \alpha v^2\frac{(\Psi - \varphi_0)^2}{b(r)}\right], \tag{7.24}$$

where $b(r) = 1 + \mu^2 r^2$ and the dimensionless parameters α, β, v, μ, and φ_0 are expressed as follows in terms of the dimensional quantities involved in the statement of the problem:

$$\alpha = \frac{T_e}{T_i}\,, \qquad \beta = \frac{8\pi T_0}{H_0^2}\,, \qquad v = \frac{e\Psi_0}{cD}\,,$$
$$\mu = \frac{\sqrt{2MT}}{D}\, r_c\,, \qquad \varphi_0 = \frac{c\mathcal{P}_0}{e\Psi_0}\,. \tag{7.25}$$

The significance of these quantities is rather clear. For instance, the characteristic ion Larmor radius is $\rho_i = \mu/v$. Notice that the explicit dependence of $n(r, \Psi)$ and $\Phi(r, \Psi)$ on the r-coordinate vanishes for $\mu \to 0$.

With Eqns (7.23) and (7.24), we obtain the expression for the current j_{pl}:

$$j_{pl}(r, \Psi) = -\beta r\left[\frac{v^2}{b(r)}(\Psi - \varphi_0) + \frac{1}{2}\frac{d\Phi_T}{d\Psi}\right] n(r, \Psi)\,. \tag{7.26}$$

It remains to determine one more functional problem parameter, viz. the thermalized potential $\Phi_T(\Psi)$. It is assumed to be of the form:

$$\Phi_T(\Psi) = q_0(\Psi - 2q_1)\Psi\,, \tag{7.27}$$

where $q_0 = \text{const}$ and $q_1 = \text{const}$ are parameters. The problem definition is now complete.

The problem was solved numerically employing the technique outlined briefly in Section 7.1. A long series of calculations was performed with different values of the parameters (7.25) and (7.27). According to the calculations, there exists a great qualitative diversity in the behavior of the stationary solutions in the model under consideration. In particular, this is true both of the density distributions and of

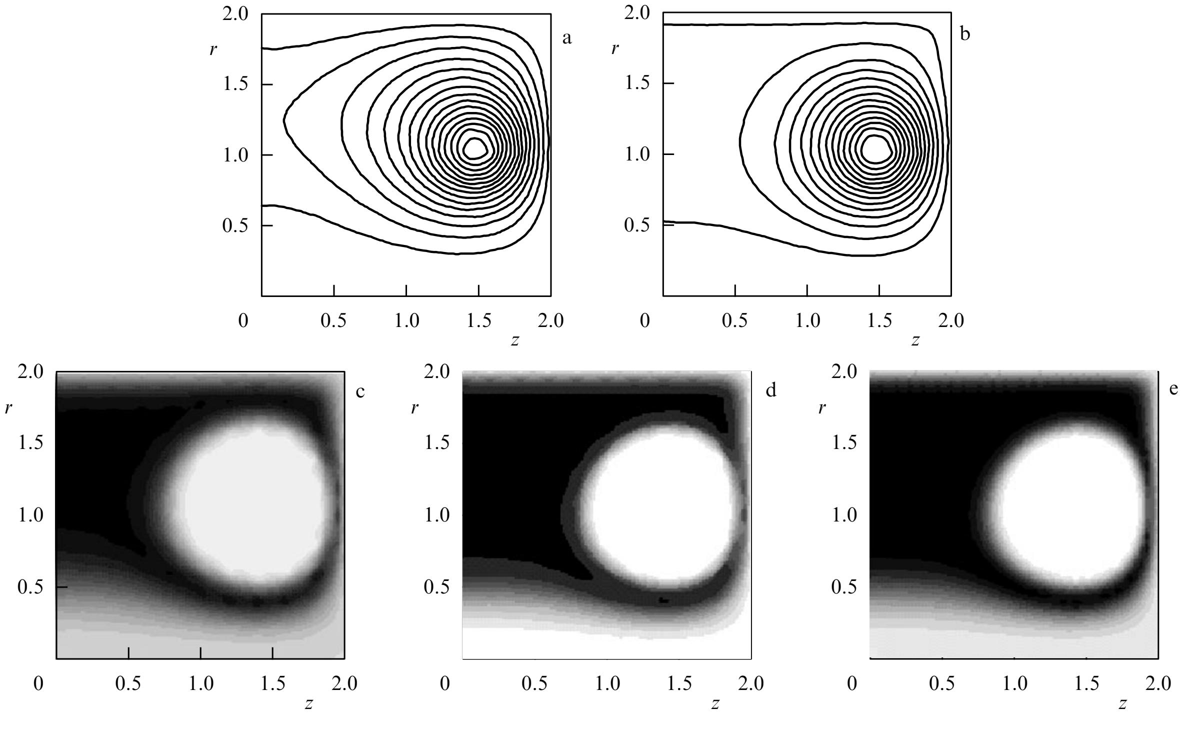

Figure 14. Distribution [in the (r, z) plane] of the vacuum magnetic field (a), the magnetic field (b), and the plasma pressure in the hybrid model (the electron case) (c), the hybrid model (the ion case) (d), and the kinetic model (e).

the resulting magnetic field configurations. One legitimate question is: are there such solutions among the solutions in the context of this model that are close, as regards their qualitative features, to the solutions obtained in the context of the GSh equation for the same configurations of the vacuum magnetic field? The cases in point are the solutions wherein the plasma is localized near the separatrices of this field.

The vacuum magnetic field is depicted in Fig. 14a for $R_{\max} = 2$, $Z_{\max} = 2$, $r_c = 1$, and $z_c = 1.5$. In the $\Psi = 0$ axis, $\Psi = \Psi_s \approx 0.092$ corresponds to a separatrix.

The Ψ-dependences of $j_{pl}(r, \Psi)$ and $n(r, \Psi)$ are rather complex, and therefore it is not easy to envision even the qualitative features of behavior of $\Psi(r, z)$ associated with the solutions of Eqn (7.16). The situation becomes somewhat simpler when the magnetic field configuration is qualitatively similar to the configuration of the vacuum field. This condition is assumed to be fulfilled.

Here we consider the results of two calculations in which the configurations of interest were realized in two different ways. Roughly speaking, in the first case this was accomplished through electrons and in the second one through ions.

We begin with the first version. Let $\varphi_0 = 0$. A consideration of the $n(r, \Psi)$ function prompts the $\Phi_T(\Psi)$ function form itself and the magnitudes of its parameters. For the plasma density to be maximum for $\Psi \approx \Psi_s$ and to drop sharply with distance away from the $\Psi = \Psi_s$ line, $\Phi_T(\Psi)$ should be at a negative minimum, sufficiently large in modulus, for $\Psi \approx \Psi_s$. Let $q_1 = \Psi_s$. Then $\Phi_T(\Psi_s) = -q_0 \Psi_s^2$. If q_0 is a sufficiently large quantity, the desired density distribution can be expected.

Let $\alpha = 1$, $\beta = 0.01$, $\nu = 0.1$, $\mu = 0.1$, and $q_0 = 5 \times 10^2$. If the pertinent magnetic field (Fig. 14b) is compared with the vacuum field, we notice that qualitative changes show up only in the domains near the separatrix of the vacuum field. It is as if the magnetic lines of force move apart near the separatrix. The density distribution (levels of the $n(r, z) \equiv n(r, \Psi(r, z))$ function) is given in Fig. 14c. The density peaks near the zero of the vacuum magnetic field and in the region adjacent to its separatrix. The minimum density values are attained in the system axis, at the side and end walls of the cylindrical casing, and in the domain enclosing the external current. Qualitatively, the pattern is similar to what was obtained on the basis of the GSh equation (see Section 7.1).

We now turn to the second case. Let $\varphi_0 \neq 0$, and let the electrons be immobile (for simplicity): $\Phi_T(\Psi) \equiv 0$. A consideration of formulas (7.23) and (7.26) suggests the following conclusions. For the density to be maximum for $\Psi \approx \Psi_s$ as before, it is required that $\varphi_0 \approx \Psi_s$ and that the parameter ν be sufficiently large. Let $\alpha = 1$, $\beta = 0.01$, $\nu = 25$, $\mu = 0.1$, and $\varphi_0 = \Psi_s = 0.092$. The magnetic field in this case is virtually the same as in the first version. The pressure distribution is given in Fig. 14d. As before, the pressure is maximum near the separatrix. The electron current is zero and, consequently, the result is entirely due to the ion current.

In the first (electron) case, the characteristic ion Larmor radius is $\rho_i = \mu/\nu = 1$. In the second (ion) case $\rho_i = 0.004$. The way to obtain the required configuration of the solution in the 'mixed' case, when the electron and ion currents are of the same order of magnitude, is rather clear.

To gain a clearer view of the ion confinement mechanisms in the cases considered above (ultimate, in a sense), there is good reason to analyze the distribution of the potential $\Phi(r, z)$. In the region adjacent to the external current ($z_c = 1.5$) the potential has a maximum in the first case and a minimum in the second. Hence, the ion confinement in the first case is primarily electrostatic in nature.

7.4 The kinetic model

Now consider briefly an example of how the general approach to the studies of axisymmetric stationary configurations, set forth in Section 7.2, is employed when the kinetic model is used both for electrons and for ions.

From the quasineutrality condition (7.12) we have

$$n_{\mathrm{i}}(r, \Phi, \Psi) = n_{\mathrm{e}}(r, \Phi, \Psi)\,.$$

Hence we find the potential $\Phi(r, \Psi)$ as a function of r and Ψ. Substituting it into the expressions for the electron and ion currents, we obtain the azimuth plasma current as a function of r and Ψ:

$$j_{\mathrm{e,i}}(r, \Psi) = \mp e \int V_\theta f_{\mathrm{e,i}}(\mathcal{E}_{\mathrm{e,i}}, \mathcal{P}_{\mathrm{e,i}})\,\mathrm{d}\mathbf{V}\Big|_{\Phi=\Phi(r,\Psi)}\,,$$

$$j_{\mathrm{pl}}(r, \Psi) = j_{\mathrm{e}}(r, \Psi) + j_{\mathrm{i}}(r, \Psi)\,. \tag{7.28}$$

We specify the distribution functions for either component, as in Eqns (7.13) and (7.22), with parameter values of their own ($T_{\mathrm{i,e}} = \mathrm{const}$, $D_{\mathrm{i,e}} = \mathrm{const}$, and $\mathcal{P}_{\mathrm{i,e0}} = \mathrm{const}$):

$$f_{\mathrm{e,i}}(\mathcal{E}_{\mathrm{e,i}}, \mathcal{P}_{\mathrm{e,i}}) \propto \exp\left[-\frac{\mathcal{E}_{\mathrm{e,i}}}{T_{\mathrm{e,i}}} - \frac{(\mathcal{P}_{\mathrm{e,i}} - \mathcal{P}_{\mathrm{e,i0}})^2}{D_{\mathrm{e,i}}^2}\right]. \tag{7.29}$$

With this selection of the functions, the calculations yield the following expressions for the required functions (we use the same units of measurements as in Section 7.3):

$$\Phi(r, \Psi) = \frac{1}{1+\alpha}\left[v_{\mathrm{i}}^2\varphi_{\mathrm{i}}^2 - v_{\mathrm{e}}^2\varphi_{\mathrm{e}}^2 + \frac{1}{2}\ln\frac{b_{\mathrm{e}}(r)}{b_{\mathrm{i}}(r)} + v_{\mathrm{e}}^2\frac{(\Psi+\varphi_{\mathrm{e}})^2}{b_{\mathrm{e}}(r)} - v_{\mathrm{i}}^2\frac{(\Psi-\varphi_{\mathrm{i}})^2}{b_{\mathrm{i}}(r)}\right],$$

$$n(r, \Psi) = b_{\mathrm{i}}(r)^{-1/[2(1+\alpha)]}\, b_{\mathrm{e}}(r)^{-\alpha/[2(1+\alpha)]} \times \exp\left\{\frac{\alpha v_{\mathrm{e}}^2}{1+\alpha}\left[\varphi_{\mathrm{e}}^2 - \frac{(\Psi+\varphi_{\mathrm{e}})^2}{b_{\mathrm{e}}(r)}\right] + \frac{v_{\mathrm{i}}^2}{1+\alpha}\left[\varphi_{\mathrm{i}}^2 - \frac{(\Psi-\varphi_{\mathrm{i}})^2}{b_{\mathrm{i}}(r)}\right]\right\},$$

$$j_{\mathrm{e}}(r, \Psi) = -\beta_{\mathrm{e}} v_{\mathrm{e}}^2 \frac{r}{b_{\mathrm{e}}(r)}(\Psi + \varphi_{\mathrm{e}})\,n(r, \Psi)\,,$$

$$j_{\mathrm{i}}(r, \Psi) = -\beta_{\mathrm{i}} v_{\mathrm{i}}^2 \frac{r}{b_{\mathrm{i}}(r)}(\Psi - \varphi_{\mathrm{i}})\,n(r, \Psi)\,, \tag{7.30}$$

in which the following dimensionless parameters appear [also see Eqn (7.25)]:

$$\beta_{\mathrm{e,i}} = \frac{8\pi T_{\mathrm{e,i}}}{H_0^2}\,,\qquad v_{\mathrm{e,i}} = \frac{e\Psi_0}{cD_{\mathrm{e,i}}}\,,\qquad \mu_{\mathrm{e,i}} = \frac{\sqrt{2m_{\mathrm{e,i}}T_{\mathrm{e,i}}}}{D_{\mathrm{e,i}}}\,r_{\mathrm{c}}\,,$$

$$\varphi_{\mathrm{e,i}} = \frac{c\mathcal{P}_{\mathrm{e,i0}}}{e\Psi_0}\,,\qquad \alpha = \frac{\beta_{\mathrm{e}}}{\beta_{\mathrm{i}}}\,, \tag{7.31}$$

where $b_{\mathrm{e,i}}(r) = 1 + \mu_{\mathrm{e,i}}^2 r^2$.

Here we consider the results of only one calculation made for the same vacuum configuration as in the case of a hybrid model. Let

$$\beta_{\mathrm{e,i}} = 0.01\,,\qquad v_{\mathrm{e}} = 0.01\,,\qquad v_{\mathrm{i}} = 25\,,\qquad \mu_{\mathrm{e}} = 0.01\,,$$

$$\mu_{\mathrm{i}} = 0.1\,,\qquad \varphi_{\mathrm{e}} = 0\,,\qquad \varphi_{\mathrm{i}} = \Psi_{\mathrm{s}} \approx 0.092\,. \tag{7.32}$$

Shown in Fig. 14e is the pressure distribution corresponding to this set of parameters. Evidently, if no significance is attached to some quantitative details of these distributions, the general qualitative pattern of plasma distribution is the same as for the hybrid model, i.e. we arrive once again at a 'crustal'-type configuration with a sharp plasma – vacuum boundary.

8. Galatea-Belt

8.1 Basic diagram

A natural extension of the family of classical toroidal multipole traps, in which only 'diamagnetic' currents flow (i.e. the net azimuth current through the (r, z) plane is zero), are configurations in which an azimuth current exists. A configuration of this kind is sketched in Fig. 4c. It has received the name Galatea-Belt. In appearance, it resembles a toroidal quadrupole with a central core, the reversal of magnetization of which gives rise to an azimuth current in the plasma. If the magnetic field induced by the current is commensurable with the magnetic field of the conductors inducing the initial quadrupole field, there appears a 'current' sheath often termed 'neutral.' Consequently, the plasma in a toroidal system assumes the configuration of a tape — a 'belt,' its mantles being engaged with the myxines.

A Galatea-Belt offers a number of obvious advantages: (1) this is a system with $\beta_0 = 1$; (2) the plasma in the belt can heat up well since the plasma layer thickness is relatively small, which increases its resistance and enhances the Joule heat release for the same azimuth current; (3) when the azimuth current decays, the plasma configuration is not disrupted but transforms into a simple multipole configuration; (4) numerous experiments to be mentioned below are indicative of the high stability of the current sheaths; (5) an installation with a belt is free of longitudinal magnetic field coils, which notably decreases the trap mass, corrects the overload of the diverter plates, and simplifies the pellet injection.

Along with these advantages, a system with a belt has some disadvantages. Noteworthy among them are the following: (1) when the core magnetization is reversed, the induced electromotive force acts not only on the plasma but on the myxine as well, and appropriate 'matching' will probably be required; (2) as is known, there is hardly any skin effect in a tokamak owing to the self-rearrangement property of its configuration whereas in a belt it may arise, substantially complicating the problem of ohmic heating.

Needless to say, other advantages and disadvantages of the belt-type trap may show up in its practical implementation. However, there is little doubt that this configuration deserves closer study.

8.2 A brief note on the current sheaths

An interest in current sheaths was first displayed by astrophysicists in connection with the problem of solar flares. A significant contribution to the solution of the problems arising in this context was made by S I Syrovatskiĭ: he instituted experimental studies of these sheaths supervised by A G Frank [65 – 67].

A sectional view of the TS-3 experimental facility is shown in Fig. 15a. A magnetic field of quadrupole geometry was induced by a system of straight current-carrying conductors located outside the chamber. The field varied virtually linearly with distance inside the chamber ($D = 10$ cm):

$$\mathbf{H} = h(y, x, 0), \qquad |H| = h|\mathbf{r}|. \tag{8.1}$$

The field gradient was variable between the limits $h = 0.4-3$ kG cm^{-1}. The initial plasma in the magnetic field was produced by an auxiliary theta-discharge which accomplished the breakdown of a neutral gas (helium or argon) filling the chamber at a pressure of $3 \times 10^{-3} - 5 \times 10^{-2}$ Torr. The initial plasma concentration was $n_e \approx 10^{14} - 10^{15}$ cm^{-3}. The electric current along the zero line of the magnetic field was generated by applying a pulsed voltage across two mesh electrodes introduced near the chamber ends; the electrode spacing filled with plasma was 40 cm. The halfperiod of the current through the plasma was $T/2 = 4.4$ µs and the peak current $I_z = 30-60$ kA. The halfperiod of the magnetic field was $T_m/2 = 400$ µs.

As follows from the experiments conducted in Ref. [66], the excitation of the electric current in the plasma directed along the zero line of the magnetic field gives rise to the formation of a plane current sheath in 0.3–1 µs, which separates the oppositely directed magnetic fields. The characteristic lateral sheath dimensions are: width $2\Delta x = 6-9$ cm, thickness $2\Delta y = 0.6-1$ cm, electric current density in the vicinity of the zero line $j_{z0} = 5-8$ kA cm^{-2}; the magnetic field component tangent to the sheath (for $x \approx 0$, $y \approx \Delta y = 0.6-1$ cm) was, as a rule, $H_x = 5-6$ kG. It was determined that the current sheath width $2\Delta x$, i.e. the largest of the two sectional dimensions, and the near-surface magnetic field H_x close to the middle of the sheath satisfy the simple theoretical relationships

$$\Delta x \approx \sqrt{\frac{4I_z}{ch}}, \tag{8.2}$$

$$H_x \leqslant h\Delta x \approx \sqrt{\frac{4I_z h}{c}} \tag{8.3}$$

over a broad range of experimental conditions. Hence, in the quadrupole magnetic field with a zero line a plasma configuration forms with $\beta \approx 1$, where

$$\beta = \frac{8\pi n_e (T_e + T_i/\bar{Z}_i)}{H_x^2}. \tag{8.4}$$

Under typical conditions, within the current sheath $n_e = 10^{16}$ cm^{-3} and $T_e + T_i/\bar{Z}_i \approx 50$ eV. In this case, inside the sheath $T_i > T_e$ ($T_i = 30-100$ eV, $T_e = 10$ eV).

The unexpected result obtained in the studies of the structure of magnetic fields of current sheaths and the electron concentration distributions was that the sheaths were found to be highly stable relative to the tearing instability growth. Indeed, the structure of the magnetic field, the distribution of electric current, as well as the uniform (along the sheath width) distribution of electron concentration remained virtually constant for a relatively long time period of the order of several microseconds, even though the reciprocal of the increment of the resistive tearing instability growth was $(1-2) \times 10^{-7}$ s in the context of the experiments under review.

There is good reason to attempt to use these properties of the current sheaths, which are formed in magnetic fields with zero lines, in the development of new magnetic traps with $\beta_0 = 1$. The first experiments with the belt configuration were conducted employing the UP-1 facility (Fig. 15b), similar to

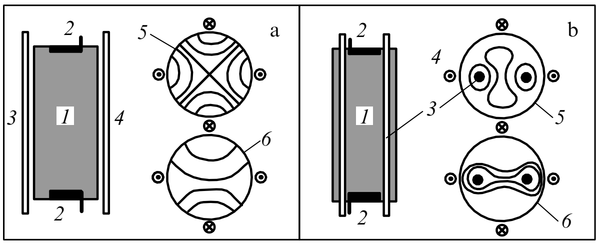

Figure 15. Rectilinear discharge devices with a current sheath and the different types of magnetic configuration. (a) — Longitudinal section of the discharge chamber of the TS-3 facility (at the left): *1* — fused silica tube with an internal diameter of 17 cm; *2* — mesh electrodes; *3*, *4* — external conductors. On the right: *5* — vacuum magnetic configuration; *6* — magnetic configuration when the discharge current in the plasma is aligned with the currents in the myxines. (b) Longitudinal section of the discharge chamber of the UP-1 facility (on the left): *1* — fused silica tube with an internal diameter of 17 cm; *2* — mesh electrodes; *3* — myxines; *4* — external conductors. On the right: *5* — configuration in the case that the current in the plasma is aligned with the current in the myxines, *6* — configuration in the case that the current in the plasma is in opposition to the current in the myxines.

TS-3, with the current-carrying conductors placed inside the vacuum chamber. The facility and the results obtained are described comprehensively in Section 8.4. Here we emphasize that there is a significant distinction between the configurations of the TS-3 and UP-1 facilities. If the direction of the TS-3 discharge current is reversed (with retention of direction of the current through external conductors), the current sheath will only rotate through 90°. Doing this on the UP-1 facility would cause a significant rearrangement of the configuration (Fig. 15b). If the current J_p through the plasma is aligned with the current through the myxines, the operating mode will be termed the 'α-mode.' If the currents are in opposition, the mode will be termed the 'β-mode.' We are concerned primarily with the α-mode because in this case the region of zero magnetic field is larger and more stable.

8.3 Static belt models

8.3.1 Formulation of the problem. Plane models of the belt with a δ-like plasma-field transition layer were considered in Section 6. Now we construct the MHD models on the basis of the GSh equation [68]. However, this way of constructing static models has a fundamental disadvantage — it requires that the magneto-baric function $P(\Psi)$ be specified *a priori*. It is clear that the form of these functions is actually determined only through the configuration formation. In doing this we will nevertheless remain within the framework of the GSh equation and consider it with model $P(\Psi)$ functions. Despite the conventionality of this approach, it yields useful information on the most general properties of the configurations we are interested in. Considering the limitedness of such an approach, we will restrict ourselves to ultimately simple models. In particular, only plane models in the (x, y)-coordinates will be treated in what follows. To do so, we first have to select the magneto-baric characteristics.

The class of model $P(\Psi)$ functions is defined by four conditions (Fig. 16a):

(1) the field in the center of the system must be zero ($x = y = 0$). Here we put $\Psi(0, 0) = 0$;

(2) the pressure should vanish or decay rapidly for $x^2 + y^2 > R_*^2$, where $R_* \geqslant 2a$ (here a is the distance of the myxine to the center of the configuration);

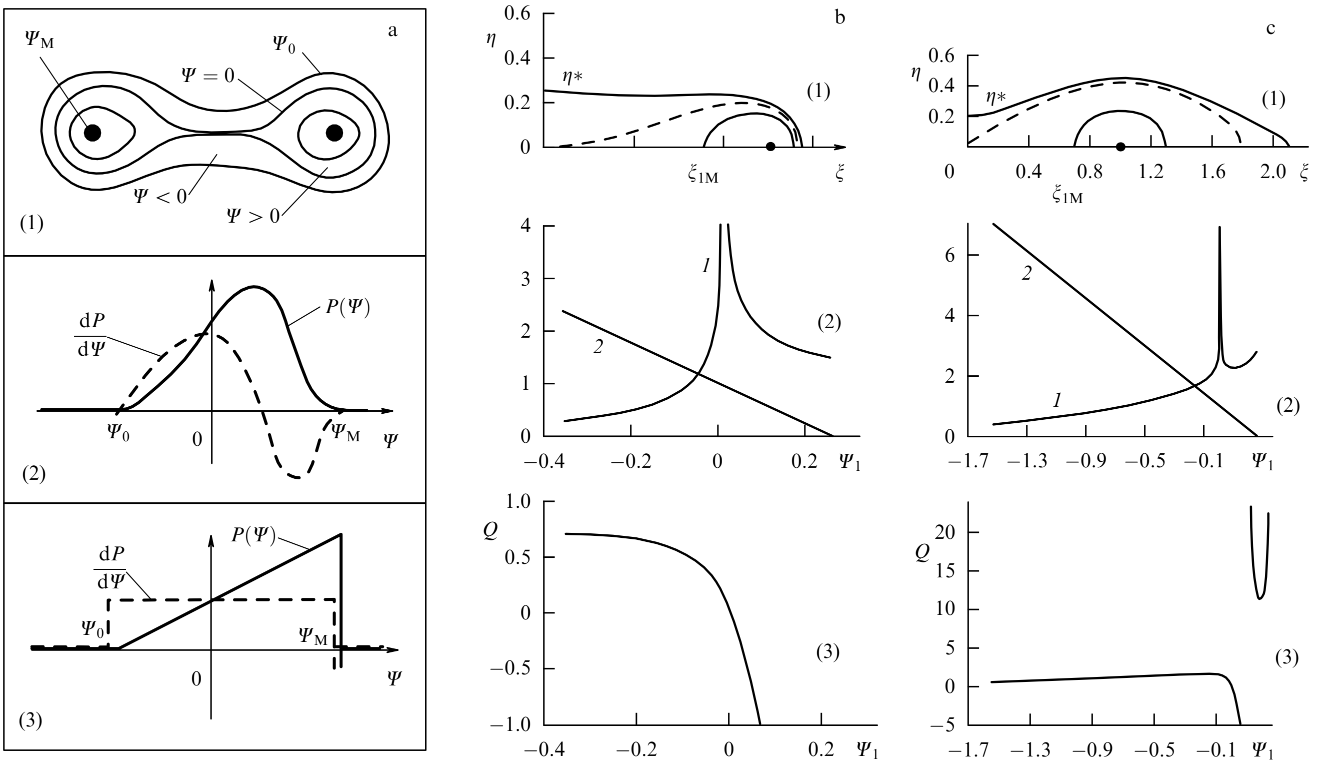

Figure 16. Calculation of the plane configurations. (a) (1) — diagram of an α-type magneto-plasma configuration; (2) — typical form of the magneto-baric function $P(\Psi)$ and the current density j_z; (3) the $P(\Psi)$ function in the form of a linear spline, taken for calculation, and the corresponding current density. (b) (1) — typical form of the magnetic belt configuration for $\lambda = 2$, $\mu = 4$; (2) — $U(\Psi)$ (curve *1*) and the dimensionless pressure (curve *2*) as functions of the dimensionless flux; (3) — $Q(\Psi)$ for the same λ and μ. (c) (1) — magnetic configuration of the belt in the double equilibrium regime ($\lambda = -0.5$, $\mu = 4$), (2) — $U(\Psi)$ (curve *1*) and the dimensionless pressure (curve *2*) as functions of the dimensionless flux; (3) — $Q(\Psi)$ for the same λ and μ.

(3) P should become zero in the neighborhood of the myxines, i.e. for $(x-a)^2 + y^2 < R_\mu^2$;

(4) the peak of the current density should be located at the center.

Assuming the current through the myxine to be directed along the z-axis and considering that the separatrix passes through the origin, where we put $\Psi = 0$, we obtain that $\Psi > 0$† inside the separatrix and $\Psi < 0$ outside it.

It follows from the foregoing that the magneto-baric characteristic and its associated current density $j_z = c\,dP(\Psi)/d\Psi$ should have the appearance of the curves plotted in Fig. 16a. The specific features of the curves are the decay of P and j_z as $\Psi \to \pm\infty$, the current density peak for $\Psi = 0$, and, in addition, the change of sign of the current density in the vicinity of the myxine ($\Psi > 0$). For the GSh equation to have simple analytical solutions, the dependence $P'(\Psi)$ should be linear. The curve plotted in Fig. 16a is far from linear, and therefore $P(\Psi)$ is conveniently approximated either by linear or by quadratic splines‡. Taking into account precisely the qualitative significance of the calculations conducted, here we consider in detail only the case of prescribing $P(\Psi)$ in the form of a linear spline [68]:

$$P(\Psi) = \begin{cases} 0\,, & \Psi < \Psi_0 < 0\,, \\ P_0\left(1 - \dfrac{\Psi}{\Psi_0}\right), & \Psi_0 < \Psi < \Psi_1\,, \\ 0, & \Psi > \Psi_1\,. \end{cases} \tag{8.5}$$

† The flux function of a single conductor is $\Psi = -(2J/c)\ln(r/b)$.

‡ The solutions of the GSh equation for the two specified cases are given in Ref. [24].

A compelling disadvantage of this approximation is the absence of current concentration in a narrow layer between the myxines. We can therefore say that the model with a linear spline represents only the current sheath itself. In what follows we employ the terms: 'belt' ($\Psi_0 < \Psi < \Psi_1$), magnetic sheath of a belt ($\Psi < \Psi_0$), magnetic sheath of a myxine ($\Psi > \Psi_1$). The GSh equations corresponding to these regions are of the form:

'belt'

$$\Delta\Psi = -4\pi P'(\Psi) - \frac{4\pi}{c} J_\mu\big[\delta(x+a) + \delta(x-a)\big]\delta(y)$$

$$= -\frac{4\pi}{c} j_0 - \frac{4\pi}{c} J_\mu\big[\delta(x+a) + \delta(x-a)\big]\delta(y)\,, \tag{8.6a}$$

where $j_0 = P_0 c/|\Psi_0| = \text{const}$, while $x = \pm a$ and $y = 0$ are the coordinates of the myxines;

magnetic sheath of a 'belt'

$$\Delta\Psi = 0\,, \tag{8.6b}$$

and magnetic myxine sheaths

$$\Delta\Psi_{(\pm)} = -\frac{4\pi}{c} J_\mu \delta(x \pm a)\delta(y)\,. \tag{8.6c}$$

Below we outline the results of an analysis of these equations performed in Ref. [68].

8.3.2. Morphology of the belts. The general solution of Eqn (8.6a) is of the form

$$\Psi = -\frac{J_\mu}{c}\left\{\ln\left[(x+a)^2+y^2\right]+\ln\left[(x-a)^2+y^2\right]\right\} - \frac{2\pi}{c}j_0y^2+\Psi_L\,, \qquad (8.7)$$

where Ψ_L is the general solution of the Laplace equation ($\Delta\Psi_L=0$). Following [68], we restrict ourselves to a particular solution of the form

$$\Psi_L = q(x^2-y^2)\,. \qquad (8.7a)$$

This expression describes the quadrupole field induced, for instance, by four conductors at infinity with alternating current directions.

Introducing the dimensionless variables

$$\xi=\frac{x}{a}\,,\qquad \eta=\frac{y}{a}\,,\qquad \Psi_1(\xi,\eta)=\frac{c}{J_\eta}\,\Psi\,,\qquad \lambda=\frac{cq}{J_\mu}\,,$$

we can write Eqn (8.7) as

$$\Psi_1 = -\left\{\mu\eta^2+\lambda(\xi^2-\eta^2) + \ln\left[\left((\xi+1)^2+\eta^2\right)\left((\xi-1)^2+\eta^2\right)\right]\right\}. \qquad (8.8)$$

Here $\mu=2\pi j_0a^2/J_\mu$. The product $\mu|\Psi_0|=2\pi a^2c^2P_0/J_\mu^2$ is in essence the β parameter calculated using the effective field $H_{\text{eff}}=J_\mu/ca$. According to expression (8.8) for Ψ, the morphology of the force lines in the belt is determined by the two parameters μ and λ. As shown by the analysis performed in Ref. [68], there is a great diversity of magnetic structures [even with the simplest form (8.7a)]. This analysis proceeded from locating the zero points of the magnetic field, i.e. the points where $\partial\Psi_1/\partial\xi=\partial\Psi_1/\partial\eta=0$. With Eqn (8.8), we find two equations

$$(\mu-\lambda)\bar\eta+\frac{\bar\eta}{(\bar\xi-1)^2+\bar\eta^2}+\frac{\bar\eta}{(\bar\xi+1)^2+\bar\eta^2}=0\,,$$
$$\lambda\bar\xi+\frac{\bar\xi-1}{(\bar\xi-1)^2+\bar\eta^2}+\frac{\bar\xi+1}{(\bar\xi+1)^2+\bar\eta^2}=0\,, \qquad (8.9)$$

which establish the relation between the $\bar\xi,\bar\eta$ coordinates of the zero points and the parameters μ, λ. The system (8.9) is linear in μ and λ for given $\bar\xi,\bar\eta$. The determinant of this system is $D=\bar\xi\bar\eta$, and therefore four essentially distinct solutions are possible in this case:

$$\begin{aligned}
&(1)\quad \bar\xi=\bar\eta=0\,,\qquad D=0\,,\\
&(2)\quad \bar\xi\equiv\bar\xi_2\neq0\,,\qquad \bar\eta=0\,,\qquad D=0\,,\\
&(3)\quad \bar\xi=0\,,\qquad \bar\eta\equiv\bar\eta_3\neq0\,,\qquad D=0\,,\\
&(4)\quad \bar\xi\equiv\bar\xi_4\neq0\,,\qquad \bar\eta\equiv\bar\eta_4\neq0\,,\qquad D\neq0\,.
\end{aligned} \qquad (8.10)$$

In case (1), the zero point is the origin, which remains a zero point for all values of μ, λ. So, the point $\bar\xi=\bar\eta=0$ is mapped onto the entire (μ,λ)-plane.

In case (2), when the zero points lie in the ξ-axis, from Eqn (8.9) we obtain

$$\bar\xi_2=\frac{\lambda-2}{\lambda}\,,\qquad \bar\eta=0\,. \qquad (8.11)$$

The condition for the existence of a real root $\bar\xi_2$ implies that the $\bar\eta=0$ line is mapped onto almost the entire (μ,λ)-plane, with the exception of the band $0<\lambda<2$. For each admissible λ there exist two zero points with the coordinates $\pm\bar\xi_2^{1/2}$, i.e. lying in the ξ-axis symmetrically on either side of the origin. The values of $|\bar\xi_2|<1$ correspond to the $\lambda>2$ region; such zero points are located between the myxines. The values of $|\bar\xi_2|>1$ correspond to the $\lambda<0$ region, and the zero points are positioned outside the myxines.

In case (3), when the zero points lie in the η-axis, we obtain

$$\bar\eta_3^2=\frac{\mu-\lambda+2}{\lambda-\mu}\,,\qquad \bar\xi=0\,, \qquad (8.12)$$

so that the $\bar\xi=0$ line is mapped onto the band $\mu<\lambda<\mu+2$ in the (μ,λ)-plane. Each admissible pair μ, λ generates two zero points located symmetrically (above and below) with respect to the origin.

Finally, in case (4) the nonzero roots $\bar\xi_4$, $\bar\eta_4$ of system (8.9) are bound by the relationships

$$\bar\eta_4^2=\frac{1}{2\lambda-\mu}-\frac{\lambda^2}{(2\lambda-\mu)^2}\,,$$
$$\bar\xi_4^2+\bar\eta_4^2=\frac{-\mu}{2\lambda-\mu}\,. \qquad (8.13)$$

One point in the parametric (μ,λ)-plane corresponds to each zero point $\bar\xi_4$, $\bar\eta_4$ of this kind. In turn, any pair of admissible values μ, λ generates four zero points (one in each quadrant of the plane) located symmetrically relative to the ξ- and η-axes. As follows from Eqns (8.13), the region of admissible values of μ and λ (i.e. the region where real roots $\bar\xi_4$, $\bar\eta_4$ exist) is defined by two simultaneous inequalities

$$\Phi_1(\mu,\lambda)\leqslant0\,,\qquad \Phi_2(\mu,\lambda)\geqslant0\,,$$
$$\Phi_1(\mu,\lambda)\equiv\lambda^2-2\lambda+\mu\,,$$
$$\Phi_2(\mu,\lambda)\equiv\lambda^2-(\mu-2\lambda)(\mu+1)\,. \qquad (8.14)$$

So, from one to nine zero points $\bar\xi$, $\bar\eta$, whose coordinates are specified by Eqns (8.10)–(8.13), can correspond to a given pair of parameters μ, λ.

The separatrix lines themselves are generated only by hyperbolic zero points, at which the condition

$$\frac{\partial^2\Psi_1}{\partial\xi^2}\,\frac{\partial^2\Psi_1}{\partial\eta^2}<\left(\frac{\partial^2\Psi_1}{\partial\xi\,\partial\eta}\right)^2 \qquad (8.15)$$

is fulfilled in addition to Eqns (8.9), and in some cases by parabolic zero points corresponding to the equality in (8.15). When the opposite inequality is fulfilled, the separatrix degenerates into a point in the (ξ,η) plane (the elliptic case). Plotted in the figures of Ref. [68] are the regions of the μ, λ parameters for which the zero points are hyperbolic and the regions of elliptic points, the boundaries defining the parabolic points.

Also notice that for $0<\lambda<\mu$ and $\mu<\lambda<0$ all the force lines, including the separatrices, are closed. In the opposite cases, the force lines (including the separatrices) may have branches going to infinity with slopes $\eta/\xi=\pm\sqrt{\lambda/(\lambda-1)}$.

8.3.3 Morphology of magnetic force lines near the center. In the consideration of the plasma configuration, the situation at the center is of prime importance. Expanding expression (8.8) in a series for $\xi \to 0$, $\eta \to 0$, we obtain

$$\Psi_1 \approx (\lambda - 2)\xi^2 + (\mu - \lambda + 2)\eta^2 - (\xi^4 + \eta^4) + 6\xi^2\eta^2 + \ldots \tag{8.16}$$

The equation of the separatrix passing through the center is $\Psi_1 = 0$. When inequality (8.15) is fulfilled, i.e. with $\{\lambda > 2, \lambda > \mu + 2\}$ or $\{\lambda < 2, \lambda < \mu + 2\}$, we have a hyperbolic point at the center of the (ξ, η) plane, with branches of the separatrix emanating from this point. The separatrix branches near the center represent two intersecting straight lines

$$\eta \approx \pm\xi\sqrt{\frac{2-\lambda}{\mu+2-\lambda}}\,. \tag{8.17}$$

Consider the region $\{\lambda \leqslant 2,\ \lambda \leqslant \mu + 2\}$ in greater detail. The rays $\{\lambda = 2,\ \mu \geqslant 0\}$ and $\{\lambda = \mu + 2,\ \mu \leqslant 0\}$ serve as its boundaries. At the first boundary, the central zero point is parabolic and the separatrix near the center appears as a horizontally oriented parabola $\eta^2 \approx \xi^4/\mu$. In this case μ is positive: the plasma current has the same direction as the current in the myxine. The plasma is concentrated here as a horizontally extended layer and we have an ultimate α-mode. If we recede from this boundary towards lower ξ, the inclination of the separatrices to the ξ-axis becomes positive and increases. If now μ be reduced for a fixed $\lambda < 0$, the inclination will increase further to attain 45° for $\mu = 0$ and become greater than 45° for negative μ. Thus occurs a transition to the β-mode. At the second boundary $\lambda = \mu + 2$ even for $\mu < 0$, and we obtain the ultimate β-mode. Near the center the separatrix branches transform into vertically oriented parabolas $\xi^2 \approx \eta^4/(-\mu)$: the plasma is concentrated as a vertical layer.

8.3.4 Frame of the belt. Solution (8.8) is formally defined in the entire (ξ, η) plane. Now consider the 'excision' of finite configurations and the construction of magnetic sheaths conjugated with them. Generally, this conjugation necessitates the fulfillment of two conditions: first, the continuity of the normal component of the magnetic field, i.e.

$$\Psi_{\rm pl}(\xi,\eta)\bigg|_{\Gamma-0} = \Psi_{\rm vac}(\xi,\eta)\bigg|_{\Gamma+0}\,, \tag{8.18}$$

and, second, the equilibrium condition

$$\left(\frac{(\nabla\Psi_{\rm pl})^2}{8\pi} + P\right)\bigg|_{\Gamma-0} = \frac{(\nabla\Psi_{\rm vac})^2}{8\pi}\bigg|_{\Gamma+0}\,. \tag{8.19}$$

We perform the excision of the plasma volume over the surfaces $\Psi = \Psi_0$ and $\Psi = \Psi_{\rm M}$ (Fig. 16a). The Ψ function and its normal derivative are specified on the plasma side of the interface. The Laplace equation is obeyed in the magnetic sheath. If we restrict ourselves to a relatively narrow sheath, the field in the sheath can be found by seeking the solution of a conventional Cauchy problem as a series in powers of v — the normal distance from Γ:

$$\Psi \approx \Psi\bigg|_{\Gamma} + v\,\frac{\partial\Psi}{\partial v}\bigg|_{\Gamma} + \frac{v^2}{2}\,\frac{\partial^2\Psi}{\partial v^2} + \ldots \tag{8.20}$$

The first two terms are determined by the boundary conditions, the third and succeeding terms can be found from the Laplace equation. A specific scheme for calculating the terms of expansion (8.20) is outlined in Ref. [68].

With the knowledge of the magnetic sheath of the belt, it can be conjugated with supported conductors which form, in concert with myxines, the magnetic configuration of the system.

And one further remark. As noted in the introductory section, the approximation of δ-like transition layers may be too coarse in some cases, requiring that they be 'spread' by setting them off by an 'edging.' Since we are dealing with an equilibrium, the edging region should also be described by the GSh equation

$$\Delta\Psi = -4\pi\,\frac{{\rm d}p_{\rm k}}{{\rm d}\Psi}\,, \tag{8.21}$$

where $p_{\rm k}(\Psi)$ is the magneto-baric characteristic in the edging region. Substituting the expansion

$$\Psi = \Psi_0(s) + v\Psi_1(s) + \frac{v^2}{2}\,\Psi_2(s) + \ldots$$

and taking into account that $\Psi_0(s)$ is constant along $\Gamma_{\rm M}$ while $\Psi_1(s) = H(s)$, the magnetic field strength along $\Gamma_{\rm M}$, we obtain

$$\Psi_2(s) = -4\pi\,\frac{{\rm d}p_{\rm k}(\Psi_0)}{{\rm d}\Psi_0}$$

and so on.

Examples of 'cut-out configurations' with $\lambda = 2$, 0, and -0.5 for $\mu > 0$ (the α-mode) are given in Fig. 16b.

8.3.5 Integral configuration characteristics. First consider the currents through the belt and the force acting on a myxine. If the external configuration boundary is the $\Psi = \Psi_0$ force line at which the pressure vanishes, three currents appear in the system: the current J_μ through the myxine, the current J_V through the plasma volume, and surface currents $J_{\rm s}$ at the boundary between the plasma and the magnetic sheath of myxines. Their magnitudes are given in Table 3. In particular, the values of $J_{\rm s}$ relate to the magnetic sheath of the myxine, its smallest distance from the configuration center being $\xi_{\rm M} = 0.7$. Also given in Table 3 are the dimensionless magnitudes of the force with which the myxines are attracted together. Notice that this force is zero for $\lambda = -0.5$. This is a consequence of the fact that, as is easy to verify,

$$F_x = \frac{J_\mu^2}{ac^2}(1 + 2\lambda)\,. \tag{8.22}$$

Indeed, when their potential is taken as $\mu\eta^2$ [see Eqn (8.8)], the intrinsic magnetic field of the currents flowing through the plasma becomes zero in the $\eta = 0$ plane, where the myxines are located. Consequently, the force acting, e.g., on the right myxine is determined only by the action of the left myxine and the 'far quadrupole.' This gives formula (8.22). Clearly for

Table 3.

λ	μ	J_V/J_μ	$J_{\rm s}/J_\mu$	$F_x ac^2/J_\mu^2$
2	2	−0.331	0.033	−5.0
2	4	−0.515	0.059	−5.0
1	2	−0.405	0.059	−3.0
1	4	−0.669	0.106	−3.0
0	2	−0.544	0.097	−1.0
0	4	−0.919	0.174	−1.0
−0.5	2	−0.818	0.133	0.0
−0.5	4	−1.377	0.235	0.0

$\lambda = -0.5$ there occurs a double equilibrium — that of the plasma and the myxines.

Now let us discuss the issue of the configuration stability with respect to convection. The most dangerous MHD instabilities of plasma configurations are those of the convective type. Therefore there is a need to consider first the stability of the belts and, especially, their peripheries with respect to convection. Although $\beta = 1$ in the central region of the belts, in the neighborhood of $\Psi = \Psi_0$ the magnitude of β nevertheless tends to zero while in the neighborhood of $\Psi = \Psi_M$, too, it can be rather small. For $\beta \ll 1$ the perturbations of the E-field are potential and the stability criterion is of the form (Longmire – Rosenbluth – Kadomtsev)

$$Q \equiv \frac{U(\mathbf{n}_0\nabla)P}{P(\mathbf{n}_0\nabla)U} < \gamma\,. \tag{8.23}$$

Here U is the specific volume of a magnetic force tube

$$U(\mu, \lambda, \Psi) = \frac{\delta V}{\delta \Psi} = \int \frac{\mathrm{d}l}{H}\,,$$

$\mathbf{n}_0$ is a unit vector of the external normal to the $\Psi = \mathrm{const}$ surface and γ is the adiabatic exponent. Figure 16b, c shows plots of the dimensionless function $U_1(\Psi_1) = UJ_\mu/a^2c$ for $\mu = 4$ and two values of λ equal to 2 and -0.5; also plotted is the dependence $Q(\Psi_1)$ for the same λ and μ. One can see that the plasma volume is stable as far as the external boundary $P = 0$ for $\lambda = 2$, with Q monotonically decaying towards the periphery and remaining negative for $\Psi_1 < 0$. As shown by a number of numerical examples, a similar situation occurs for different $\mu > 0$ if $\lambda \geqslant 0$. For lower λ, the periphery can become unstable. In particular, for $\lambda = -0.5$ only the internal region with $\Psi_1 \leqslant 0.1$ is stable, which corresponds to the necessity of truncating the configuration for nonzero pressure $P \approx 0.6P_0$. This fact is consistent with what was stated in Section 3.1 — holding the myxines adversely affects the plasma confinement.

8.3.6 Numerical simulation of the formation of the Galatea-Belt configuration. In the groups supervised by K V Brushlinskiĭ [69] and G I Dudnikova [70], dedicated codes were developed and preliminary 2-D simulations of the formation of the Galatea-Belt configurations were performed. A system of the MHD equations was solved in a rectangular range; the solution was shown to reach the quasistationary stage corresponding to the static solutions with a single-valued magneto-baric characteristic $P(\Psi)$. As shown in Ref. [70], in the α-mode it is possible to induce a magnetic sheath around the myxines virtually devoid of plasma by changing the current through them. At present (1998), work is underway to calculate the dynamics of the belt configuration in the axisymmetric case with ohmic heating.

8.4 Experimental modeling of the formation of the Galatea-Belt configuration

In the Institute of General Physics, Russian Academy of Sciences, an experimental UP-1 facility (Fig. 15b) intended for the studies on Galatea-Belt formation in a rectilinear discharge was devised under the supervision of A G Frank [71]. Configurationally, it is close to the facility for the studies of current sheaths. In UP-1 the discharge is likewise accomplished in a 1-m-long fused silica tube 18 cm in diameter. The myxines 2 cm in diameter are insulation-coated. The UP-1 experiments were conducted with maximum current in the myxines $J_\mu = 35$ kA and a halfperiod of 180 μs. The characteristic magnitude of discharge current in the plasma was $J_p = 17-18$ kA and the halfperiod about 5–6 μs. The discharges were accomplished without pre-ionization for an initial pressure of $\sim 3 \times 10^{-2}$ Torr when the working gas was Ar and 0.2 Torr in the case of He.

The plasma emission, recorded through a mesh electrode using interference light color filters and a streak camera, at different points of time is shown in Fig. 17. The use of interference light filters made it possible to take photographs of the discharge in different spectral lines and thus to

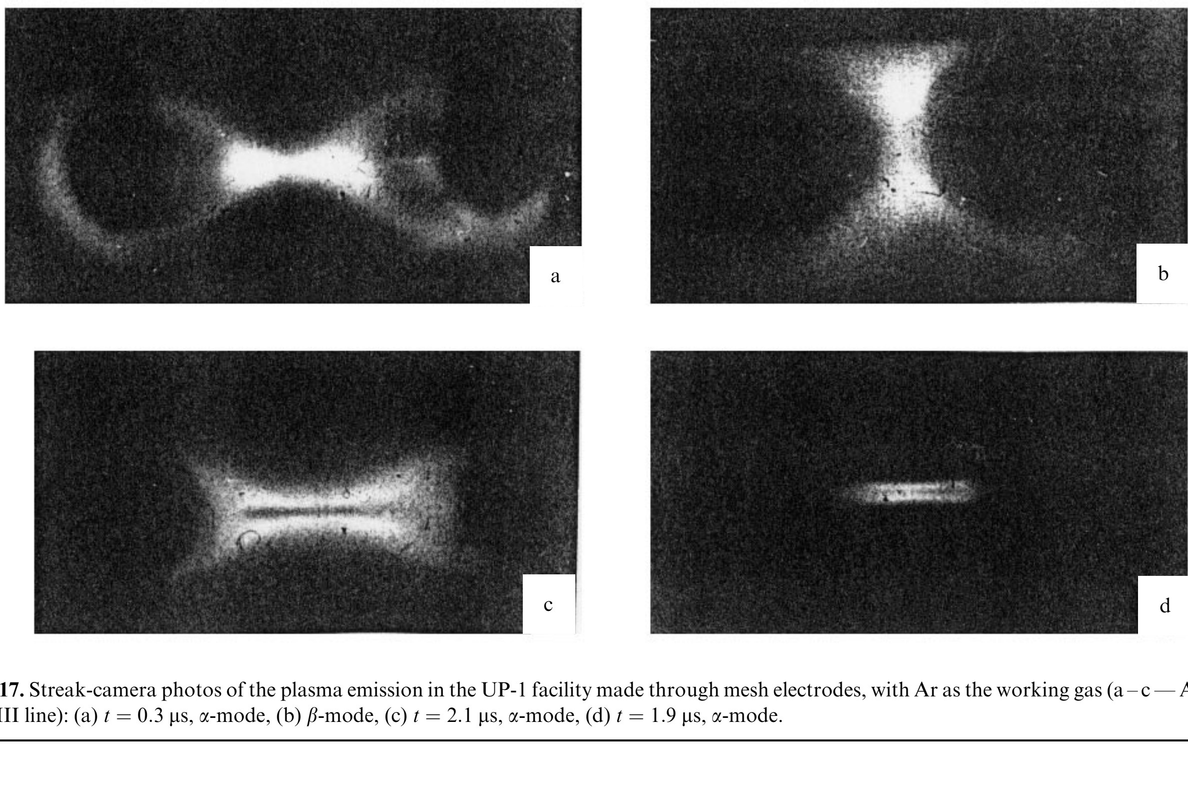

Figure 17. Streak-camera photos of the plasma emission in the UP-1 facility made through mesh electrodes, with Ar as the working gas (a – c — ArII line, d — CIII line): (a) $t = 0.3$ μs, α-mode, (b) β-mode, (c) $t = 2.1$ μs, α-mode, (d) $t = 1.9$ μs, α-mode.

judge the general properties of the plasma configuration. Frames a, c, and d relate to the α-mode and frame b to the β-mode. At the initial stage of discharge the current sheath and the mantles around the myxines are clearly visible (frame a). Subsequently (frames c and d) the mantles disappear due to the plasma contact with the myxines and the chamber walls, for no care was taken in these experiments to form the magnetic sheaths of myxines while the diameter of the discharge chamber was too small. Black strips are evident in the center of the pictures (c, d). Their appearance results from depletion of the corresponding atoms and ions with increasing electron temperature. The most surprising thing about these 'black holes' $\leqslant 1$ mm thick is that they produce sharp images, even though the length of the plasma column is ~ 1 m. This fact indicates conclusively that the configuration under discussion is very stable.

Spectroscopic measurements of density n_e and T_e in Ar averaged over the current sheath yielded the values $n_e \sim 10^{15}$ cm^{-3} and $T_e \sim 30$ eV for the current magnitudes specified above [72].

9. Electric-discharge traps

With the exception of Section 8, plasma confinement has been dealt with so far. Now we will touch on how the plasma can be produced in Galateas by an electrode discharge. This is how virtually all fusion traps came into being. But here the cases in point are peculiar systems which can be termed 'electric-discharge traps' (EDTs) [73]. In EDTs, the electric field and the flowing current serve many functions: accomplish the ionization of the entering working substance; heat the ions (directly and indirectly, via electrons); provide particle confinement not only by the magnetic field, but by the electric field as well; they can give rise to acceleration of the plasma or its components; and, lastly, in some cases accomplish autorecuperation, i.e. energy withdrawal from a significant fraction of particles escaping the trap.

Here we outline the experiments on three EDTs of different types — an 'electrostatic' plasma trap (ESPT), a toroidal electric-discharge multipole trap (EDT-M), and three-coil Galateas of the Galatea-A type (EDT-A).

The EDT discharges are characterized by a high electron temperature and therefore, as a rule, are blue in color irrespective of the kind of gas. This was clearly demonstrated on EDT-M where Xe, Ar, N_2, and He served as the working substance. The kind of gas could not be identified by eye. It was therefore proposed to term them 'celestines' ('blue').

Theoretically, the EDTs have not been adequately studied. However, there is good reason to make a brief review of the experiments for two reasons. First, amazingly high plasma parameters were obtained for modest expenditures and, second, they are little known to physicists; hopefully, familiarization with the experiments will foster this avenue of experimental and theoretical investigation.

9.1 Electrostatic plasma trap (ESPT)

This trap was proposed by V V Zhukov and A I Morozov in 1969. The impetus to its invention was given by the plasma lens experiment [74, 75] conducted with a hydrogen ion beam of ~ 1 A in a moderate vacuum ($\sim 10^{-4}$ Torr). Under these conditions, the ionization of the residual gas occurred in the lens volume (a non-self-maintained discharge was initiated) in crossed poloidal (E, H)-fields and, naturally, the resulting ions were accelerated towards the lens axis. The surprising thing was that a dark spot (channel) ~ 1 mm in diameter and ~ 10 cm in length was clearly visible when viewing a rather bright emission region along the lens axis. The spot was due to the deflection of the resulting radially moving low-energy ions induced by the magnetic field. The very fact of dark spot formation is indicative of stability of the plasma configuration. Naturally, the idea was conceived in designing a magnetoelectric trap of the mirror-type. A diffusion-type trap was made — a chain of five cells (Fig. 18a) [31, 76, 77]. Basically, the trap design was as follows: each cell constituted a magnetic bottle with a magnetic field ~ 200 Oe in the axis at the cell center and ~ 1000 Oe in the mirrors. An anti-turn was placed in the medium cell plane to induce a zero magnetic field in some circle. This zero-field circle was intended to suppress azimuthally asymmetric perturbations†. However, the role of the zero-field circle was not limited exclusively to stabilization. This separatrix surface intersected the electrode to which positive voltage was applied. As a result, it played the part of the anode of the discharge circuit. The role of the cathode was fulfilled by the axial magnetic line which met either the chamber walls or a special axial electrode.

In this way a radial electric field was induced in the trap volume. To make the potential distribution across the coaxial magnetic surfaces more uniform, systems of coaxial electrodes connected to a voltage divider were placed at the trap ends.

The equipotential lines inside the cell constructed on the basis of probe measurements for $U_p = 500$ V are given in Fig. 18b; plotted in Fig. 18c is the U_p-dependence of the depth Φ_{max} of the potential well in the central cell. It is evident that the value of Φ_{max} in this case exceeds one-half the value of U_p.

The ESPT operation is as follows. Hydrogen (or deuterium) is delivered to the central cell to become ionized in the cloud of azimuthally drifting electrons. The resulting ions accelerate towards the trap axis and move further in the radial direction. Most of the ions in this case cannot cross the separatrix surface, which is at the anode potential $\Phi_a = U_p$, because the ions are produced at a potential $\Phi_* < U_p$. They can escape the potential barrier $\Phi_a - \Phi_*$ only due to classical or anomalous collisions. When the system is stabilized well and classical collisions are the governing factor, it is easily seen that the ions crossing the anode surface and reaching the chamber walls, which are at the anode potential, impart a relatively small fraction of energy to them. The main fraction of the energy $e\Phi_a$ goes to the electric circuit which induces the electric field in the trap. Consequently, the trap itself is a recuperator. Improving the recuperation efficiency is favored by a specific feature of Coulomb collisions: they occur primarily at large distances and are associated with the transfer of small portions of energy. So, the Fokker – Planck nature of the energy variation for the bulk of the ions causes them to approach the anode separatrix with a small energy scatter and to escape it with a low velocity.

Of course, the ions do not move strictly along the trap radii. Moreover, the cell dimensions are so selected that a sufficiently strong randomization of ion motion occurs in the (r, z)-plane. In this case, the cell chain behaves like a diffusion

† More recently, in the late 80s, anti-turns were incorporated in the 'Taro' trap for the same purpose [78].

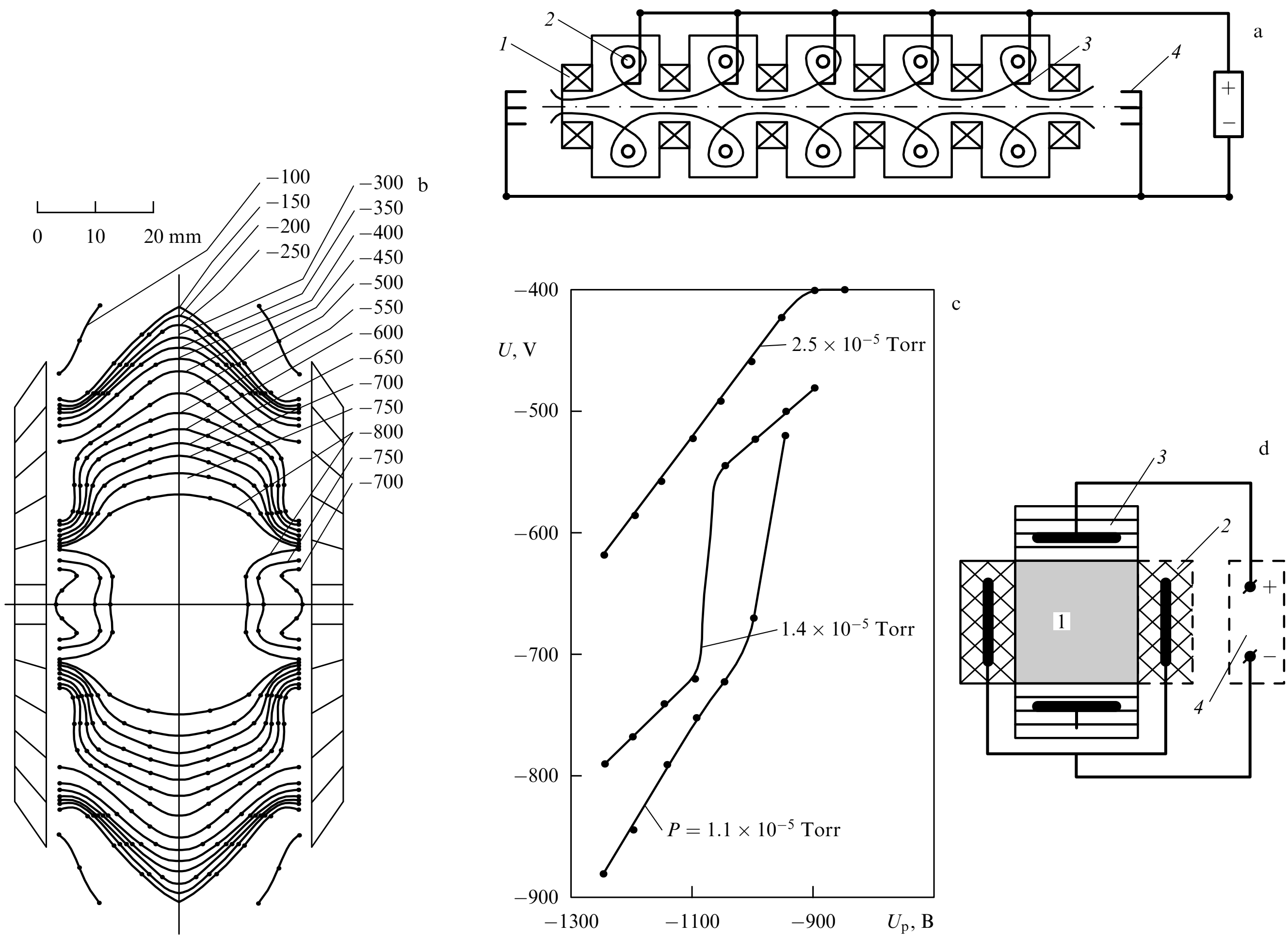

Figure 18. Magnetoelectric ESPT trap: (a) schematic diagram: *1* — mirror coils, *2* — 'anti-turn,' *3* — anode, *4* — sectional cathode; (b) distribution of the floating potential in the central ESPT cell for $U_{\mathrm{p}} = -1250$ V, $H_{\mathrm{pr}} \approx 4$ kOe; (c) dependence of the well depth on U_{p} and the pressure in the vacuum chamber; (d) functional diagram of the ESPT as a plasma 'decay'-mode recuperator: *1* — plasma volume, *2* — ion barrier, *3* — electron barrier, *4* — energy receiver.

trap and the particle lifetime

$$\tau_{\mathrm{p}}^{(N)} \propto N^2 \tau_{\mathrm{p}}^1 ,$$

where N is the number of cells and τ_{p}^1 is the average particle lifetime in one cell.

In an ESPT the energy is recuperated not only from the ions. In principle, to a large extent the electron energy can be recovered, too. This is because the plasma density peaks in the central cell of the trap and reduces to a small value near the ESPT ends. This is responsible for a 'thermal' potential difference

$$\delta\Phi \approx \frac{kT_{\mathrm{e}}}{e} \ln \frac{n_{\max}}{n_{\min}} .$$

across the axis. In consequence, those electrons that move towards the trap ends give up a significant part of their thermal energy to the electric circuit of the system.

It is valid to say that an ESPT behaves, with respect to the charged particles inside of it, as a kind of thermoelement in which the cathode and the anode are surrounded respectively by ion and electron barriers (Fig. 18d).

The barrier for electrons is induced by the magnetic field between the axis and the separatrix, and the barrier for ions by the crimps of the equipotential lines along the trap. That is why in experimental studies attention was above all given to the resultant potential well†.

9.2 Electric-discharge quadrupole EDT-M Galatea trap ('Avos'ka')

The next Galatea studied in the electric-discharge mode was the toroidal quadrupole EDT-M trap (Fig. 19a). It was proposed by A I Morozov and implemented by A I Bugrova, A S Lipatov, and V K Kharchevnikov [5, 79–81]. The trap consisted of two parallel rings with currents flowing in one direction. The major and minor ring radii were 30 cm and 2 cm, respectively. The coils were wrapped in foil connected electrically to the chamber walls. Rigid braces were used to obviate the attraction of the coils to one another. The coil separation was 10 cm. The experiments were conducted primarily for two values of ampere-turns in the myxines: $J_\mu = 1500$ A and $J_\mu = 12000$ A. The z-component of the field as a function of radius in the medium (between the coils) plane is plotted in Fig. 19a. Noteworthy is the effect of toricity responsible for a radial shift of the magnetic field zero. Specifically, if two parallel conductors rather than two rings

† Unfortunately, for several reasons the experimental studies on the ESPT did not last long, and only fragmentary results were obtained during that period.

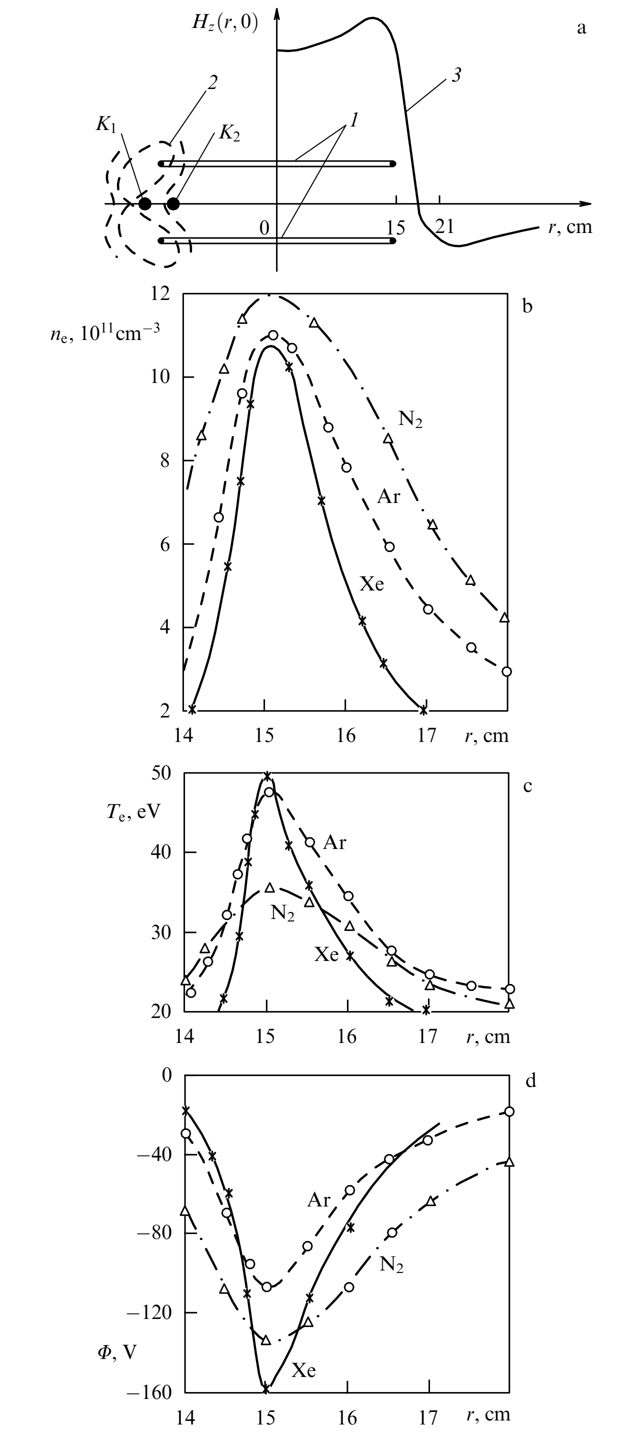

Figure 19. Quadrupole electric-discharge EDT-M Galatea trap: (a) schematic and magnetic field of the Galatea: *1* — myxines, *2* — separatrix, *3* — radial dependence of H_z in the medium plane ($z = 0$), K_1 — position of the cathode in the barrier regime, K_2 — position of the cathode in the mirror regime; (b – d) dependences of the local discharge parameters on r in different gases for $z = 0$ and $H_b^* = 140$ Oe. (The mirror regimes $U_p = 200$ V, $\dot{m} = 2$ mg s^{-1}, $J_p(\mathrm{Xe}) = 300$ mA, $J_p(\mathrm{Ar}) = 270$ mA, $J_p(\mathrm{N_2}) = 200$ mA.)

were dealt with, the zero of the field would be located between them. But owing to toricity it is located at $R_0 = 17.5$ cm instead of $R_c = 15$ cm. The second important manifestation of toricity is the field strength asymmetry with respect to $r = R_c$. For $r < R_c$ the field has a maximum of $(H_z)_{\max} \approx 80$ Oe at $r_1 = 11$ cm, whereas for $r > R_c$ it peaks at $R_\delta \approx 21$ cm and the field (the 'barrier field') at this point amounts to ~ 20 Oe. Referring to the figure, the field decays slowly beyond the barrier.

The plasma in the trap was produced by a straight discharge between an incandescent tungsten filament and the chamber. In principle, sustaining the pressure in the chamber at $\sim 10^{-4}$ Torr would suffice to maintain a discharge. However, the discharge was more stable in the flow-type mode. In this mode, a tube ~ 3 mm in diameter was placed near the discharge to deliver the gas subsequently drawn away by a pump. For a voltage of $\leqslant 100$ V, a discharge was initiated between the incandescent cathode and the chamber, its color being blue irrespective of the sort of gas.

Despite its exceptional simplicity, studies of the EDT-M characteristics and the processes therein present specific difficulties. They arise from the novelty of the situation involved and a large number of independent parameters, such as the intermyxine distance, the myxine cross section diameter, the currents through the myxines, the locations of the cathode and the gas supply, the cathode heat, and the voltage across the discharge. The first series of papers dates back to the early 90s (see the references cited above). Valuable results were obtained, which we discuss below.

First and foremost, it was discovered that there exist two forms of discharge. In one of them, which will be named the 'mirror form,' the main glow was confined to the plasma ring (plasmoid), with a small diameter of $\sim 2 - 2.5$ cm. In this case, the plasma glow in the vicinity of the separatrix enclosing the myxines was quite weak. This part of the configuration was termed 'mantle.' The 'mirror form' was observed when the distance of the cathode to the system axis was ~ 13.5 cm. For $J_\mu = 1500$ A, the magnetic field intensity was ~ 50 Oe and for $J_\mu = 12000$ A it was ~ 400 Oe.

If the cathode is moved in the radial direction, the plasmoid, too, moves along with it. The discharge pattern changes substantially when the cathode is in the immediate vicinity ($r_0 \approx 17$ cm) of the zero of the vacuum magnetic field. In this case, the plasma occupies the immediate neighborhood of the separatrix along its entire length. This was named the 'barrier form' of the discharge. The volt-ampere discharge characteristics for a constant cathode heat are similar in both regimes but the barrier-discharge voltage is lower. The typical magnitudes of discharge current are $\sim 200 - 400$ mA and of the voltage $\sim 200 - 400$ V. Lastly, the mirror discharge is transparent-blue whereas the barrier one is less transparent and its glow is bluish-white.

As expected, probe measurements revealed that higher plasma parameters were inherent in the mirror regime, which therefore received primary emphasis at that time. The radial distributions of the density, the electron temperature, and the electric potential in the medium plane in this regime, with a current of 12000 ampere-turns flowing through the myxines, are plotted in Fig. 19b – d. Referring to the figure, the parameters obtained with different gases are close to each other: $n_{\mathrm{e\,max}} \sim 10^{12}$ cm^{-3}, $T_{\mathrm{e\,max}} \sim 50$ eV, the potential well depth $\Phi_{\max} \approx -150$ V for the discharge voltage $U_p \sim 200$ V. These data are unique. Such a high electron temperature in a rectilinear low-current stationary discharge, we believe, has been attained for the first time. The high electron temperature accounts for the similarity of blue glow in different gases. That is why it was suggested that the name 'celestines'† be

† Celestis — sky-blue.

used for the blue discharges realized in the EDT-M-type systems. Several significant conclusions, above all about the ion component, can be drawn from the experimental data cited above. The Larmor ion radii in the magnetic fields involved are high ($\geqslant 100$ cm), and hence the ions are confined in the trap by the electrostatic field ('reside in a potential well'). The average ion energy can be estimated from the well profile and the electron density distribution:

$$\bar{\mathcal{E}}_{\rm i} \approx \frac{1}{3}\, e|\Phi_{\max}|\,,$$

where $\Phi_{\max}$ is the well depth. In the case of Fig. 19d, this yields $\mathcal{E}_{\rm i} \sim 50$ eV. The ion escape along the lines of force is hindered by the convergence of the equipotential lines near the myxines, i.e. the formation of electric 'mirrors' rather than magnetic ones and the conservation, to a degree, of the transverse adiabatic invariant

$$J_{\perp,\rm i} = V_{\perp,\rm i} h = \text{const}\,.$$

Here $V_{\perp,\rm i}$ is the ion velocity component in the direction normal to the equipotential lines and h is the distance between the surfaces with equal potentials.

On the strength of the above considerations, even though they are undoubtedly subject to refinement, the form of the discharge under discussion was termed the 'mirror' regime.

It is not the mere color that makes the celestines remarkable. Also impressive is their low-current property exhibited for a high discharge voltage, relatively large system dimensions, and very weak magnetic fields. With the data given in Fig. 19, we estimate the classical conductivity by the formula

$$\sigma_\perp = \frac{e^2 n_{\rm e}^2 c^2}{\sigma_0 H^2}\,,$$

to obtain a value in reasonable agreement with the conductivity estimated from the discharge parameters $J_{\rm p}$ and $U_{\rm p}$. These same data make it possible to estimate the magnitude of β in the mirror regime (from the vacuum field in the cathode region). Hence we have $\beta \sim 0.1$. Estimating the mirror-regime energy times by the formula

$$\tau_E = \frac{3}{2}\,\frac{\int n(T_{\rm i} + T_{\rm e})\,{\rm d}^3 r}{J_{\rm p} U_{\rm p}}$$

gives $\tau_E \sim 10$ μs for $J_\mu = 1500$ A and $\tau_E \sim 70$ μs for $J_\mu = 12000$ A.

The studies of the barrier regime commenced only recently (in late 1997). The name 'barrier regime' arose from the fact that plasma in this case fills the region of the zero of magnetic field and the minimum confining field is the barrier field. The strength of this field is $H_{\rm b} \approx 20$ Oe for $J_\mu = 1500$ A and $H_{\rm b} \sim 140$ Oe for $J_\mu = 12000$ A. Preliminary data have now been obtained for a weak field: $n_{\rm e\,max} \sim 5 \times 10^{10}$ cm^{-3}, $T_{\rm e\,max} \sim 28$ eV, $\Phi_{\max} \approx -25$ V. To these values correspond the classical conductivity, $\beta_{\rm b} \sim 0.1$, and $\tau_E \sim 40$ μs. A significant increase in τ_E is associated with a drastic increase in the volume occupied by the plasma.

Despite the incompleteness of the available data, the results of the barrier regime research are highly optimistic. In this connection, efforts are underway to develop an 'Octupole' Galatea trap, with an average diameter of the plasma volume of 60 cm. The barrier field in this trap can attain a magnitude of 1000 Oe.

9.3 Electric-discharge version of Galatea-A

In the Moscow Institute of Radio Engineering and Electronics, too, experiments were conducted on electric-discharge versions of Galatea-A which received the name 'Gala' [82]. As already noted in Section 2.3, this system of three coils makes it possible to obtain a diversity of magnetic and, accordingly, plasma configurations by varying the magnitude and the sense of the current J_μ in the central myxine with respect to the current $J_{\rm pr}$ in the mirror coils. The two most notable configurations are depicted in Fig. 20a, b. As in the case of EDT-M, there is an incandescent cathode and a delivery of xenon to its neighborhood. The experiments were made for a constant number of turns in the mirror coils to provide one and the same field $H_{\rm pr} \sim 100$ Oe in the mirrors. The volt-ampere discharge characteristics for different field configurations are presented in Fig. 20c. Referring to the figure, they are close to the characteristics observed on EDT-M for similar parameters of the magnetic field.

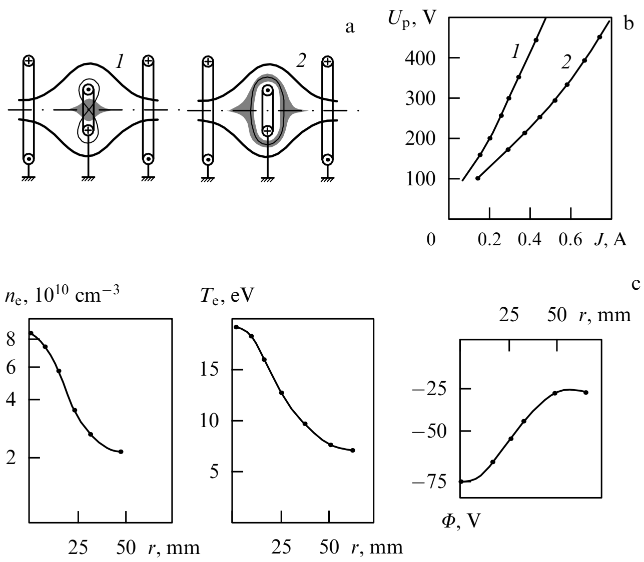

Figure 20. Three-coil electric-discharge traps of the Galatea-A type: (a) Gala model and two magnetic configurations *1* and *2*, (b) volt-ampere characteristics for these configurations at $H_{\rm pr} = 150$ Oe, (c) radial distributions of the electric density, the electron temperature, and the electric potential for $z = 0$ for configuration *1*.

10. Conclusions

Though far from complete, the information on Galateas summarized in this review nevertheless allows the following conclusions:

(1) The technical difficulties arising from the magnetic suspension of myxines and their operation in reactor conditions can be overcome with present-day technologies.

(2) The orientation of research to the development of traps with $\beta_0 \approx 1$ is justified both from scientific and practical standpoints.

(3) Galateas are widely diversified, and this provides additional reason to regard them as promising systems.

(4) The scope of experimental and theoretical research has now been defined. Of vital importance are studies of the plasma – field transition layer.

(5) Electric-discharge traps are an important tool for producing and confining plasmas with particle energies $\sim 10-100$ eV.

(6) Unlike low-β traps, Galateas, or 'magnetic vessels,' constitute a unique tool for many plasma technologies and for hypertemperature reactors (D^3He, DD etc.).

Acknowledgements

The studies presented here were performed analytically, numerically, and to a degree experimentally. Some of them were performed under the auspices of the Russian Foundation for Basic Research and the Russian Ministry of Nuclear Energy.

The work on this review would have been impossible without the active participation of our colleague-investigators in Galatea research, whose contributions are represented in the body of the review and in the references cited. The authors are deeply grateful to all of them. We would also like to express our appreciation to the colleagues who participated actively in the discussion of this series of papers. They are V D Shafranov, V I Il'gesonis, A A Rukhadze, and B B Kadomtsev who stimulated us into writing this review. The authors' special gratitude is due to A I Bugrova for establishing and conducting the first studies on electric-discharge Galateas.

References

1. Braginskiĭ S I, Kadomtsev B B, in *Fizika Plazmy i Problema Upravlyaemykh Termoyadernykh Reaktsiĭ* Vol. 3 (Plasma Physics and Thermonuclear Research) (Ed. M A Leontovich) (Moscow: Izd. AN SSSR, 1958) p. 300
2. Berkowitz J, Grad H, Rubin H, in *Fizika Goryacheĭ Plazmy i Termoyadernye Reaktsii* Vol. 1 (The Physics of Hot Plasmas and Thermonuclear Reactions) (Proceedings of the Second International Conference on the Peaceful Uses of Atomic Energy, Geneva, 1958) (Moscow: Atomizdat, 1959) p. 109
3. Berkowitz J et al., in *Fizika Goryacheĭ Plazmy i Termoyadernye Reaktsii* Vol. 1 (The Physics of Hot Plasmas and Thermonuclear Reactions) (Proceedings of the Second International Conference on the Peaceful Uses of Atomic Energy, Geneva, 1958) (Moscow: Atomizdat, 1959) p. 146
4. Firsov O B, in *Fizika Plazmy i Problema Upravlyaemykh Termoyadernykh Reaktsiĭ* Vol. 3 (Plasma Physics and Thermonuclear Research) (Ed. M A Leontovich) (Moscow: Izd. AN SSSR, 1958) p. 327
5. Bugrova A I et al. *Pis'ma Zh. Tekh. Fiz.* **18** (24) 54 (1992) [*Sov. Tech. Phys. Lett.* **18** 815 (1992)]; *Fiz. Plazmy* **19** 972 (1993) [*Plasma Phys. Rep.* **19** 505 (1993)]
6. Morozov A I *Pis'ma Zh. Tekh. Fiz.* **16** (15) 86 (1990) [*Sov. Tech. Phys. Lett.* **16** 597 (1990)]
7. Morozov A I *Fiz. Plazmy* **18** 305 (1992) [*Sov. J. Plasma Phys.* **18** 159 (1992)]
8. Sakharov A D, in *Fizika Plazmy i Problema Upravlyaemykh Termoyadernykh Reaktsiĭ* Vol. 1 (Plasma Physics and Thermonuclear Research) (Ed. M A Leontovich) (Moscow: Izd. AN SSSR, 1958) p. 20
9. Orlinskiĭ D V, in *Fizika Plazmy i Problema Upravlyaemykh Termoyadernykh Reaktsiĭ* Vol. 4 (Plasma Physics and Thermonuclear Research) (Ed. M A Leontovich) (Moscow: Izd. AN SSSR, 1958) p. 49
10. Yoshikawa S *Nucl. Fusion* **13** 433 (1973)
11. Kerst D W, Ohkawa T *Nuovo Cimento* **22** 784 (1961)
12. Kerst D W et al. *Phys. Rev. Lett.* **15** 396 (1965)
13. Ohkawa T et al., in *Proc. Conf. Culham, Vienna, 1965* Vol. 2 (Vienna: IAEA, 1966) p. 531
14. Demidenko I I, Lomino N S, Padalka V G *Zh. Tekh. Fiz.* **40** 1217 (1970)
15. Skornyakov G V *Zh. Tekh. Fiz.* **32** 777 (1962) [*Sov. Phys. Tech. Phys.* **7** 571 (1963)]
16. Peregood B P, Lehnert B *Nucl. Instrum. Methods* **180** 357 (1981)
17. Prager S C *Nucl. Instrum. Methods Phys. Res.* **207** 187 (1983)
18. Hasegawa A *Comments Plasma Phys. and Controlled Fusion* **11** 147 (1987)
19. Moor R D AIAA Pap., No. 69-270 (1969) p. 1
20. Morozov A I *Pis'ma Zh. Tekh. Fiz.* **16** (15) 89 (1990) [*Sov. Tech. Phys. Lett.* **16** 598 (1990)]
21. Zykov V G, Preprint of the Kharkov Institute of Physics and Technology, No. 79-12 (Kharkov: KhIFT, 1979) p. 44
22. Morozov A I, Pustovitov V D *Fiz. Plazmy* **17** 1276 (1991) [*Sov. J. Plasma Phys.* **17** 740 (1991)]
23. Brushlinskiĭ K V, Morozov A I, Petrovskaya N B *Mat. Modelirovanie* (in press)
24. Morozov A I, Frank A G *Fiz. Plazmy* **20** 982 (1994) [*Plasma Phys. Rep.* **20** 879 (1994)]
25. Morozov A I *Nucl. Fusion Suppl.* **3** 3 (1969)
26. Post R F *Fiz. Plazmy* **23** 816 (1997)
27. Budker G I, in *Proc. 4 Europ. Conf. on Controlled Fusion and Plasma Physics, Moscow, 1973* Vol. 2 (Dubna, 1974) p. 136
28. Morozov A I, Solov'ev L S, in *Voprosy Teorii Plazmy* Vol. 8 (Reviews of Plasma Physics) (Ed. M A Leontovich) (Moscow: Atomizdat, 1974) p. 3
29. Brushlinskiĭ K V, Morozov A I, in *Voprosy Teorii Plazmy* Vol. 8 (Reviews of Plasma Physics) (Ed. M A Leontovich) (Moscow: Atomizdat, 1974) p. 88
30. Morozov A I *Fiz. Plazmy* **16** 131 (1990) [*Sov. J. Plasma Phys.* **16** 69 (1990)]
31. Zhukov V V, Morozov A I, Shchepkin G Ya *Pis'ma Zh. Eksp. Teor. Fiz.* **9** 24 (1969) [*JETP Lett.* **9** 14 (1969)]
32. Morozov A I, Solov'ev L S, in *Voprosy Teorii Plazmy* Vol. 2 (Reviews of Plasma Physics) (Ed. M A Leontovich) (Moscow: Gosatomizdat, 1963) p. 3
33. Markov B A, Morozov A I *Pis'ma Zh. Tekh. Fiz.* **20** (10) 1 (1994) [*Tech. Phys. Lett.* **20** 384 (1994)]
34. Markov B A, Morozov A I, Sveshnikov A G *Mat. Modelirovanie* **8** (11) 59 (1996)
35. Tamm I E *Osnovy Teorii Elektrichestva* (Principles of the Theory of Electricity) (Moscow: Nauka, 1976)
36. Morozov A I, Khripunov V I *Fiz. Plazmy* **18** 838 (1992) [*Sov. J. Plasma Phys.* **18** 435 (1992)]
37. Morozov A I, Nevrovskiĭ V A, Pistunovich V I *Pis'ma Zh. Tekh. Fiz.* [*Tech. Phys. Lett.*] (in press)
38. Briesmeister J (Ed.) MSNP-A General Monte Karlo Code for Neutron and Photon Transport, Version 3A, LA-7396-M, Rev. 2, September (1986)
39. Braginskiĭ S I, in *Voprosy Teorii Plazmy* Vol. 1 (Reviews of Plasma Physics) (Ed. M A Leontovich) (Moscow: Gosatomizdat, 1963) p. 183
40. Morozov A I, Pastukhov V P *Fiz. Plazmy* **18** 790 (1992) [*Sov. J. Plasma Phys.* **18** 410 (1992)]
41. Pastukhov V P, Sokolov A Yu *Nucl. Fusion* **32** 1725 (1992)
42. Sokolov A Yu *Fiz. Plazmy* **19** 1454 (1993) [*Plasma Phys. Rep.* **19** 766 (1993)]
43. Kesner J, Mauel M *Fiz. Plazmy* **23** 801 (1997)
44. Hasegawa A, Chen L, Mauel M E *Nucl. Fusion* **30** 2405 (1991)
45. Teller E et al. *Fusion Technol.* **22** 82 (1992)
46. Mauel M E, Kesner J *The Dipol Plasma Confinement Concept, IAEA Technical Committee Meeting on Innovative Approaches to Fusion Energy, Pleasanton, California, USA, October 20 – 22, 1997*
47. Morozov A I *Fiz. Plazmy* **17** 124 (1991) [*Sov. J. Plasma Phys.* **17** 71 (1991)]
48. Brushlinskiĭ K V, Ratnikova T A, Tuzova N B *Mat. Modelirovanie* **2** (11) 45 (1990); Brushlinskiĭ K V, Ryaben'kiĭ V S, Tuzova N B *Zh. Vychisl. Mat. Mat. Fiz.* **32** 1929 (1992)
49. Zueva N M, Mikhaĭlova M S, Morozov A I *Fiz. Plazmy* **18** 664 (1992) [*Sov. J. Plasma Phys.* **18** 346 (1992)]
50. Morozov A I *Fiz. Plazmy* **17** 395 (1991) [*Sov. J. Plasma Phys.* **17** 231 (1991)]

51. Morozov A I, Solov'ev L S *Zh. Eksp. Teor. Fiz.* **40** 1316 (1961) [*Sov. Phys. JETP* **13** 927 (1961)]
52. Demidenko I I, Lomino N S, Padalka V G *Zh. Tekh. Fiz.* **40** 2326 (1970)
53. Morozov A I, in *Plazmennye Uskoriteli* (Plasma Accelerators) (Ed. L A Artsimovich) (Moscow: Mashinostroenie, 1973) p. 282
54. Shafranov V D *Zh. Eksp. Teor. Fiz.* **33** 710 (1957) [*Sov. Phys. JETP* **6** 545 (1958)]
55. Morozov A I, Savel'ev V V *Fiz. Plazmy* **19** 977 (1993) [*Plasma Phys. Rep.* **19** 508 (1993)]
56. Savel'ev V V *Fiz. Plazmy* **21** 216 (1995) [*Plasma Phys. Rep.* **21** 205 (1995)]
57. Birkhoff G, Zarantonello E H *Jets, Wakes and Cavities* (Applied Mathematics and Mechanics, Vol. 2) (New York: Academic Press, 1957) [Translated into Russian (Moscow: Mir, 1964)]
58. Gurevich M I *Teoriya Struĭ Ideal'noĭ Zhidkosti* (Theory of Jets in Ideal Fluids) (Moscow: Nauka, 1979) [Translated into English (New York: Academic Press, 1965)]
59. Maĭkov A R, Morozov A I, Sveshnikov A G *Fiz. Plazmy* **22** 93 (1996) [*Plasma Phys. Rep.* **22** 87 (1996)]
60. Landau L D, Lifshits E M *Elektrodinamika Sploshnykh Sred* (Electrodynamics of Continuous Media) (Moscow: Nauka, 1982) [Translated into English (Oxford: Pergamon Press, 1960)]
61. Samarskiĭ A A, Gulin A V *Chislennye Metody* (Numerical Techniques) (Moscow: Nauka, 1989)
62. Ferraro V C *J. Geophys. Res.* **52** 15 (1952)
63. Morozov A I, in *Trudy Soveshchaniya po Maloradioaktivnomu Termoyadernomu Sintezu na Osnove* D – ^{3}He (Proceedings of the Conference on Weakly Radiactive D – ^{3}He-Based Nuclear Fusion) (Moscow: I.V. Kurchatov Institute of Atomic Energy, 1991) p. 133
64. Morozov A I, Savel'ev V V *Fiz. Plazmy* **21** 209 (1995) [*Plasma Phys. Rep.* **21** 199 (1995)]
65. Syrovatskiĭ S I *Zh. Eksp. Teor. Fiz.* **60** 1727 (1971) [*Sov. Phys. JETP* **33** 934 (1971)]
66. Syrovatskiĭ S I, Frank A G, Khodzhaev A Z *Pis'ma Zh. Eksp. Teor. Fiz.* **15** 138 (1972) [*JETP Lett.* **15** 94 (1972)]
67. Frank A G *Tr. Fiz. Inst. Akad. Nauk SSSR* **160** 93 (1985)
68. Morozov A I, Murzina M V *Fiz. Plazmy* **22** 551 (1996) [*Plasma Phys. Rep.* **22** 500 (1996)]
69. Brushlinskiĭ K V, Gorshenin K P, Morozov A I *Pis'ma Zh. Tekh. Fiz.* **21** (22) 67 (1995) [*Tech. Phys. Lett.* **21** 935 (1995)]; Brushlinskiĭ K V, Gorshenin K P *Mat. Modelirovanie* **9** (5) 28 (1997)
70. Dudnikova G I, Morozov A I, Fedoruk M P *Fiz. Plazmy* **23** 387 (1997)
71. Bogdanov S Yu et al. *Pis'ma Zh. Tekh. Fiz.* **21** (24) 5 (1995) [*Tech. Phys. Lett.* **21** 995 (1995)]
72. Bogdanov S Yu et al. *Fiz. Plazmy* **24** 467 (1998)
73. Bugrova A I et al. *Pis'ma Zh. Tekh. Fiz.* **18** (24) 54 (1992) [*Sov. Tech. Phys. Lett.* **18** 815 (1992)]
74. Morozov A I, Lebedev S V, in *Voprosy Teorii Plazmy* Vol. 8 (Reviews of Plasma Physics) (Ed. M A Leontovich) (Moscow: Atomizdat, 1974) p. 247
75. Zhukov V V, Morozov A I, Shchepkin G Ya *Pis'ma Zh. Eksp. Teor. Fiz.* **9** 24 (1969) [*JETP Lett.* **9** 14 (1969)]
76. Morozov A I, in *Plazmennye Uskoriteli* (Plasma Accelerators) (Ed. L A Artsimovich) (Moscow: Mashinostroenie, 1973) p. 83
77. Morozov A I *6-European Conf. on Control Fusion and Plasma Phys., Moscow, USSR, June, 1973* Vol. 2, p. 285
78. Lane B et al. *Nucl. Fusion* **22** 577 (1982)
79. Bugrova A I et al. *Pis'ma Zh. Tekh. Fiz.* **18** (8) 1 (1992) [*Sov. Tech. Phys. Lett.* **18** 242 (1992)]; Bugrova A I et al. *Pis'ma Zh. Tekh. Fiz.* **18** (24) 54 (1992) [*Sov. Tech. Phys. Lett.* **18** 815 (1992)]
80. Bugrova A I et al. *Fiz. Plazmy* **19** 972 (1993) [*Plasma Phys. Rep.* **19** 505 (1993)]
81. Bugrova A I et al. *Fiz. Plazmy* **19** 1411 (1993) [*Plasma Phys. Rep.* **19** 741 (1993)]
82. Bugrova A I et al. *Pis'ma Zh. Tekh. Fiz.* **20** (19) 51 (1994) [*Sov. Tech. Phys. Lett.* **20** 788 (1994)]